Tesis Doctoral

Reconocimiento de acciones en videos de profundidad

Ubalde, Sebastián

2016-03-22

Universidad de Buenos Aires

Facultad de Ciencias Exctas y Naturales

Departamento de Computación

Reconocimiento de acciones en videos de profundidad

Tesis presentada para optar al título de Doctor de la Universidad de Buenos Aires en el área Cs. de la Computación

Sebastián UBALDE

Directora de tesis: Marta E. Mejail

Consejera de estudios: Marta E. Mejail

Buenos Aires, 2015

Reconocimiento de acciones en videos de profundidad

Resumen El problema de reconocer automáticamente una acción llevada a cabo en un video está recibiendo mucha atención en la comunidad de visión por computadora, con aplicaciones que van desde el reconocimiento de personas hasta la interacción persona-computador. Podemos pensar al cuerpo humano como un sistema de segmentos rígidos conectados por articulaciones, y al movimiento del cuerpo como una transformación continua de la configuración espacial de dichos segmentos. La llegada de cámaras de profundidad de bajo costo hizo posible el desarrollo de un algoritmo de seguimiento de personas preciso y eficiente, que obtiene la ubicación 3D de varias articulaciones del esqueleto humano en tiempo real. Esta tesis presenta contribuciones al modelado de la evolución temporal de los esqueletos.

El modelado de la evolución temporal de descriptores de esqueleto plantea varios desafíos. En primer lugar, la posición 3D estimada para las articulaciones suele ser imprecisa. En segundo lugar, las acciones humanas presentan gran variabilidad intra-clase. Esta variabilidad puede encontrarse no sólo en la configuración de los esqueletos por separado (por ejemplo, la misma acción da lugar a diferentes configuraciones para diestros y para zurdos) sino también en la dinámica de la acción: diferentes personas pueden ejecutar una misma acción a distintas velocidades; las acciones que involucran movimientos periódicos (como aplaudir) pueden presentar diferentes cantidades de repeticiones de esos movimientos; dos videos de la misma acción puede estar no-alineados temporalmente; etc. Por último, acciones diferentes pueden involucrar configuraciones de esqueleto y movimientos similares, dando lugar a un escenario de gran similaridad inter-clase. En este trabajo exploramos dos enfoques para hacer frente a estas dificultades.

En el primer enfoque presentamos una extensión a *Edit Distance on Real sequence* (EDR), una medida de similaridad entre series temporales robusta y precisa. Proponemos dos mejoras clave a EDR: una función de costo *suave* para el alineamiento de puntos y un algoritmo de alineamiento modifica-

do basado en el concepto de *Instancia-a-Clase* (I2C, por el término en inglés: *Instance-to-Class*) . La función de distancia resultante tiene en cuenta el ordenamiento temporal de las secuencias comparadas, no requiere aprendizaje de parámetros y es altamente tolerante al ruido y al desfasaje temporal. Además, mejora los resultados de métodos no-paramétricos de clasificación de secuencias, sobre todo en casos de alta variabilidad intra-clase y pocos datos de entrenamiento.

En el segundo enfoque, reconocemos que la cantidad de esqueletos discriminativos en una secuencia puede ser baja. Los esqueletos restantes pueden ser ruidosos, tener configuraciones comunes a varias acciones (por ejemplo, la configuración correspondiente a un esqueleto sentado e inmóvil) u ocurrir en instantes de tiempo poco comunes para la acción del video. Por lo tanto, el problema puede ser naturalmente encarado como uno de *Aprendizaje Multi Instancia* (MIL por el término en inglés *Multiple Instance Learning*). En MIL, las instancias de entrenamiento se organizan en conjuntos o *bags*. Cada bag de entrenamiento tiene asignada una etiqueta que indica la clase a la que pertenece. Un bag etiquetado con una determinada clase contiene instancias que son características de la clase, pero puede (y generalmente así ocurre) también contener instancias que no lo son. Siguiendo esta idea, representamos los videos como bags de descriptores de esqueleto con marcas de tiempo, y proponemos un framework basado en MIL para el reconocimiento de acciones. Nuestro enfoque resulta muy tolerante al ruido, la variabilidad intra-clase y la similaridad inter-clase. El framework propuesto es simple y provee un mecanismo claro para regular la tolerancia al ruido, a la poca alineación temporal y a la variación en las velocidades de ejecución.

Evaluamos los enfoques presentados en cuatro bases de datos públicas capturadas con cámaras de profundidad. En todos los casos, se trata de bases desafiantes. Los resultados muestran una comparación favorable de nuestras propuestas respecto al estado del arte.

Palabras clave: Video de profundidad, Aprendizaje Multi Instancia, Citation-kNN, Edit Distance on Real sequence, Instancia-a-Clase

Action recognition in depth videos

Abstract The problem of automatically identifying an action performed in a video is receiving a great deal of attention in the computer vision community, with applications ranging from people recognition to human computer interaction. We can think the human body as an articulated system of rigid segments connected by joints, and human motion as a continuous transformation of the spatial arrangement of those segments. The arrival of low-cost depth cameras has made possible the development of an accurate and efficient human body tracking algorithm, that computes the 3D location of several skeleton joints in real time. This thesis presents contributions concerning the modeling of the skeletons temporal evolution.

Modeling the temporal evolution of skeleton descriptors is a challenging task. First, the estimated location of the 3D joints are usually inaccurate. Second, human actions have large intra-class variability. This variability may be found not only in the spatial configuration of individual skeletons (for example, the same action involves different configurations for right-handed and left-handed people) but also on the action dynamics: different people have different execution speeds; actions with periodic movements (like clapping) may involve different numbers of repetitions; two videos of the same action may be temporally misaligned; etc. Finally, different actions may involve similar skeletal configurations, as well as similar movements, effectively yielding large inter-class similarity. We explore two approaches to the problem that aim at tackling this difficulties.

In the first approach, we present an extension to the *Edit Distance on Real sequence* (EDR), a robust and accurate similarity measure between time series. We introduce two key improvements to EDR: a weighted matching scheme for the points in the series and a modified aligning algorithm based on the concept of *Instance-to-Class* distance. The resulting distance function takes into account temporal ordering, requires no learning of parameters and is highly tolerant to noise and temporal misalignment. Furthermore,

it improves the results of non-parametric sequence classification methods, specially in cases of large intra-class variability and small training sets.

In the second approach, we explicitly acknowledge that the number of discriminative skeletons in a sequence might be low. The rest of the skeletons might be noisy or too person-specific, have a configuration common to several actions (for example, a *sit still* configuration), or occur at uncommon frames. Thus, the problem can be naturally treated as a Multiple Instance Learning (MIL) problem. In MIL, training instances are organized into bags. A bag from a given class contains some instances that are characteristic of that class, but might (and most probably will) contain instances that are not. Following this idea, we represent videos as bags of time-stamped skeleton descriptors, and we propose a new MIL framework for action recognition from skeleton sequences. We found that our approach is highly tolerant to noise, intra-class variability and inter-class similarity. The proposed framework is simple and provides a clear way of regulating tolerance to noise, temporal misalignment and variations in execution speed.

We evaluate the proposed approaches on four publicly available challenging datasets captured by depth cameras, and we show that they compare favorably against other state-of-the-art methods.

Keywords: Depth video, Multiple Instance Learning, Citation-kNN, Edit Distance on Real sequence, Instance-to-Class

Contents

1 Introduction **16**

1.1 Problem description 17

1.1.1 Action recognition in depth videos 18

1.2 Contributions 22

1.3 Publications 23

1.4 Organization of the thesis 25

1 Introducción **26**

1.1 Descripción del problema 27

1.1.1 Reconocimiento de acciones en videos de profundidad 29

1.2 Contribuciones 33

1.3 Publicaciones 34

1.4 Organización de la tesis 36

2 Prior works and datasets **37**

2.1 Related Work 37

2.1.1 Skeleton-based action recognition review 37

2.2 Datasets 43

2.2.1 MSRDailyActivity3D dataset 44

2.2.2 MSRAction3D dataset 45

2.2.3 UTKinect dataset 46

2.2.4 Florence3D dataset 48

2.3 Resumen 49

3 Action recognition using Instance-to-Class Edit Distance on Real sequence **50**
3.1 Introduction . . . 50
3.2 Recognizing actions using Instance-to-Class Edit Distance on Real sequence . . . 53
3.2.1 Comparing time series . . . 54
3.2.2 A new time series similarity measure . . . 62
3.2.3 Action recognition with I2CEDR . . . 74
3.3 Results . . . 80
3.3.1 Evaluation of the proposed EDR extensions . . . 80
3.3.2 Comparison of the proposed EDR extensions with other elastic matching similarity measures . . . 82
3.3.3 Robustness analysis . . . 84
3.3.4 Comparison with the state-of-the-art . . . 87
3.4 Resumen . . . 89

4 Action recognition using Citation-kNN on bags of time-stamped poses **91**
4.1 Introduction . . . 91
4.2 Recognizing actions with Citation-kNN on bags of time-stamped poses . . . 93
4.2.1 Multiple Instance Learning . . . 93
4.2.2 Citation-kNN . . . 94
4.2.3 Modified Citation-kNN . . . 98
4.2.4 Citation-kNN on bags of time-stamped poses . . . 99
4.3 Results . . . 111
4.3.1 Parameter selection . . . 111
4.3.2 Parameter influence . . . 112
4.3.3 Evaluation of the main components of the action recognition procedure . . . 116
4.3.4 Robustness analysis . . . 118
4.3.5 Comparation with the state-of-the-art . . . 123
4.4 Resumen . . . 125

5 Conclusions and perspective **127**

5 Conclusiones y perspectiva **130**

Bibliography **133**

List of Figures

1.1 Four examples of the challenges involved in RGB-based action recognition. Figures 1.1a and 1.1b show frames of videos that have quite different appearance despite being instances of the same action. Figures 1.1c and 1.1d show frames of videos that have similar appearance even though they correspond to different actions. See text for details. 19

1.2 RGB (1.2a) and depth (1.2b) sequences for an instance of the *cheer up* action. 19

1.3 Two widely used depth devices: Microsoft Kinect (1.3a) and Asus Xtion PRO LIVE (1.3b). 20

1.4 Joints tracked by Kinect. 21

1.1 Cuatro ejemplos de los desafíos involucrados en el reconocimiento de acciones basado en RGB. Las figuras 1.1a y 1.1b muestran frames de videos que tienen apariencia considerablemente diferente a pesar de ser instancias de la misma acción. Las figuras 1.1c y 1.1d muestran frames de videos que tienen apariencia similar pese a que corresponden a acciones diferentes. Ver el texto para más detalles. 29

1.2 Secuencias de frames RGB (1.2a) y de profundidad (1.2b) para una instancia de la acción *cheer up*. 30

1.3 Dos sensores de profundidad ampliamente utilizados: Microsoft Kinect (1.3a) y Asus Xtion PRO LIVE (1.3b). 30

1.4 Articulaciones localizadas por Kinect. 31

2.1 Example RGB frames of the MSRDailyActivity3D dataset. . . 45
2.2 Example depth frames of the MSRAction3D dataset. 46
2.3 Example frames of the UTKinect dataset. 47
2.4 Example frames of the Florence3D dataset. 48

3.1 A schematic example of a warping path. 56
3.2 A schematic example of a trace. 60
3.3 A schematic example of an extended trace. 68
3.4 Traces and EDRS distances between a query sequence A and two training sequences C_1^1 (3.4a) and C_2^1 (3.4b). The computed distances are larger than expected. See text for description. . . 70
3.5 Traces and EDRS distances between a query sequence A and two training sequences C_1^2 (3.5a) and C_2^2 (3.5b). See text for description. 71
3.6 Extended traces and I2CEDR distances between a query sequence A and two sets of training sequences C^1 and C^2. See text for description. 72
3.7 Evaluation of the proposed EDR extensions. The original EDR distance is referred to as *Hard*, while *Soft* and *I2C* denote EDRS and I2CEDR respectively. The term *I2C-P* denotes the use of I2CEDR combined with the multi-part approach. See text for details. 81
3.8 Comparison of I2CEDR with other elastic matching similarity measures. The presented functions EDRS (referred as *EDR Soft*) and I2CEDR (referred as *I2C-EDR*) are compared with four other measures: Frechet, Dynamic Time Warping (*DTW*), Instance-to-Class Frechet (*I2C-Frechet*) and Instance-to-Class Dynamic Time Warping (*I2C-DTW*). See text for details. 83
3.9 Relationship between the relative accuracy and the noise standard variation for several methods on two datasets: MSRDailyActivity3D (3.9a) and UTKinect (3.9b). 85

3.10 Relationship between the relative accuracy and the temporal misalignment for several methods on two datasets: MSRDailyActivity3D (3.10a) and UTKinect (3.10b). 86

4.1 The traditional kNN method for combining neighbors labels to obtain the label of a query is not directly applicable to the MIL setting. The figure illustrates how false positive instances contained in positive bags attract negative bags. For example, given $\{P_1, P_2, N_1\}$ as training bags, N_2 will be classified as positive when the minimal Hausdorff distance is used. 97

4.2 Illustration of the Hausdorff distance between two bags of skeleton descriptors, corresponding to the actions *cheer up* and *drink*. Figure 4.2a describes the directed Hausdorff distance from the *cheer up* bag to the *drink* bag. Figure 4.2b describes the distances for the directed Hausdorff distance from the *drink* bag to the *cheer up* bag. Each descriptor in the source bag is linked by an arrow to its nearest neighbor in the target bag. The distance to such nearest neighbor is indicated both by the color of the arrow (following the color scale shown on the right side) and by the number next to the arrow. See text for details. 103

4.3 Illustration of the Hausdorff distance between a query bag and two training bags of skeleton descriptors. The query bag corresponds to the action *sit down*. Training bags are labeled with the actions *sit down* and *stand up*. Figure 4.3a describes the directed Hausdorff distance from the *stand up* bag to the query bag. Figure 4.3b describes the directed Hausdorff distance from the *sit down* training bag to the query bag. Temporal order is not considered. Descriptors in the source bag are linked by an arrow to their nearest neighbors in the target bag. The distance to such nearest neighbor is indicated both by the color of the arrow (following the color scale shown on the right side) and by the number next to the arrow. See text for details. 104

4.4 Illustration of the Hausdorff distance between a query bag and two training bags of skeleton descriptors. The compared bags are the same as in Figure 4.3. Different from the scenario illustrated in that Figure, the example shown here takes into account temporal information. See text for details. 106

4.5 Illustration of the Hausdorff distance between a query bag and two training bags of skeleton descriptors. The query bag corresponds to the action *cheer up*. Training bags are labeled with the actions *cheer up* and *drink*. Figure 4.5a describes the directed Hausdorff distance from the *cheer up* bag to the query bag. Figure 4.5b describes the directed Hausdorff distance from the query bag to the *cheer up* training bag. One of the descriptors in the *cheer up* training bag is very noisy. Descriptors in the source bag are linked by an arrow to their nearest neighbors in the target bag. The distance to such nearest neighbor is indicated both by the color of the arrow (following the color scale shown on the right side) and by the number next to the arrow. See text for details. 108

4.6 Parameter influence for two of the four considered datasets. . 113

4.7 Parameter influence for two of the four considered datasets. . 114

4.8 Confusion matrices for the UTKinect dataset. Figure 4.8a shows the results obtained when time information is ignored. Figure 4.8b shows the results obtained when taking temporal information into account. 119
4.9 Confusion matrices for the MSRDailyActivity3D dataset. In Figure 4.9a time information is ignored, while in Figure 4.9b it is not. 120
4.10 Relationship between the relative accuracy and the noise standard variation for several methods on two datasets: MSRDailyActivity3D (4.10a) and UTKinect (4.10b). 122
4.11 Relationship between the relative accuracy and the temporal misalignment for several methods on two datasets: MSRDailyActivity3D (4.11a) and UTKinect (4.11b). 123

Chapter 1

Introduction

Action recognition is a growing topic in computer vision research. Generally speaking, it consists of identifying which of a predefined set of actions is performed in a given video. The problem is usually approached using machine learning techniques, that tend to deal robustly with the complexities found in real data.

Automatically identifying an action performed in a video can be a valuable tool in many applications. A common example is the analysis of surveillance videos [Cha02]. Many security systems are based on the the data captured by several cameras. When the number of cameras is large, it can be hard or even impossible for human controllers to manually detect important events in the videos.

Closely related is the use of video understanding techniques for the purpose of elderly and children care in indoor environments such as smart homes and smart hospitals [SS15]. Monitoring and automatically recognizing daily activities can be of great help for assisting the residents, as well as for describing their functional and health status. Yet another related application is automatic video summarization, that provides short videos using only the important scenes from the original video.

Another common example is content-based search in video databases [HXL+11]. The ability to automatically obtain textual data describing a video avoids the need for manual annotation, and can be crucial for the development of more useful and informative datasets.

Human-computer interaction is a further field that benefits from improvements in action recognition techniques. For example, such techniques can be used to provide interfaces for people with motion impairments, easing their interaction with computers or other people [ZHJR11]. Another common application is the development of video games that let the user interact with the console/computer without the need for a game controller [RKH11].

Behavior-based biometrics has also received much attention in the last years. Unlike classical biometrics (such as fingerprints-based), they obtain data for identification without interfering with the activity of the person. A typical example is gait recognition [SPL+05]. A related use concerns the automatic guidance of a patients movements in rehabilitation systems.

Therefore, new developments in action recognition methods, such as the ones presented in this work, can be of great interest for a wide range of applications.

1.1 Problem description

This thesis focus on the problem of action recognition from depth videos. In this section, we give a general introduction to the problem and we clarify several aspects about it. Specifically, we make explicit what we understand by *action recognition*, and describe how the problem changes depending on the type of video data employed. In doing so, we pay special attention to depth data, as this is the one used in this work.

Given a list of possible actions and a video showing an actor performing any one of them, the ultimate goal in the considered problem is to recognize the action being performed. To clarify the meaning of the termn *action*, the taxonomy defined in [MHK06] can be used. The work distinguishes between *action primitives* (or *movements*), *actions* and *activities*. Action primitives are atomic motions, and can be considered as the building blocks of actions. Activities in turn are made up of several actions. As an example, *cooking* can be thought of as an activity, involving several actions such as *chopping* and *stirring*. *Chopping* can in turn be decomposed in several action

primitives, such as *taking a knife* and *cutting a vegetable*. The actions considered in the thesis can be thought of as belonging to the action primitive category. Note, however, that the granularity of the primitives may vary depending on the application, and some of the actions considered in this work can be very well seen as simple exemplars of the *action* category.

A large number of works have been proposed for action recognition from RGB videos. This type of video data poses several challenges. On the one hand, the appearance of an action can vary considerably in different videos. This may be due to changes in lighting conditions, occlusions, viewpoint, actor's clothing, execution style, etc. Figures 1.1a and 1.1b show examples of videos that have quite different appearance despite being instances of the same action. The former corresponds to the action *play game* and the latter to the action *use vacuum cleaner*. On the other hand, different actions can look very similar to each other. This is illustrated in Figure 1.1c, that compares frames from the actions *drink* and *call cellphone*. Another example of this phenomena can be seen in Figure 1.1d, that shows frames from the actions *read* and *write*.

The difficulties mentioned above have been partially mitigated with the arrival of low cost depth sensors. Section 1.1.1 introduces some of the technologies used for depth sensing, and explain their advantages over traditional RGB videos. In particular, it highlights the possibility of inferring an actor's pose based on depth information, which is crucial for the methods presented in the thesis.

1.1.1 Action recognition in depth videos

The advent of low cost depth sensors opened up new options to address classical difficulties in action recognition. Typical depth sensors consist of an infrared laser projector and an infrared camera. Combined, the camera and the projector can be used to create a *depth map*, which encodes distance information between the objects in the scene and the camera. Most of the devices are also coupled with an RGB camera. Figure 1.2 shows three different RGB frames and their associated depth maps. Frames were extracted

(a) (b)

(c) (d)

Figure 1.1: Four examples of the challenges involved in RGB-based action recognition. Figures 1.1a and 1.1b show frames of videos that have quite different appearance despite being instances of the same action. Figures 1.1c and 1.1d show frames of videos that have similar appearance even though they correspond to different actions. See text for details.

from a video corresponding to the *cheer up* action.

An example of this kind of technologies is the Microsoft Kinect. It calculates depth images at 320 × 240 or 640 × 480 resolution and at 30 frames per second. See Figure 1.3a for a visual description of the device. Another widely used sensor is the Asus Xtion PRO LIVE, that offers either 60 320 × 240 depth frames per second or 30 640 × 480 depth frames per second. The device is depicted in Figure 1.3b.

Many of the problems faced by RGB-based action recognitions methods

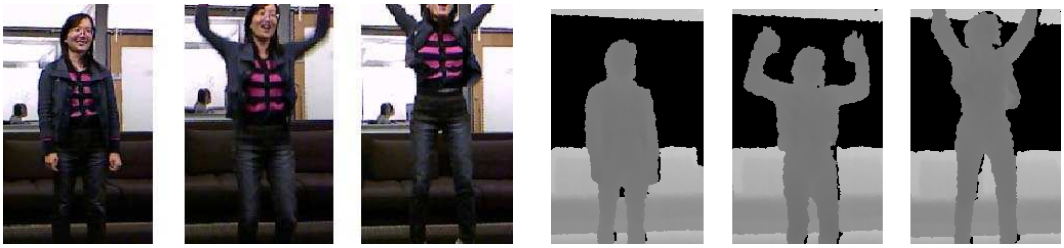

(a) (b)

Figure 1.2: RGB (1.2a) and depth (1.2b) sequences for an instance of the *cheer up* action.

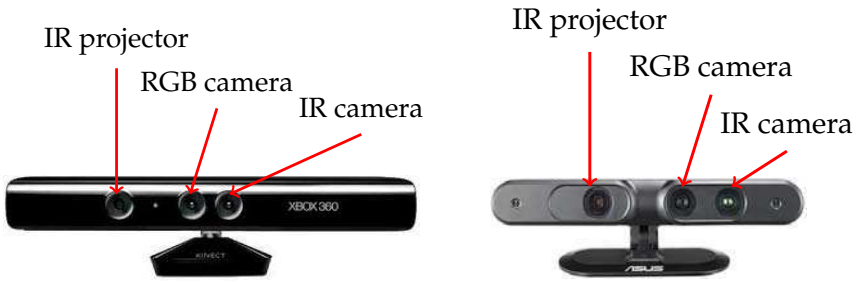

(a) (b)

Figure 1.3: Two widely used depth devices: Microsoft Kinect (1.3a) and Asus Xtion PRO LIVE (1.3b).

are eased when working with depth videos. Such videos are less affected by environmental conditions than conventional RGB data. More importantly, they provide additional information that makes 3D reconstruction possible. In particular, an accurate estimation of a person's pose can be computed from depth information, including the location of several skeleton joints at each frame of a video. The temporal evolution of the human skeleton across a video is a valuable tool for interpreting the action being performed. The action recognition methods presented in this thesis are fully based on such skeleton information. Therefore, in the following we describe how it can be extracted from the raw depth data. Furthermore, we explain the specific challenges involved in skeleton-based action recognition.

Skeleton-based action recognition

The current standard method for skeleton estimation from depth data is presented in the work of Shotton et al. [SSK+13]. The method labels each pixel in a depth image as being either part of the human body, the background, or unknown, and predicts the 3D position of several body joints (hand, wrist, elbow, etc.). A description of the localized joints is shown in Fig. 1.4. Note that a skeleton can be thought of as a tree. For example, the hip center can be seen as the root with 3 subtrees, corresponding to the left leg, the right leg and the upper body.

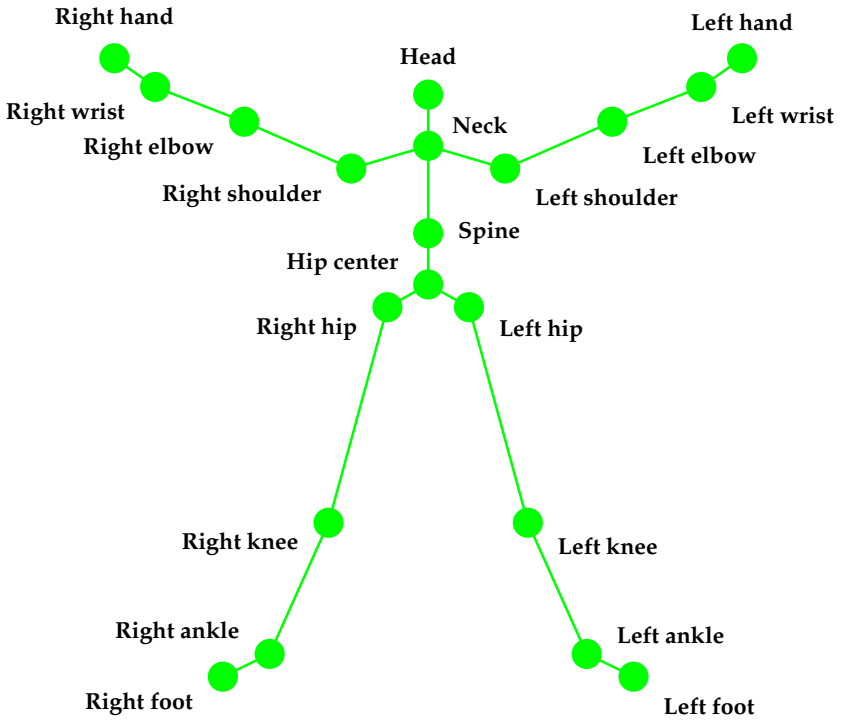

Figure 1.4: Joints tracked by Kinect.

Most of the public datasets for action recognition from depth videos provide skeleton data. In the vast majority of the cases (including the datasets used for the experiments in this thesis, described in Section 2.2), skeleton information was obtained using the Microsoft Kinect tracking system built on top of the work in [SSK+13].

While skeleton data provides useful information for action recognition, it also poses new challenges. Moreover, it is far from eradicating many of the inherent difficulties of the problem. Previous work in skeleton-based action recognition has focused mainly in two issues. The first one is the design of suitable spatio-temporal skeleton descriptors and proper distance functions for comparing them. The second one is the modeling of their temporal evolution. The rest of the thesis focuses mainly on this second task.

Modeling the temporal evolution of skeleton descriptors is challenging. First, 3D joints estimated from the detph image are usually inaccurate, due to the noise present in the depth image. Second, human actions present large intra-class variability. This variability may be found not only in the spatial configuration of individual skeletons (for example, the same action

would involve different configurations for right and left handed people) but also on the action dynamics: different people would probably have different execution speeds; the number of repetitions may change in actions involving periodic movements (like *waving*); temporal misalignment may exist between videos of the same action; etc. Finally, different actions may involve similar skeletal configurations, as well as similar movements, effectively yielding large inter-class similarity.

This work focuses on skeleton-based action recognition. Therefore, the rest of the thesis considers an action execution as represented by a sequence of skeletons, encoding the temporal evolution of the actor's pose, and proposes a new machine learning techniques that aim at overcoming the problems commented in the previous paragraph.

1.2 Contributions

In this thesis we present two novel methods for skeleton-based action recognition. The goal of the presented methods is to predict the action label of a query skeleton sequence, based on previously labeled training sequences.

The first method is strongly based in a new distance function between time series. We call such distance *Instance-to-Class Edit Distance on Real sequence* (I2CEDR). The proposed distance can be seen as belonging to a group of techniques that measure the similarity between two sequences of points by finding optimal alignments between the points, according to a chosen cost function. The novel I2CEDR is obtained as the result of two key changes to one of such techniques, known as Edit Distance on Real sequence (EDR) [CÖO05]. First, a soft cost mechanism is introduced for aligning the points. Second, the notion of *Instance-to-Class* (I2C) [BSI08] distance is incorporated into the function. The first change aims at making EDR a more accurate measure, by allowing small differences between aligned points to be taken into account. The second change aims at improving the results of non-parametric [BSI08] sequence classification methods based on EDR, specially in cases of large intra-class variability and small training sets. The proposed measure takes into account temporal ordering and requires no

learning of parameters. An efficient dynamic programming algorithm is presented for computing I2CEDR. Our method shows considerable robustness to noise and temporal misalignment. Thorough experiments on four popular datasets support the superiority of our approach over other methods using distance functions based on sequence alignment. Further, when coupled with a robust skeleton descriptor, the performance of our approach is comparable to the state-of-the-art.

The second method proposes a novel Multiple Instance Learning (MIL) [FF10] approach to the problem. A new representation for skeleton sequences is described, that allows for effective sequence classification using a classic and simple MIL technique [WZ00] known as Citation-kNN. This technique adapts the k-Nearest Neighbors (kNN) approach to the multiple instance setting. We introduce three changes to the standard Citation-kNN formulation. First, we present a natural extension to multi-class classification. Second, we adjust the neighbor voting mechanism by incorporating distance-weighted votes. Third, we adapt it to work on videos represented by multiple sequences, each corresponding to the temporal evolution of a different body part. We experimentally validate the benefits of the proposed representation for skeleton sequences and the improvements brought by the modified Citation-kNN. Extensive tests show that the proposed method is very tolerant to noise and temporal misalignment. Further, the role played by the different parameters is exposed. Results show that the combination of a reasonably robust skeleton descriptor with our approach for sequence representation and classification leads to state-of-the-art results. Despite the simplicity of the method, highly competitive results are achieved in four popular datasets. We believe this supports the appropriateness of the MIL approach to the problem, and opens the door to further research in that direction.

1.3 Publications

The development of this thesis has lead to several works. Some of them have already been published, while others are submitted or to be submitted.

Journal Papers:

- Sebastián Ubalde, Norberto Goussies and Marta Mejail, *Efficient Descriptor Tree Growing For Fast Action Recognition*. Pattern Recognition Letters, 0167-8655, 2013.

- Norberto A. Goussies, Sebastián Ubalde and Marta Mejail, *Transfer Learning Decision Forests for Gesture Recognition*. Journal of Machine Learning Research, 15:3667-3690, 2014.

Peer-reviewed Conference Papers:

- Sebastián Ubalde and Norberto A. Goussies, *Fast Non-Parametric Action Recognition*. Proceedings of the 17th Iberoamerican Congress on Pattern Recognition, CIARP 2012, Buenos Aires, Argentina, Septiembre 3-6, 2012. Proceedings. Lecture Notes in Computer Science 7441 Springer 2012.

- Sebastián Ubalde, Zicheng Liu and Marta Mejail, *Detecting Subtle Object Interactions Using Kinect*. Proceedings of the 19th Iberoamerican Congress on Pattern Recognition, CIARP 2014, Puerto Vallarta, Mexico, Noviembre 2-4. Lecture Notes in Computer Science 8827, 770-777, Springer, 2014.

- Norberto Goussies, Sebastián Ubalde, Francisco Gómez Fernández and Marta Mejail, *Optical Character Recognition Using Transfer Learning Decision Forests*. IEEE International Conference on Image Processing, ICIP 2014, 309-4313, IEEE, 2014.

Submitted:

- Sebastián Ubalde, Francisco Gómez Fernández and Marta Mejail, *Skeleton-based Action Recognition Using Citation-kNN on Bags of Time-stamped Pose Descriptors*. IEEE International Conference on Image Processing, ICIP 2016.

To be submitted:

- Sebastián Ubalde and Marta Mejail,*Skeleton-based Action Recognition Using Instance-to-Class Edit Distance on Real sequence*. IEEE International Conference on Pattern Recognition, ICPR 2016.

1.4 Organization of the thesis

This thesis is organized as follows. We discuss previous works and describe the datasets used in the experiments in Chapter 2. The first novel method presented in the thesis is explained in Chapter 3. The second main contribution is introduced in Chapter 4. Both chapters 3 and 4 include thorough experiments for the proposed methods. Finally, Chapter 5 concludes and comments on future work.

Capítulo 1

Introducción

El reconocimiento de acciones es un tema de creciente interés en el campo de la visión por computadora. En términos generales, consiste en identificar cuál de un conjunto predefinido de acciones es ejecutada en un video dado. El problema es generalmente encarado usando técnicas de aprendizaje automático (o *machine learning*), que tienden a lidiar de manera robusta con las complejidades típicas de los datos de la realidad.

La identificación automática de la acción ejecutada en un video puede ser una herramienta valiosa para muchas aplicaciones. Un ejemplo común es el análisis de videos de vigilancia [Cha02]. Muchos sistemas de seguridad se basan en los datos capturados por varias cámaras. Cuando el número de cámaras es grande, puede ser difícil, o incluso imposible, detectar manualmente eventos importantes en los videos.

Una aplicación muy relacionada a la anterior es el uso de técnicas de comprensión de videos para el cuidado de ancianos y niños en predios cerrados como las casas y los hospitales inteligentes [SS15]. El monitoreo y el reconocimiento automático de actividades diarias puede ser de gran ayuda en la asistencia de los residentes, así como en la obtención de informes acerca de sus capacidades funcionales y su salud. Otra aplicación relacionada es el resumen automático de videos, que intenta obtener videos cortos a partir de las escenas importantes del video original.

Otro ejemplo común es la búsqueda basada en contenido en bases de datos de videos [HXL+11]. La habilidad de obtener de manera automática

descripciones textuales de un video dado evita la necesidad de realizar anotaciones manuales, y puede ser crucial para el desarrollo de bases de datos más útiles e informativas.

La interacción humano-computadora es otro campo de aplicación que se beneficia de las mejoras en las técnicas de reconocimiento de acciones. Por ejemplo, dichas técnicas pueden ser usadas para proveer interfaces para personas con movilidad reducida, facilitando su interacción con computadoras y con otras personas [ZHJR11]. Otro ejemplo es el desarrollo de video juegos que permiten que el usuario interactúe con la consola/computadora sin la necesidad de usar un dispositivo físico [RKH11].

La biometría basada en comportamiento ha recibido también mucha atención en los últimos años. A diferencia de las herramientas biométricas clásicas (como las huellas digitales), las técnicas basadas en comportamiento obtienen datos para identificación sin interferir con la actividad de la persona. Un ejemplo típico es la identificación a partir del modo de andar de las personas [SPL+05]. Un uso relacionado es el desarrollo de herramientas que guíen de manera automática a pacientes en rehabilitación por problemas motrices.

En resumen, nuevos desarrollos en métodos de reconocimiento de acciones, como los presentados en este trabajo, pueden ser de gran interés para una amplia gama de aplicaciones.

1.1 Descripción del problema

Esta tesis se enfoca en el problema del reconocimiento de acciones en videos de profundidad. En esta sección damos una introducción general al problema y clarificamos varios aspectos del mismo. Más específicamente, hacemos explícito qué entendemos por *reconocimiento de acciones*, y describimos cómo el problema cambia dependiendo del tipo de datos de video considerado. Prestamos especial atención a la descripción de los datos de profundidad, que son los utilizados en este trabajo.

Dada una lista de posibles acciones y un video en el que se muestra a un actor llevando a cabo una de ellas, el objetivo del problema considerado es

reconocer la acción siendo ejecutada. Para aclarar el significado del término *acción*, se puede utilizar la taxonomía definida en [MHK06]. Dicho trabajo distingue entre *acciones primitivas* (o *movimientos*), *acciones* y *actividades*. Las acciones primitivas son movimientos atómicos, y pueden ser considerados como las piezas básicas con las que se "construyen" las acciones. Las actividades, por su parte, están constituidas por varias acciones. Por ejemplo, *cocinar* puede ser interpretada como una actividad que involucra varias acciones como *cortar* y *revolver*. A su vez, *cortar* puede descomponerse in varias acciones primitivas, como *agarrar un cuchillo* y *cortar un vegetal*. Las acciones consideradas en la tesis pueden pensarse como pertenecientes a la categoría de *acción primitiva*. No obstante, es importante tener en cuenta que la granularidad de las acciones primitivas puede variar dependiendo de la aplicación, y alguna de las acciones consideradas en este trabajo pueden ser vistas como ejemplares sencillos de la categoría *acción*.

Un gran número de trabajos ha sido propuesto para reconocimiento de acciones a partir de videos RGB. Este tipo de datos de video plantea varios desafíos. Por un lado, la apariencia de una acción puede variar considerablemente en diferentes videos. Esto puede deberse a cambios en la iluminación, oclusiones, ubicación de la cámara, indumentaria, estilo de ejecución, etc. Las figuras 1.1a and 1.1b muestran ejemplos de videos que tienen apariencia muy diferente pese a mostrar instancias de la misma acción. El primero corresponde a la acción *jugar videojuego* y el segundo a la acción *usar aspiradora*. Por otro lado, acciones diferentes pueden verse muy similares entre sí. Esto se ilustra en la figura 1.1c, que compara frames de las acciones *tomar* y *llamar por teléfono*. Otro ejemplo puede verse en la figura 1.1d, que muestra frames para las acciones *leer* y *escribir*.

Las dificultades mencionadas más arriba han sido parcialmente mitigadas con la llegada de sensores de profundidad de bajo costo. La sección 1.1.1 comenta algunas de las tecnologías usadas para sensado de profundidad y explica sus ventajas sobre los videos RGB tradicionales. En particular, resalta la posibilidad de inferir la pose de un actor a partir de la información de profundidad, lo cual es crucial para los métodos presentados en esta tesis.

(a) (b)

(c) (d)

Figura 1.1: Cuatro ejemplos de los desafíos involucrados en el reconocimiento de acciones basado en RGB. Las figuras 1.1a y 1.1b muestran frames de videos que tienen apariencia considerablemente diferente a pesar de ser instancias de la misma acción. Las figuras 1.1c y 1.1d muestran frames de videos que tienen apariencia similar pese a que corresponden a acciones diferentes. Ver el texto para más detalles.

1.1.1 Reconocimiento de acciones en videos de profundidad

El advenimiento de sensores de profundidad de bajo costo abrió nuevas opciones para encarar algunas dificultades clásicas del problema de reconocimiento de acciones. Un sensor de profundidad típico consiste en un proyector de laser infrarrojo y una cámara infrarroja. Combinados, la cámara y el proyector pueden usarse para crear un *mapa de profundidad*, que codifica la información de distancia entre los objetos en la escena y la cámara. La mayoría de los dispositivos están equipados también con una cámara RGB. La figura 1.2 muestra tres frames RGB diferentes y sus mapas de profundidad asociados. Los frames fueron extraídos de un video correspondiente a la acción *alentar*.

Un ejemplo de este tipo de tecnologías es Microsoft Kinect. El dispositivo calcula imágenes de profundidad con una resolución de 320×240 o 640×480 a 30 frames por segundo. La figura 1.3a muestra una descripción del mismo. Otro ejemplo es Asus Xtion PRO LIVE, que ofrece 60 frames de 320×240 por segundo, o 30 frames de 640×480 por segundo. El dispositivo

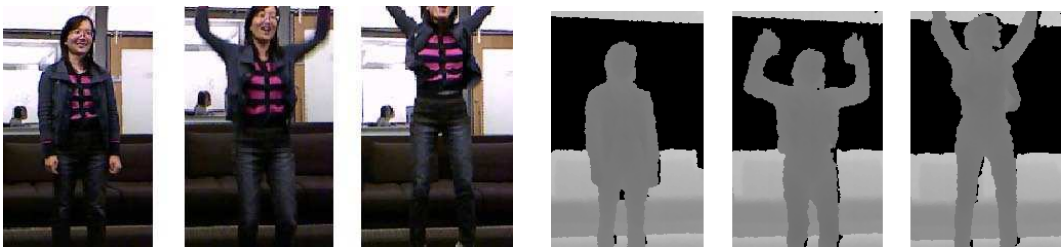

(a) (b)

Figura 1.2: Secuencias de frames RGB (1.2a) y de profundidad (1.2b) para una instancia de la acción *cheer up*.

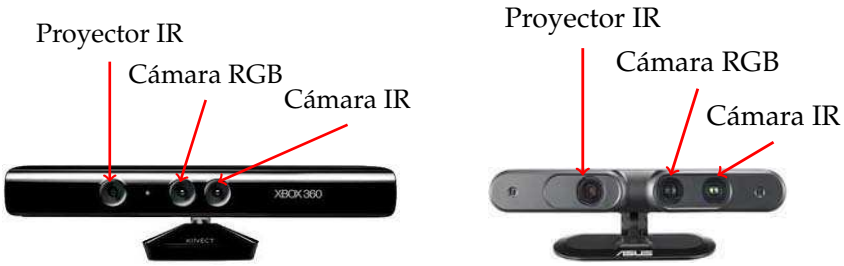

(a) (b)

Figura 1.3: Dos sensores de profundidad ampliamente utilizados: Microsoft Kinect (1.3a) y Asus Xtion PRO LIVE (1.3b).

puede verse en la figura 1.3b.

Muchos de los problemas enfrentados por métodos de reconocimiento de acciones en videos RGB son simplificados al trabajar con videos de profundidad. Dichos videos son menos afectados por las condiciones del entorno que los videos RGB convencionales. Más importante aún, proveen información adicional que hace posible realizar reconstrucciones 3D. En particular, es posible estimar con precisión la pose de una persona a partir de los datos de profundidad, incluyendo la ubicación de varias articulaciones del esqueleto humano en cada frame de un video. La evolución temporal del esqueleto humano a lo largo de un video es una herramienta valiosa para interpretar la acción ejecutada. Los métodos de reconocimiento de acciones presentados en esta tesis están basados en su totalidad en dicha información del esqueleto. Por lo tanto, a continuación describimos cómo puede ser

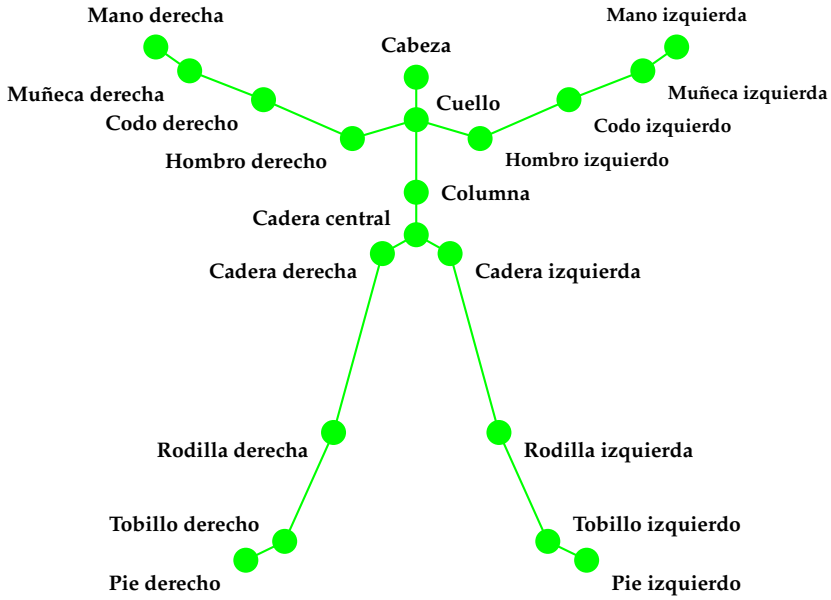

Figura 1.4: Articulaciones localizadas por Kinect.

extraída a partir de los datos de profundidad en bruto. Además, explicamos los desafíos específicos involucrados en el reconocimiento de acciones basado en esqueletos.

Reconocimiento de acciones basado en esqueletos

Actualmente, el método estándar para estimar esqueletos a partir de los datos de profundidad es el presentado en el trabajo de Shotton et al. [SSK+13]. El método etiqueta cada pixel en la imagen de profundidad como correspondiente al cuerpo humano, al fondo, o como indefinido. A partir de ese etiquetado, predice la posición 3D de varias articulaciones del cuerpo humano (manos, muñecas, codos, etc.). Una descripción de las articulaciones localizadas se muestra en la figura 1.4. Nótese que un esqueleto puede pensarse como un árbol. Por ejemplo, el centro de la cadera puede ser visto como la raíz de un árbol con 3 subárboles, correspondientes a las piernas izquierda y derecha, y a la parte superior del cuerpo.

La mayoría de las bases de datos públicas para reconocimiento de acciones en videos de profundidad proveen información de esqueleto. En la gran mayoría de los casos (incluyendo las bases de datos usadas para los experimentos de esta tesis, descriptos en la sección 2.2), la información de

esqueleto se obtuvo usando el sistema de seguimiento de Microsoft Kinect, desarrollado a partir del trabajo en [SSK+13]

Si bien la información de esqueleto es útil para el reconocimiento de acciones, también plantea nuevos desafíos. Además, su uso no altera muchas de las dificultades inherentes al problema. Los trabajos anteriores en reconocimiento de acciones basado en esqueletos se han enfocado principalmente en dos aspectos. El primero el diseño de descriptores de esqueleto adecuados, y de funciones para compararlos de manera efectiva. El segundo es el modelado de la evolución temporal de dichos descriptores. El resto de la tesis se enfoca principalmente en el segundo aspecto.

El modelado de la evolución temporal de descriptores de esqueleto es una tarea desafiante. En primer lugar, las ubicaciones 3D de las articulaciones estimadas a partir de imágenes de profundidad suelen ser imprecisas, debido al ruido encontrado en la imagen de profundidad. En segundo lugar, las acciones humanas presentan alta variabilidad intra-clase. Dicha variabilidad puede encontrarse no sólo en la configuración espacial de cada esqueleto (por ejemplo, la misma acción involucra diferentes configuraciones dependiendo de la mano hábil de la persona), sino también en la dinámica de la acción: diferentes personas probablemente tengan diferentes velocidades de ejecución; el número de repeticiones puede cambiar en acciones que involucran movimientos periódicos (como *agitar los brazos*); diferentes videos de la misma acción pueden estar desfasados temporalmente; etc. Por último, acciones diferentes pueden parecerse tanto en términos de configuraciones de esqueleto como de movimientos, generando alta similaridad inter-clase.

Este trabajo se enfoca en el reconocimiento de acciones basado en esqueletos. Por lo tanto, el resto de la tesis considera que la ejecución de una acción está representada por una secuencia de esqueletos, que codifica la evolución temporal de la pose del actor. Con dicha representación en mente, presenta nuevas técnicas de aprendizaje automático que apuntan a superar los problemas comentados en el párrafo anterior.

1.2 Contribuciones

En esta tesis presentamos dos métodos novedosos para el reconocimiento de acciones basado en esqueletos. El objetivo de dichos métodos es predecir la etiqueta de una secuencia de esqueletos dada, a partir de secuencias de entrenamiento etiquetadas. La etiqueta, en nuestro caso, indica la acción ejecutada en la secuencia.

El primer método esta fuertemente basado en una nueva función de distancia entre series temporales. Llamamos *Instance-to-Class Edit Distance on Real sequence* (I2CEDR) a dicha función. La misma puede pensarse como perteneciente a un grupo de técnicas que mide la similaridad entre dos secuencias de puntos a través del cálculo de un alineamiento óptimo entre los puntos, de acuerdo a una determinada función de costo. La novedosa I2CEDR se obtiene como resultado de dos cambios clave a una de las técnicas del mencionado grupo, conocida como *Edit Distance on Real sequence* (EDR) [CÖO05]. Por un lado, una función de costo *suave* es propuesta para el alineamiento de puntos. Por otro, la noción de *Instancia-a-Clase* (I2C, por el término en inglés *Instance-to-Class*) es incorporada al cálculo de la distancia. El primer cambio apunta a hacer de EDR una medida más precisa, permitiendo que pequeñas diferencias entre los puntos alineados sean tenidas en cuenta. El segundo busca mejorar los resultados de métodos de clasificación de secuencias no-paramétricos [BSI08], sobre todo en casos de alta variabilidad intra-clase y pocos datos de entrenamiento. La medida propuesta tiene en cuenta el ordenamiento temporal entre los puntos alineados, y no requiere aprender parámetros. Un algoritmo de programación dinámica eficiente es presentado para computar I2CEDR. Nuestro método muestra una robustez considerable frente al ruido y al desfasaje temporal. Los detallados experimentos en cuatro bases de datos frecuentemente utilizadas en la literatura avalan la superioridad de nuestro enfoque frente a otros métodos que utilizan funciones de distancia basadas en alineamiento de puntos. Además, cuando se lo usa en conjunto con descriptor de esqueleto robusto, el rendimiento de nuestro enfoque resulta comparable al estado del arte.

El segundo método propone un novedoso enfoque de *Aprendizaje Mul-*

ti Instancia (MIL por el término en inglés *Multiple Instance Learning*) [FF10] para el problema. Una nueva representación para secuencias de esqueleto es presentada. La misma permite clasificar secuencias de manera efectiva usando una técnica de MIL clásica y simple, conocida como Citation-kNN [WZ00]. Dicha técnica adapta el enfoque de *k vecinos más cercanos* (kNN por el término en inglés *k-nearest-neighbors*) al contexto de MIL. Proponemos tres cambios a la formulación estándar de Citation-kNN. Primero, presentamos una extensión natural a la clasificación multi-clase. Luego, ajustamos el mecanismo de voto de los vecinos más cercanos incorporando pesos de acuerdo a la distancia del vecino. Por último, adaptamos la técnica para trabajar sobre múltiples secuencias obtenidas a partir de la secuencia original a clasificar, lo cual permite emplear un enfoque multi-parte al trabajar con secuencias de esqueletos. Validamos experimentalmente tanto los beneficios de la representación presentada como las mejoras logradas mediante los cambios a Citation-kNN. Los detallados experimentos muestran que el método es muy tolerante al ruido y al desfasaje temporal. Además, permiten analizar el rol jugado por cada parámetro del método. Los resultados muestran que la combinación de un descriptor de esqueleto razonablemente robusto con nuestro enfoque para representar y clasificar secuencias permite obtener resultados comparables al estado del arte. A pesar de tratarse de un método simple, se obtienen resultados altamente competitivos en cuatro bases de datos frecuentemente utilizadas en la literatura. Creemos que esto avala la pertinencia del enfoque basado en MIL para el problema, y abre la puerta a nuevas investigaciones en esa dirección.

1.3 Publicaciones

El desarrollo de esta tesis ha dado lugar a varios trabajos. Algunos de ellos ya han sido publicados, mientras que otros han sido enviados o lo serán en un futuro cercano:

Revistas internacionales con arbitraje:

- Sebastián Ubalde, Norberto Goussies y Marta Mejail, *Efficient Descriptor Tree Growing For Fast Action Recognition*. Pattern Recognition Let-

ters, 0167-8655, 2013.

- Norberto A. Goussies, Sebastián Ubalde y Marta Mejail, *Transfer Learning Decision Forests for Gesture Recognition*. Journal of Machine Learning Research, 15:3667-3690, 2014.

Actas de conferencias de congresos internacionales con arbitraje:

- Sebastián Ubalde y Norberto A. Goussies, *Fast Non-Parametric Action Recognition*. Proceedings of the 17th Iberoamerican Congress on Pattern Recognition, CIARP 2012, Buenos Aires, Argentina, Septiembre 3-6, 2012. Proceedings. Lecture Notes in Computer Science 7441 Springer 2012.

- Sebastián Ubalde, Zicheng Liu y Marta Mejail, *Detecting Subtle Object Interactions Using Kinect*. Proceedings of the 19th Iberoamerican Congress on Pattern Recognition, CIARP 2014, Puerto Vallarta, Mexico, Noviembre 2-4. Lecture Notes in Computer Science 8827, 770-777, Springer, 2014.

- Norberto Goussies, Sebastián Ubalde, Francisco Gómez Fernández y Marta Mejail, *Optical Character Recognition Using Transfer Learning Decision Forests*. IEEE International Conference on Image Processing, ICIP 2014, 309-4313, IEEE, 2014.

Enviados:

- Sebastián Ubalde, Francisco Gómez Fernández y Marta Mejail, *Skeleton-based Action Recognition Using Citation-kNN on Bags of Time-stamped Pose Descriptors*. IEEE International Conference on Image Processing, ICIP 2016.

A ser enviados próximamente:

- Sebastián Ubalde y Marta Mejail,*Skeleton-based Action Recognition Using Instance-to-Class Edit Distance on Real sequence*. IEEE International Conference on Pattern Recognition, ICPR 2016.

1.4 Organización de la tesis

Esta tesis se organiza de la siguiente manera. En el capítulo 2 repasamos trabajo previo y describimos las bases de datos utilizadas en los experimentos. En el capítulo 3 explicamos el primer método presentado en la tesis. En el capítulo 4 presentamos la segunda contribución principal del trabajo. Tanto el capítulo 3 como el 4 incluyen experimentos detallados para los métodos propuestos. Por último, en el capítulo 5 transmitimos nuestras conclusiones y comentamos posibles opciones de trabajo futuro.

Chapter 2

Prior works and datasets

This chapter discusses related works and presents the datasets used to test our methods. Section 2.1 gives an overview of previous works on action recognition related to the methods presented in the thesis. Section 2.2 describes four public datasets used in the exeriments of sections 3.3 and 4.3.

2.1 Related Work

In this section we review state-of-the-art approaches for action recognition from depth videos. More precisely, the review covers skeleton-based methods, that predict the action performed in a video using only the sequence of skeletons estimated from the depth maps (see Section 1.1.1). Many methods [OL13, wan12, LZL10, LS13, YZT12] in the literature work directly on the raw depth map, without relying on skeleton information. Those methods are not considered in the review. Moreover, note that several works present hybrid solutions, that combine skeletal data with raw depth information. When describing such works, we focus on the skeleton-based aspects of their solutions. Finally, surveys on traditional action recognition from RGB data can be found in [WRB11, Pop10, MHK06].

2.1.1 Skeleton-based action recognition review

Previous work in skeleton-based action recognition has focused mainly in two issues. The first one is the design of suitable spatio-temporal skeleton

descriptors and proper distance functions for comparing them. The second one is the modeling of their temporal evolution. This section reviews common approaches to the problem, paying special attention to their contributions on both aspects.

The work in [YT12] presents a new skeleton descriptor that combines information about the static posture, the local motion and the overall motion of the actor. Variants of this descriptor have been used in several works since its introduction in [YT12]. To capture the static posture, the relative positions of the joints within the same skeleton are computed. To represent the motion information, the relative positions are computed between the skeleton and its temporal predecessor. Similarly, overall motion is described by calculating the relative positions between the skeleton and the first skeleton in the sequence. To deal with redundancy and noise, PCA is applied to the original descriptor. Classification of new sequences is achieved using the Naive-Bayes-Nearest-Neighbor (NBNN) method [BSI08], that avoids descriptor quantization and offers good generalization capabilities by considering Video-to-Class distance instead of the classical Video-to-Video distance. Further, informative skeleton selection is performed using the raw depth information.

Seidenari et al. [SVB+13] describe skeletons using four kinematic chains. The torso joints are considered as composing a single rigid part. Such part serves as the root of the four chains. The rest of the joints are organized into first (those adjacent to the torso) and second degree (those connected to the torso trough a first degree joint) joints. The first degree joints are expressed in a coordinate system relative to the torso, while the second degree joints are expressed in a coordinate system relative to its parent joint. In both cases, Cartesian coordinates are used to avoid the gimbal lock problem. Similar to [YT12], the NBNN method is used for classification. In this case, however, an extra feature is added to the skeleton descriptors to account for temporal information. Further, several NBNN classifiers are combined to independently align different body parts.

Wang et al. [WLWY12a] use the (static) relative position of the joints presented in [YT12] as the skeleton descriptor, and present the *Fourier Tempo-*

ral Pyramid (FTP) to capture the temporal structure of the action. To mitigate the effect of noisy data and temporal misalignment, FTPs compute the evolution of the low-frequency Fourier coefficients along the video, using a pyramid structure inspired by [LSP06]. Given a set of joints, the notion of *actionlet* is defined as the concatenation of the FTP for each joint in the set. A data mining method is proposed to select discriminative actionlets. Further, a Multiple Kernel Learning (MKL) approach is used to combine the discriminative power of the mined actionlets.

Gowayyed et al. [GTHES13] describe the trajectory of each joint using Histograms of Oriented Displacements (HOD). Specifically, for each pair of consecutive joint positions, the length and orientation angle of the associated displacement vector are calculated. The length of the vector is added to the corresponding bin in an histogram of orientation angles. To capture global temporal information, histograms are organized into a pyramid, similar to the one considered in [WLWY12a]. The final descriptor is obtained by concatenating the pyramids of each joint. The proposed representation is speed invariant, and is fast to compute.

The work in [LN06] uses the 3D joint positions as skeleton descriptors, and model temporal dynamics using Continuous Hidden Markov Models (CHMM). They observe that low accuracy can be obtained when a single descriptor (i.e. the coordinates of each of the joints) is used to represent a skeleton. Therefore, they consider instead several lower-dimensional descriptors, each corresponding to a single joint or a combination of related joints. The motion model of each lower-dimensional descriptor is learned with a separate CHMM. Each trained CHMM is considered a weak classifier, that nevertheless has reasonably good performance and different discriminative power for different actions. Because of that, the authors combine them using AdaBoost [FS97] to obtain a stronger classifier.

Xia et al. [XCA12] introduce a new skeleton descriptor and use k-means clustering to represent each skeleton by a *posture visual word*. The temporal evolution of those words is modeled using Discrete Hidden Markov Models (DHMM). Specifically, joint locations are casted into the bins of a spherical histogram centered at the actor's hip and aligned with the actor's direction.

To gain robustness against pose variability, each joint votes for several bins (its actual bin and the surrounding 3D bins), and voting is done trough a Gaussian weight function. Histograms are reprojected using linear discriminant analysis (LDA) to select relevant bins, and k-means is used to cluster the reprojected vectors into the posture words. As a result, each action sequence is encoded as a sequence of posture words, which is in turn fed into the DHMM training algorithm.

Focusing on the recognition of domestic activities, the work in [SPSS11] presents a carefully hand-crafted skeleton descriptor that includes the relative position of specific joints, such as the feet and hands with respect to the torso, or the hands with respect to the head. Half-space quaternions are used to achieve a compact representation of the joint's orientation. Motion information of several selected joints is also incorporated into the descriptor. The temporal evolution of the descriptors is modeled using a two-layered Maximum Entropy Markov Model (MEMM), that considers activities as composed of a set of sub-activities. The top-layer represents activities, and the bottom layer represent their associated sub-activities. The association between activities and sub-activities is efficiently determined during inference using a dynamic programming algorithm.

The work in [DWW15] uses the raw joint locations as descriptors, and leaves the extraction of meaningful features to several Recurrent Neural Networks (RNN) connected in a hierarchical fashion. Different to perceptrons, RNNs are neural networks with cyclical connections between cells. Such recurrent connections can be seen as leading to memorization of previous inputs. For time sequences, this allows for temporal context to be taken into account. The commented work decomposes skeletons into five parts (two arms, two legs and one trunk) and feed them into five Bidirectional RNNs (BRNN). The outputs of the trunk network are concatenated with the outputs of the other four networks, and the resulting vectors are fed into four BRNNs that model the movements of neighboring body parts. A similar scheme is used to obtain two further high level representations, corresponding to the lower body, upper body and full body. The final output is fed into a single-layer perceptron. To overcome the vanishing gra-

dient problem [G+12], the highest level network (corresponding to the full body) uses a Long Short-Term Memory (LSTM) architecture [HS97]. LSTM networks consists of a set of recurrently connected memory blocks. Each block contains one or more self-connected memory cells and three multiplicative gates: the input, output and forget gates. The multiplicative gates allow LSTM memory cells to store and access information over long periods of time.

Based on the observation that not all skeletons in a sequence are discriminative about the performed action, the authors in [VZQ15] add a differential gating scheme to the traditional LSTM network that quantifies the change in information gain caused by successive skeletons. Such quantification is measured by the so call *Derivative of States* (DoS). A large value of DoS corresponds to skeletons with salient motion information and instruct the gate units to allow more information to enter the memory cell. The chosen skeleton descriptor combines joint locations, pairwise angles between limbs, pairwise joint distances and joint velocities.

[ZCG13] uses the same skeleton descriptor as in [YT12], but considers a Bag-of-Words (BoW) approach for temporal modeling. Similar to [XCA12], training descriptors are quantized using k-means clustering, and the cluster centers are used as posture visual words. For a given sequence, each descriptor in the sequence is mapped to its nearest word, and a histogram is built by counting the number of descriptors associated with each word. Histograms are used to train a random forest, that is used for classification of new instances.

Wang et al. [WWY13] divide joints into five groups using the same criteria as in [DWW15]. Using the training data, a dictionary of posture words is learned for each group by clustering the poses of its associated joints. Each posture word represents a certain pose of the joints in the group. Data mining techniques are applied to obtain distinctive sets of both co-occurring spatial configurations of posture words (which are called *spatial-part-sets*) and co-occurring sequences of posture words (called *temporal-part-sets*). A BoW approach is then applied to condense the information in the part-sets. Specifically, sequences are represented by histograms that count the pres-

ence of distinctive part-sets, and SVM is used for classification.

Similar to [DWW15], the raw joint locations are used in [RDE11] as descriptors. The authors observe that not all joints have the same importance when trying to decide if a skeleton sequence corresponds to a particular action. For example, lower body joints should have little or non influence in deciding if the actor is clapping hands or not. Based on such observation, their approach associates a weight to each joint depending on its discriminative power. For a given joint, measures representing its intra/inter action variability are learned from the training data. The former is obtained by averaging the DTW distance between all possible pairs of sequences labeled with the same action. The latter is computed by averaging the DTW distance between all the remaining pairs. In both cases, only the descriptor coordinates associated with the considered joint are used. The (normalized) difference between the inter-action variability and the intra-action variability determines the final weight of the joint. Specifically, larger differences correspond to larger weights. New sequences are classified by comparing them to each training sequence using DTW distance. The learned weights are plugged into the distance function used to compare points in DTW (see Section 3.2.1).

Relational binary features are proposed in [MR06] as skeleton descriptors, in an attempt to discard uninformative details while retaining important pose characteristics. Such features describe geometric relations between joints using boolean values. For example, one feature might describe the left hand position as being above (value zero) or below (value one) the head. Temporal evolution is modeled using the concept of *motion templates* (MTs). An MT is learned for each action using a procedure that aligns all the sequences for that action using DTW. For a given action, its associated MT aims at capturing the essence of the action, by identifying periods in time where certain binary features consistently assume the same value in all the sequences of that action. Classification of a new sequence is achieved by computing the DTW distance between the sequence an each training MT. A special function is proposed to measure the distance between points in DTW (see Section 3.2.1), that accounts only for the pose features associated

with consistent periods in the MT, and discards the rest.

A novel skeleton descriptor is described in [VAC14]. Given two body limbs, the translation and rotation matrices required to take one limb to the position and orientation of the other is used to represent their relative 3D geometry. Such matrices are members of the special Euclidean group $SE(3)$ [MLSS94], which is a Lie group. Therefore, by considering every pair of limbs, skeletons are described by points in the Lie group $SE(3) \times \ldots \times SE(3)$, where $\times$ indicates the direct product between Lie groups. As such Lie group is a curved manifold, points are further map to its lie algebra $\mathfrak{se}(3) \times \ldots \times \mathfrak{se}(3)$, to ease temporal modeling and classification. Skeleton sequences are thus represented as curves in the mentioned Lie algebra. Moreover, a nominal curve is computed for each action, and all the training curves are warped to their corresponding nominal curve using DTW. Finally, the FTP representation of [WLWY12a] is used to describe sequences, and classification is performed using SVM.

The work in [OBT13] represents skeletons by the relative azimuth and elevation angles of each joint with respect with its parent. Considering such representation, each joint can be associated with two temporal series, describing the evolution of the two angles along the action sequence. Temporal modeling is achieved by computing the distance between every possible pair of series. Therefore, if m is the number of angles in the skeleton representation (and thus the number of series), the action sequence is represented by a vector of $\frac{m(m-1)}{2}$ elements. The authors found that simple distance functions between series (e.g. the Euclidean distance) lead to better results for this representation than more complex functions such as DTW. A linear SVM is used for classification.

2.2 Datasets

This section describes the four datasets used in our experiments: MSRDailyActivity3D, MSRAction3D, UTKinect and Florence3D. In every case, videos show a single actor performing an action. Each video is labeled according to the performed action. Skeleton data is provided for all the videos.

For each dataset, we present a general overview, we show example frames and we describe the training/testing setting followed in the experiments. Specifically, we detail which videos are considered as training data and which videos are used for testing. Moreover, we make explicit how the performance measure (namely, the average class accuracy) reported in sections 3.3 and 4.3 is computed. Further, we indicate which part of the data was used for parameter optimization via leave-one-actor-out cross-validation (i.e all sequences belonging to the same person are associated with the same fold).

2.2.1 MSRDailyActivity3D dataset

The MSRDailyActivity3D dataset [WLWY12a] consists of several action sequences captured with a Kinect device. It was designed with daily activities in mind. As such, actions take place in a living room containing a sofa, and the actor interacts with typical objects found in domestic spaces. There are 16 actions: *drink*, *eat*, *read book*, *call cellphone*, *write on a paper*, *use laptop*, *use vacuum cleaner*, *cheer up*, *stay still*, *toss paper*, *play game*, *lay down on sofa*, *walk*, *play guitar*, *stand up* and *sit down*. Ten different subjects are recorded. If possible, each subject performs an action twice: one standing next to the sofa and the other sitting on the sofa. Overall, there are $16 \times 2 \times 10 = 320$ action sequences. Figure 2.1 shows some example RGB frames.

This dataset is very challenging. First, the presence of the sofa makes skeleton tracking difficult. As a consequence, joint positions are quite noisy and inaccurate. Second, many actions involve similar sets of subtle body movements, such as *read book* or *write on a paper*, that are hard to differentiate from one another based solely on skeleton information. Finally, the wide diversity of actors, positions and performing styles leads to large intra-class variability.

The typical experimental setting on this dataset uses the videos corresponding to half of the subjects as training data, and the videos corresponding to the remaining subjects as testing data. In the experiments described in sections 3.3 and 4.3, average class accuracy is computed following such

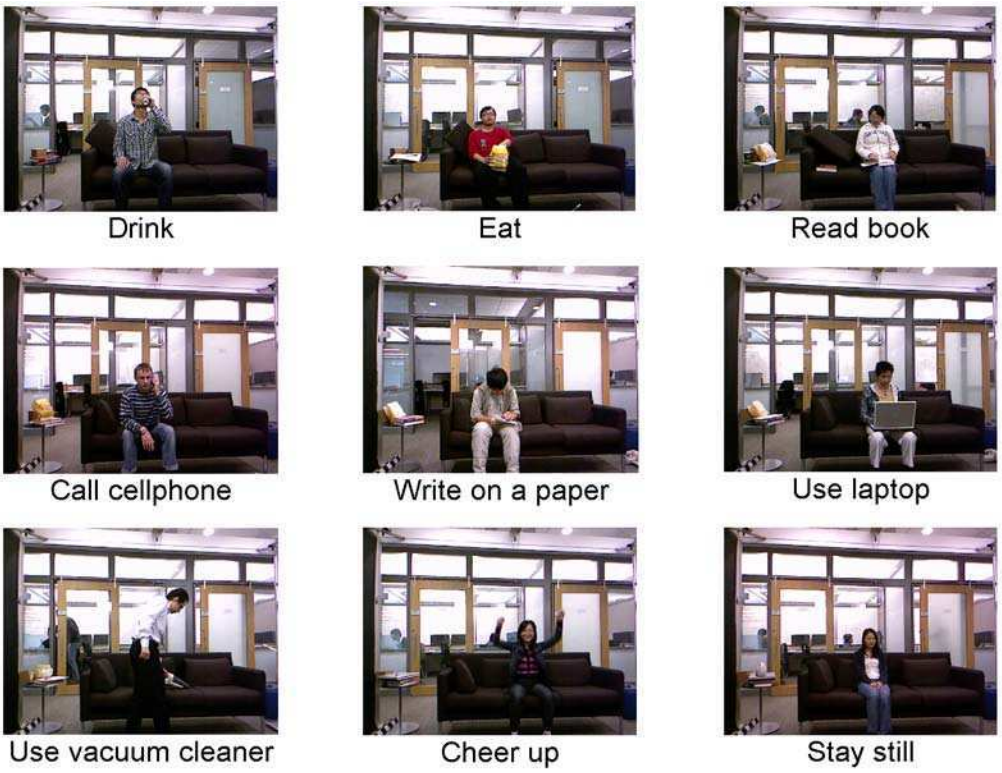

Figure 2.1: Example RGB frames of the MSRDailyActivity3D dataset.

typical setting. For parameter selection, we optimize the average class accuracy via leave-one-actor-out cross-validation on the training data.

2.2.2 MSRAction3D dataset

The action sequences in the MSRAction3D dataset [LZL10] were captured with a depth sensor similar to the Kinect device. The actions were chosen in the context of hands-free game console interaction. Therefore, they cover the various movements of arms, legs, torso and their combinations. There are 20 actions: *high arm wave*, *horizontal arm wave*, *hammer*, *hand catch*, *forward punch*, *high throw*, *draw x*, *draw tick*, *draw circle*, *hand clap*, *two hand wave*, *side-boxing*, *bend*, *forward kick*, *side kick*, *jogging*, *tennis swing*, *tennis serve*, *golf swing*, *pickup & throw*. Each action was performed by 10 subjects for 2 or 3 times. Overall, the dataset includes 577 action sequences. Figure 2.2 shows example depth frames.

This is undoubtedly the most popular dataset in the literature. Despite a somewhat low intra-class variability (subjects are facing the camera during

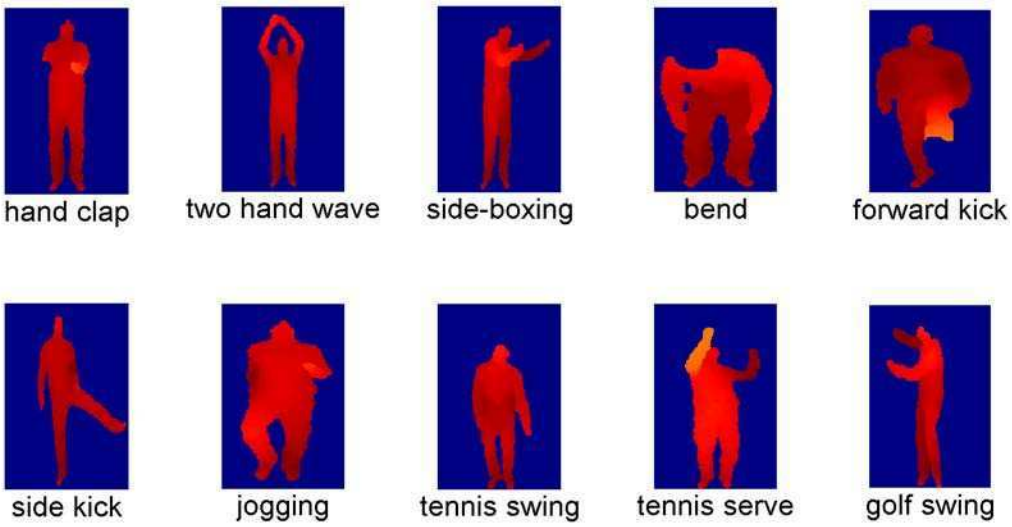

Figure 2.2: Example depth frames of the MSRAction3D dataset.

the performance and use their right arm or leg whenever the action involves a single arm or leg), it is also considerably challenging. Specifically, many of the actions are highly similar to each other, leading to a large inter-class similarity.

The typical experimental setting presented in [LZL10] divides the dataset into three subsets $AS1$, $AS2$ and $AS3$, each having 8 actions. Subsets $AS1$ and $AS2$ are intended to group actions with similar movement, while subset $AS3$ is intended to group complex actions together. For each subset, such typical setting follows a cross-subject scheme (presented in [LZL10]), that uses half of the subjects for training and the remaining half for testing. In the experiments described in sections 3.3 and 4.3, average class accuracy is computed by averaging the results for $AS1$, $AS2$ and $AS3$. For parameter selection, we optimize the average class accuracy via leave-one-actor-out cross-validation on the training subjects, using a single set of 20 actions.

2.2.3 UTKinect dataset

The UTKinect dataset [XCA12] was collected using a Kinect device, with focus on indoor activities. It includes 10 actions: *walk*, *sit down*, *stand up*, *pick up*, *carry*, *throw*, *push*, *pull*, *wave* and *clap hands*. Each action is performed

Figure 2.3: Example frames of the UTKinect dataset.

twice by 10 actors, for a total of $10 \times 2 \times 19 = 200$ videos. Figure 2.3 shows some example frames.

The dataset is challenging for several reasons. First, sequences where captured from different views. Second, sequences corresponding to the same action can be very different from each other. For example, some actors pick up objects with one hand while others do it with both hands. Third, the duration of the action sequences can vary considerably, ranging from 5 to 120 frames. Finally, body parts might be out of the scene or occluded by objects, hurting the performance of the skeleton tracker.

In our experiments, we used the cross-subject setting from [ZCG13], that uses half of the subjects for training and the remaining subjects for testing. Average class accuracy reported in sections 3.3 and 4.3 for our methods is computed following such setting. For parameter selection, we optimize the average class accuracy via leave-one-actor-out cross-validation on the training data.

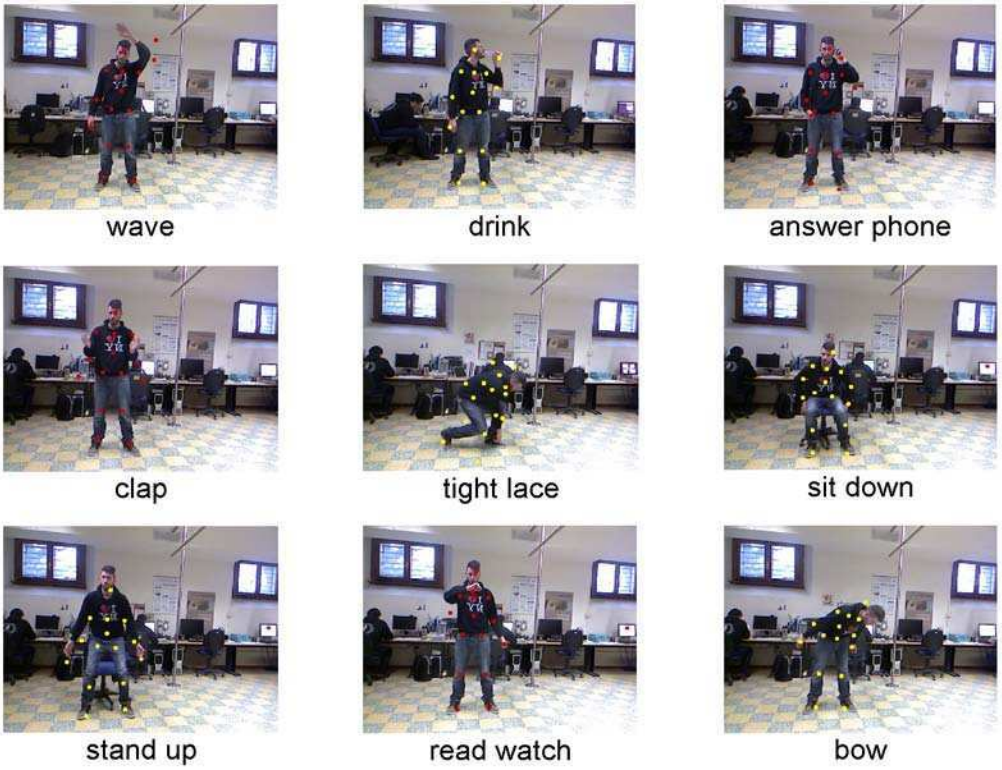

Figure 2.4: Example frames of the Florence3D dataset.

2.2.4 Florence3D dataset

This dataset was captured using a Kinect device for the work in [SVB+13]. It contains 9 actions: *wave*, *drink from a bottle*, *answer phone*, *clap*, *tight lace*, *sit down*, *stand up*, *read watch* and *bow*. Each action was performed by 10 subjects for 2 or 3 times. Overall, there are 215 action sequences. Figure 2.4 shows example frames.

This dataset has considerable intra-class variability. For example, some subjects perform a given action using their left hand, while some other use their right hand. Furthermore, several actions involve the same set of movements, like *drink from a bottle* and *answer phone*.

As with the UTKinect dataset, we used the cross-subject setting from [ZCG13] to obtain the average class accuracy reported in sections 3.3 and 4.3, and optimize the average class accuracy via leave-one-actor-out cross-validation on the training data for parameter selection.

2.3 Resumen

En este capítulo se hace un repaso de los principales trabajos relacionados existentes en la literatura para el problema encarado en la tesis, y se describen las cuatro bases de datos utilizadas en los experimentos de las secciones 3.3 y 4.3.

La revisión del estado del arte (sección 2.1) se concentra en aquellos métodos de reconocimiento de acciones en videos de profundidad basados en secuencias de esqueletos. Muchos trabajos utilizan directamente la información de profundidad, descartando la información correspondiente al esqueleto. Dichos trabajos no son considerados en la revisión, ya que su enfoque se encuentra demasiado alejado del considerado en la tesis. Asimismo, para las técnicas híbridas que consideran tanto la información de esqueleto como la información de profundidad, la revisión sólo tiene en cuenta los aspectos de las mismas relacionados al esqueleto.

Por cada trabajo comentado, se describen principalmente dos aspectos del mismo. El primero involucra el descriptor de esqueleto considerado y/o la medida de similaridad utilizada para comparar descriptores. El segundo es el enfoque elegido para modelar la evolución temporal de los descriptores.

La sección 2.2 describe las bases de datos utilizadas en los experimentos de la tesis. Se trata de cuatro bases datos que incluyen información de esqueleto, en su mayor parte obtenida usando el algoritmo de seguimiento incluido con Microsoft Kinect, basado en el trabajo de [SSK+13]. Por cada base, se describen las acciones consideradas, se muestran imágenes de ejemplo y se comentan las características principales de sus videos, enfocándose en aquellas más desafiantes. Además, se explica qué parte de los videos es usada para entrenamiento, y qué parte para testing. Asimismo, se detalla cómo se calculan las medidas de performance reportadas en las secciones de resultados.

Chapter 3

Action recognition using Instance-to-Class Edit Distance on Real sequence

This chapter describes one of the two novel methods for action recognition presented in the thesis. At its core lies a new technique for comparing sequences, obtained as the result of two modifications to a popular distance function between sequences. Section 3.1 motivates our method by focusing on specific aspects of the previous works. Section 3.2 presents the mentioned technique and the proposed approach for action recognition. Finally, Section 3.3 experimentally evaluates our method and compares it with the state-of-the-art.

3.1 Introduction

Modeling the temporal evolution of skeleton descriptors is a challenging task. The reasons, discussed in detail in Section 1.1.1, are mainly related to the noisy skeletons, and the inherently large intra-class variability/inter-class similarity. A detailed description of common approaches to the problem of skeleton-based action recognition can be found in Section 2.1.1. We now present a general review of such approaches, focusing specially in the temporal evolution model proposed by each particular method.

Several works use generative models such as Hidden Markov Models (HMM) [LN06, XCA12, SPSS11]. These methods suffer with limited amount of training data, as their training algorithms are prone to overfitting. Moreover, many works are based on Motion Capture (MoCap) data [BW95]. Skeletons computed from depth maps sequences are generally more noisy than those obtained through MoCap systems. When the difference between the actions is small, determining the number of states (as required in HMM) is usually difficult, which undermines the performance of these models.

Recurrent Neural Networks have also been employed, with relative success [VZQ15, DWW15]. These are very flexible classifiers for time series, that can model contextual time information. However, they tend to overfit when the amount of available training data is limited, as is usually the case in action recognition problems. Further, the amount of context information that can be used in practice tends to be very limited, as the signal of a given input decays too fast as to influence the network at distant time steps, an effect commonly known as the *vanishing gradient problem*. Early stopping, input noise and weight noise are among the most popular techniques to deal with the overfiting problem, while long short-term memory LSTM proved effective against the gradient problem [G+12]. While promising results are reported for these methods on certain datasets (see for example Table 4.2), careful tuning is required to successfully take advantage of the above commented techniques.

Other approaches [WLWY12a, GTHES13, VAC14] build a high level pyramidal description of the temporal sequence based on the skeletons features. Wang et al. [WLWY12a] present the Fourier Temporal Pyramid (FTP). To mitigate the effect of noisy data and temporal misalignment, they compute the evolution of the low-frequency Fourier coefficients along the video, using a pyramid structure. In [GTHES13], the trajectory of each joint is described using Histograms of Oriented Displacements (HOD), and a pyramid structure similar to the one used in [WLWY12a] to account for temporal information. [VAC14] also considers the same pyramid representation, but sequences belonging to the same action are warped to a nominal curve for that action using Dynamic Time Warping before computing the pyramid.

The main problem with these approaches is that the temporal structure of the sequence is only roughly captured by the pyramid representation.

Similarly, some works follow a Bag-of-Words approach [ZCG13,WWY13]. Employing a clustering technique, base descriptors are quantized into words, yielding a codebook. Videos are then represented as histograms of quantized descriptors. The main problem with these sort of approaches is that discriminative information is considerably reduced in descriptor quantization [BSI08]. Moreover, global time information is discarded as only the presence of words is taken into account, but not their temporal positions. The works in [YT12, SVB+13] avoid descriptor quantization by using the Naive-Bayes-Nearest-Neighbor (NBNN) [BSI08] method for classification. However, temporal information is only roughly encoded in the descriptors. This fact, coupled with the independence assumption underlying NBNN (namely, that descriptors are i.i.d. given the action class), can lead to inaccurate temporal representations. In addition, when considerably different densities in descriptor space exist among the actions, classification might be biased towards certain classes.

More related to our approach is the usage of Dynamic Temporal Warping (DTW) [RDE11,MR06,VAC14,VSRCC09,GD+95,SMA11]. DTW is probably the most popular technique among a group of related similarity measures that allow non-linear alignments between time series. It is undoubtedly the most used within the group for the problem of action recognition from skeletal data. Other similarity measures in the group include the Frechet distance [EM94], the Edit Distance with Real Penalty [CN04], the Longest Common Subsequence [VKG02] and the Edit Distance on Real Sequence [CÖO05].

These similarity measures present certain features that make them attractive for the problem of action recognition from skeletal sequences. On the one hand, they have the ability to deal with non-linear variations in the time dimension (different speeds, temporal misalignment, etc.). On the other, they specifically take into account the temporal order of the data when aligning series. That is, if position i in series X is aligned to position j in sequence Y, then positions larger than i in X can only be aligned to

positions larger than j in Y.

However, the performance of classification methods based on these measures heavily depends on the approach used to compare the points in the series. Even with a considerably robust approach, results can suffer in cases of very noisy data (such as skeletons computed from depth images).

In this chapter, we present a distance function that aims at mitigating these problems. Our proposal extends the Edit Distance on Real sequence (EDR) [CÖO05], a robust and accurate similarity measure between time series. We introduce two key improvements to EDR: a weighted matching scheme for the points in the series and a modified aligning algorithm based on the concept of Instance-to-Class [BSI08] distance. The resulting distance function takes into account temporal ordering, requires no learning of parameters and is highly tolerant to noise and temporal misalignment.

We describe a method for action recognition on skeleton sequences based on the presented distance function, and perform extensive experiments on four datasets, comparing our approach with other methods. The presented method proves superior to other approaches based on distance functions between time series. Further, results show that, when coupled with a robust skeleton descriptor, its performance is comparable to the state of the art.

3.2 Recognizing actions using Instance-to-Class Edit Distance on Real sequence

This section presents a new method for skeleton-based action recognition. Its core component is a new approach to the temporal modeling of skeletal sequences, based on a novel technique for comparing time series.

Section 3.2.1 formalizes the notion of time series and reviews classical techniques for comparing them, focusing on those computing distance functions defined over the raw series representation. The main problems of such techniques in dealing with realistic data are highlighted. Section 3.2.2 introduces a new similarity measure as an extension to a particular technique. Finally, Section 3.2.3 describes the complete action classification method, in-

cluding the role played in it by the proposed measure.

3.2.1 Comparing time series

A time series is a sequence of d dimensional points $A = (a_1, a_2, \ldots, a_N)$, $a_i \in \mathbb{R}^d \quad \forall\ 1 \leq i \leq N$, usually produced by an underlying movement during which values are sampled at uniformly spaced time instants. Note that some works use the term *trajectory* for this kind of sequence. In the following, we use the terms *series*, *time series* and *sequence* interchangeably. In addition, we shall talk of *similarity measure*, while most of the time we are actually measuring *dissimilarity*. Further, we usually employ the term *distance* or *distance function* when referring to similarity measures (note that by *distance* we do not necessarily mean a distance metric).

Many techniques have been used for comparing time series, with contributions coming from a variety of domains. All of them focus either on a specific format for representing the series, or on a particular distance function for measuring the similarity between different series.

Among the ones focusing on series representation, Piecewise Linear Approximation (PLA) is a popular choice [Pav73,SZ96] for noise filtering. This technique approximates the original series using a sequence of linear functions. Transformation to the frequency domain is another common procedure [HKT99, PM02, WLWY12a]. Typical transformations are the Discrete Fourier Transform (DFT) and the Discrete Wavelet Transform (DWT). Representing the original series by its DFT or DWT coefficients is an effective way of dealing with temporal misalignment. Further, discarding coefficients corresponding to high frequency components can lead to significant noise robustness. Feature-based representations have also been employed several times [MWLF05,WWY13]. Local segments are quantized into *words*, and the series is represented by histograms (or *pyramids*) of word occurrences. Also frequent is the use of model-based techniques [XY04], that allow for prior knowledge about the process generating the series to be taken advantage of. Once a model for such process is trained, similarity is based on the likelihood that a series was generated by that model. Hidden Markov

Model is a classical example.

More related to our approach are techniques based on distance functions defined over raw series representations. The most basic options align the ith point on one time series with the ith point on the other, and sum the distance between each of the aligned points. These sort of measures are very sensitive to distortions in the time dimension and will typically produce poor similarity scores for many real world problems.

Non-linear (elastic) alignment methods have been proposed to overcome this weakness of basic distance functions. These techniques allow similar points to match even if they are out of phase in the time axis. Several distance measures using this kind of elastic matching can be found in the literature. In the following we describe three relevant examples. We pay special attention to one of them, called Edit Distance on Real sequence, as our proposed method (Section 3.2.2) builds upon this particular technique

Elastic matching over raw series representations

The first two examples of elastic distances described in this section are Frechet and Dynamic Time Warping. Both can be explained using a structure called *warping path*. Therefore, we introduce such structure before explaining the distances.

Let $A = (a_1, a_2, \dots a_N)$ and $B = (b_1, b_2, \dots, b_M)$ be times series, with $a_i, b_j \in \mathbb{R}^d \quad \forall\ 1 \leq i \leq N$ and $1 \leq j \leq M$. An (N, M)-warping path (or simply a warping path when N and M are clear) is a sequence $p = (p_1, \dots, p_L)$, with $p_t = (i_t, j_t) \in [1, N] \times [1, M]$ for $1 \leq t \leq L$, satisfying the following conditions:

(i) Boundary condition: $p_1 = (1, 1)$ and $p_L = (N, M)$.

(ii) Monotonicity condition: $i_1 \leq i_2 \leq \dots \leq n_L$ and $j_1 \leq j_2 \leq \dots \leq j_L$.

(iii) Continuity condition: $i_t - i_{t-1} \leq 1$, $j_t - j_{t-1} \leq 1$ and $\|p_t - p_{t-1}\| \neq 0$ $\forall\ 1 < t \leq L$

A warping path $p = (p_1, \dots, p_L)$ defines an alignment between series A and B where the element $a_{i_t}$of A is paired with the element b_{j_t} of B. Condi-

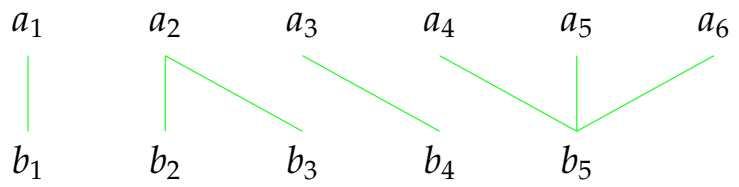

Figure 3.1: A schematic example of a warping path.

tion (i) enforces that the first (last) elements of A and B are aligned to each other. I.e., no portions of the sequences are left out of the alignment. Condition (ii) states that, whenever position i in A is matched to position j in B, positions larger or equal than i in A can only be matched to positions larger or equal than j in B. Finally, condition (iii) requires that no element in A or B is omitted and there are no replications in the alignment. Figure 3.1 shows an example warping path.

Both Frechet distance and DTW optimize, over all possible warping paths, some measure that depends on the cost of aligning points a_{i_t} and b_{j_t}. The main difference between them lies in the optimized measure. We next present the Frechet distance and describe its chosen measure. In doing so, we point out potential problems of such measure. Then we introduce DTW and explain why it uses a more robust measure than Frechet.

Given sequences $A = (a_1, a_2, \ldots, a_N)$ and $B = (b_1, b_2, \ldots, b_M)$, the Frechet distance between them $Fre(A, B)$ can be defined recursively as:

$$Fre(A,B) = \begin{cases} 0 & \text{if } N = M = 0 \\ \infty & \text{if } NM = 0 \\ \max \left\{ \begin{array}{l} cost(a_1, b_1), \\ \quad \min \left\{ \begin{array}{l} Fre(Rest(A), Rest(B)), \\ Fre(Rest(A), B), \\ Fre(A, Rest(B)) \end{array} \right. \end{array} \right. & Otherwise \end{cases} \tag{3.1}$$

where $Rest(S)$ denotes the subsequence of S obtained by removing its first point and $cost(a, b) = d(a, b)$, with $d(\cdot)$ a given L_p distance.

The measure optimized by Frechet over all possible warping paths is

the *maximum cost*. Given a warping path $p = (p_1, \ldots, p_L)$ between $A = (a_1, a_2, \ldots, a_N)$ and $B = (b_1, b_2, \ldots, b_M)$, with $p_t = (i_t, j_t) \in [1, N] \times [1, M]$, the maximum cost $mc_p(A, B)$ is defined as:

$$mc_p(A, B) = \max_{t=1,\ldots,L} cost(a_{i_t}, b_{j_t}) \tag{3.2}$$

where $cost(\cdot)$ is defined as in Equation 3.1.

The Frechet distance between A and B is therefore the maximum cost of a warping path $p*$ for which the maximum cost is minimum:

$$Fre(A, B) = mc_{p^*}(A, B) \tag{3.3}$$

Frechet distance is defined in terms of the maximum cost of a warping path. This dependence on a maximum measure undermines it robustness for many real world scenarios. The computed distance can be severely distorted by noise and outliers. Sum or average-based measures, on the other hand, help to smooth out computations, and are typically more tolerant to the presence of these artifacts. Dynamic Time Warping is an example of such measures.

Given sequences $A = (a_1, a_2, \ldots, a_N)$ and $B = (b_1, b_2, \ldots, b_M)$, the DTW distance between them $DTW(A, B)$ can be defined recursively as:

$$DTW(A, B) = \begin{cases} 0 & \text{if } N = M = 0 \\ \infty & \text{if } NM = 0 \\ cost(a_1, b_1) + & \\ \min \left\{ \begin{array}{l} DTW(Rest(A), Rest(B)) \\ DTW(Rest(A), B), \\ DTW(A, Rest(B)) \end{array} \right\} & Otherwise \end{cases} \tag{3.4}$$

where again $Rest(S)$ denotes the subsequence of S obtained by removing its first point and $cost(a, b) = d(a, b)$, with $d(\cdot)$ a given L_p distance.

The measure optimized by DTW over all possible warping paths is the *total cost*. Given a warping path $p = (p_1, \ldots, p_L)$ between $A = (a_1, a_2, \ldots, a_N)$

and $B = (b_1, b_2, \ldots, b_M)$, with $p_t = (i_t, j_t) \in [1, N] \times [1, M]$, the total cost $tc_p(A, B)$ is defined as:

$$tc_p(A, B) = \sum_{t=1}^{L} cost(a_{i_t}, b_{j_t}) \tag{3.5}$$

where $cost(\cdot)$ is defined as in Equation 3.1.

The DTW distance between A and B is therefore the total cost of a warping path $p*$ for which the total cost is minimum:

$$DTW(A, B) = tc_{p^*}(A, B) \tag{3.6}$$

DTW performance deteriorates with noisy data as, when matching all the points (recall condition (iii) in the definition of warping path), it also matches the outliers, distorting the true distance between sequences. The distortion can be severe because L_p norms are used to compute the distance between the aligned points. Edit Distance on Real sequence (EDR), presented next, overcomes these problems.

EDR is based on the Edit Distance (ED) [WF74], also refered to as Levenshtein distance. Given a source sequence A and a target sequence B, the ED between them is the number of insert, delete or replace operations needed to convert A into B. Determining the operations that need to be applied requires the ability to compare the individual elements in the sequences. ED measures the similarity between sequences of discrete symbols. As a consequence, elements are compared for equality. EDR, however, works on sequences of points in $\mathbb{R}^d$. As such, it compares elements based on proximity. Specifically, a threshold $\epsilon \in \mathbb{R}$ is used for point matching. Two points a_i and b_j from sequences A and B respectively are said to match if $d(a_i, b_j) < \epsilon$, where $d(.)$ is a given distance function.

The EDR between two sequences A and B is the number of insert, delete and replace operations needed to transform A into a sequence E that *matches* B. Two sequences A and B are said to match if they have the same length and each element in A matches the correspondent element in B. In other words:

$$match(A,B) \equiv |A| = |B| \wedge \ (d(a_i,b_i) < \epsilon \ \ \forall 1 \leq i \leq |A|) \tag{3.7}$$

where ϵ is the threshold used for element matching, $d(\cdot)$ is a distance function between points and $|\cdot|$ denotes length.

Formally, given sequences $A = (a_1, a_2, \ldots, a_N)$ and $B = (b_1, b_2, \ldots, b_M)$, and a real number ϵ, EDR is defined as:

$$EDR_\epsilon(A,B) = \begin{cases} N & \text{if } M = 0 \\ M & \text{if } N = 0 \\ \min \begin{cases} EDR_\epsilon(Rest(A), Rest(B)) \\ \quad + cost_{edr}(\epsilon, a_1, b_1), \\ EDR_\epsilon(Rest(A), B) + 1, \\ EDR_\epsilon(A, Rest(B) + 1) \end{cases} & Otherwise \end{cases} \tag{3.8}$$

where $Rest(S)$ again denotes the subsequence of S obtained by removing its first point and $cost_{edr}(\cdot)$ is defined for a given distance function $d(\cdot)$ between points as follows:

$$cost_{edr}(\epsilon, a, b) = \begin{cases} 0 & \text{if } d(a,b) < \epsilon \\ 1 & Otherwise \end{cases} \tag{3.9}$$

The criteria used for setting the value of ϵ strongly depends on the considered distance function between points $d(\cdot)$. A common choice is for $d(\cdot)$ to be the Euclidean distance and for ϵ to be set to $\min(\Psi(A), \Psi(B))$ where $\Psi(A)$ and $\Psi(B)$ are the sum of the coordinate-wise standard deviations of A and B respectively. The two last terms in the minimization in Equation 3.8 correspond to delete and insert operations respectively, while the first term corresponds either to a match or to a replacement.

Just as DTW optimizes a measure over all possible warping paths, EDR does it over all possible instances of a structure called *trace*. Intuitively, given sequences A and B and a threshold value ϵ, a trace describes how a series of edit operations transforms A into a sequence E that matches a sequence B, but ignoring the order in which changes happen and any redundancy in the series of operations.

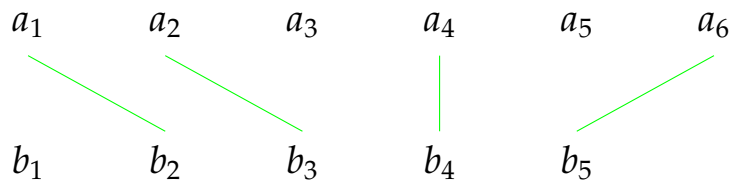

Figure 3.2: A schematic example of a trace.

Let $A = (a_1, a_2, \ldots a_N)$ and $B = (b_1, b_2, \ldots, b_M)$ be times series, with $a_i, b_j \in \mathbb{R}^d \quad \forall\ 1 \leq i \leq N$ and $1 \leq j \leq M$. An (N, M)-trace t (or simply a trace when N and M are clear) is a set of ordered pairs (i, j) of integers satisfying:

(i) $1 \leq i \leq N, 1 \leq j \leq M$

(ii) for any two distinct tuples (i_1, j_1) and (i_2, j_2) in t:

  (a) $i_1 \neq i_2$ and $j_1 \neq j_2$;
  (b) $i_1 < i_2 \iff j_1 < j_2$.

A tuple (i, j) can be seen as a line joining point i of sequence A with point j of sequence B. We say that the line (i, j) *touches* positions i and j, and that points a_i and b_j are *connected*. Condition (i) states that i and j are actually withing the limits of the sequences. Condition (iia) ensures each position (either in A or in B) is touched by at most one line. Condition (iib) states that lines cannot cross. A line (i, j) indicates either a match or a replacement operation. If $d(a_i, b_j) < \epsilon$, a_i matches b_j and a_i is left unchanged. Otherwise, a_i is replaced by b_j. Positions of A not touched by any line represent points of A deleted by the series of operations. Similarly, untouched positions of B represent points inserted in A. An example trace is shown in figure 3.2.

Traces are very similar to warping paths. However, they differ from them in two ways. First, in a warping path a point from one of the sequences may be connected to several points from the other sequence, while in a trace each point is connected to at most one other point. Second, in a warping path every point is connected to at least one other point, while in a trace points may not be part of any connection.

The measure optimized by EDR over all possible traces is the *edit cost*.

Given a trace t between $A = (a_1, a_2, \ldots, a_N)$ and $B = (b_1, b_2, \ldots, b_M)$, and a threshold value ϵ, the edit cost $ec_t(\epsilon, A, B)$ is defined as:

$$ec_t(\epsilon, A, B) = I + D + \sum_{(i,j)\in t} cost_{edr}(\epsilon, a_i, b_j) \tag{3.10}$$

where I and D are the number of positions in A and B respectively left untouched by lines in the trace, and $cost_{edr}(\cdot)$ is definied as in Equation 3.9.

For a given ϵ, $EDR_\epsilon(A, B)$ is therefore the edit cost of a trace t^* for which the edit cost is minimum:

$$EDR_\epsilon(A, B) = ec_{t^*}(\epsilon, A, B) \tag{3.11}$$

Like warping paths, traces define alignments between sequences. Therefore, both DTW and EDR optimize a cost over all possible alignments. This optimization process gives them the ability to deal with temporal misalignment. However, they crucially differ in the considered alignments and the criteria used to assign costs to each alignment. On the one hand, EDR allows unmatched points (corresponding to positions not touched by any line in Figure 3.2). This is different from DTW, that requires all points to be matched (as illustrated in the example of Figure 3.1 by the absence of unconnected points). On the other hand, EDR quantizes distances between points to 0 or 1 when computing the cost of a given alignment, whereas DTW uses the raw distance between points. The combination of this two elements (i.e. allowing unmatched points and quantizing distances), makes EDR more robust than DTW to noise and outliers.

The EDR definition in Equation 3.8 suggests that an algorithm for computing the distance can be obtained using a dynamic programming approach. The algorithm stores the cumulative distance in a matrix $D \in \mathbb{R}^{(N+1)\times(M+1)}$ indexed from zero (N and M are the number of elements in the sequences). The cost of the optimal trace between the first i elements of A and the first j elements of B is stored at $D_{i,j}$. An initialization step sets $D_{0,j} = j$ and $D_{i,0} = i \; \forall \; 0 \leq i \leq n$ and $0 \leq j \leq m$. As the value in $D_{i,j}$ can be computed from the values of $D_{i-1,j}$, $D_{i,j-1}$ and $D_{i-1,j-1}$, carrying out computations in a specific order allows the algorithm to reuse previous results.

When the algorithm finishes, the EDR distance between A and B is stored at $D_{n,m}$. The pseudo-code of the dynamic programming algorithm is shown in Algorithm 1. It is not difficult to see that the temporal complexity of the algorithm is in $\mathcal{O}(NM)$.

Algorithm 1 Compute EDR distance between 2 time series

Require: Time series $A = (a_1, a_2, \dots a_N)$ and $B = (b_1, b_2, \dots, b_M)$, matching threshold $\epsilon \in \mathbb{R}$

function EDR(ϵ, A, B)
  $D \leftarrow$ *new matrix* $\in \mathbb{R}^{(N+1)\times(M+1)}$
  $D_{i,0} \leftarrow i \ \ \forall\, 0 \leq i \leq N$
  $D_{0,j} \leftarrow j \ \ \forall\, 0 \leq j \leq M$
  for $i \leftarrow 1, N$ **do**
    for $j \leftarrow 1, M$ **do**
      $ins \leftarrow D_{i,j-1} + 1$
      $del \leftarrow D_{i-1,j} + 1$
      $mr \leftarrow D_{i-1,j-1} + cost_{edr}(\epsilon, a_i, b_j)$
      $D_{i,j} \leftarrow \min(ins, del, mr)$
    end for
  end for
  return $D_{N,M}$
end function

3.2.2 A new time series similarity measure

In this section we present new similarity measure between time series, based on EDR. This novel distance function is the result of two improvements to the original EDR, which we introduce in an incremental fashion.

The first improvement introduces a soft cost for comparing points. We call *Edit Distance on Real sequence with Soft matching* (EDRS) the distance function obtained by adding the soft cost mechanism to EDR. The second improvement incorporates the notion of Instance-to-Class (I2C) distance to EDRS. The resulting technique is called *Instance-to-Class Edit Distance on Real*

sequence (I2CEDR). For each new distance presented in this section, we discuss its benefits and illustrate them with examples. Finally, we describe a dynamic programming algorithm for computing I2CEDR.

Edit Distance on Real sequence with Soft matching

In EDR, matched points add zero to the final distance computation, because no cost is assigned to aligned points lying within ϵ from each other. On the other hand, points separated by a distance slightly larger than the matching threshold can only by aligned at a cost of 1 (via a replacement). This hard criteria for assigning penalties undermines the accuracy of the method. With this problem in mind, we introduce a soft matching approach, that assigns a lower penalty to closer points and a larger one to distant points. The penalty increases gradually up to the matching threshold. As in EDR, the cost of aligning points that lie at distances larger than ϵ is 1. The resulting distance function can help to reveal and capture very small differences between sequences while retaining noise robustness.

Several functions can be chosen for assigning penalties. We use a linear function, that multiples the distance between the points by $\frac{1}{\epsilon}$. The choice is lead by the simplicity of the function and the good experimental results.

Equation 3.12 formally defines the Edit Distance on Real sequence with Soft matching (EDRS) between two sequences $A = (a_1, a_2, \ldots, a_N)$ and $B = (b_1, b_2, \ldots, b_M)$, for a given matching threshold ϵ. The definition of EDRS is the same as EDR (Equation 3.8), except for the cost assigned to aligned points, which appears in bold:

$$EDRS_\epsilon(A,B) = \begin{cases} N & \text{if } M = 0 \\ M & \text{if } N = 0 \\ \min \begin{cases} EDRS_\epsilon(Rest(A), Rest(B)) \\ \quad + \boldsymbol{cost_{edrs}(\epsilon, a_1, b_1)}, \\ EDRS_\epsilon(Rest(A), B) + 1, \\ EDRS_\epsilon(A, Rest(B) + 1) \end{cases} & Otherwise \end{cases} \tag{3.12}$$

where $Rest(S)$ again denotes the subsequence of S obtained by removing its first point, and $cost_{edrs}(\cdot)$ is defined as:

$$cost_{edrs}(\epsilon, a, b) = \begin{cases} \frac{d(a,b)}{\epsilon} & \text{if } d(a,b) < \epsilon \\ 1 & Otherwise \end{cases} \tag{3.13}$$

In all our experiments, we chose $d(\cdot)$ to be the Euclidean distance and set the value of ϵ to $\min(\Psi(A), \Psi(B))$ where $\Psi(A)$ and $\Psi(B)$ are the sum of the coordinate-wise standard deviations of A and B respectively.

In EDRS, insertions, deletions and replacement operations have a cost of of 1, just as in EDR. However, different to EDR, matchings might also add up to the final cost of a given trace. In other words, EDRS optimizes a different measure than EDR over all possible traces. We call such measure the *soft edit cost*. Given a trace t between $A = (a_1, a_2, \ldots, a_N)$ and $B = (b_1, b_2, \ldots, b_M)$, and a threshold value ϵ, the soft edit cost $sec_t(\epsilon, A, B)$ is defined as:

$$sec_t(\epsilon, A, B) = I + D + \sum_{(i,j)\in t} cost_{edrs}(\epsilon, a_i, b_j) \tag{3.14}$$

where I and D are, as in Equation 3.10, the number of positions in A and B respectively left untouched by lines in the trace, and $cost_{edrs}(\cdot)$ is definied as in Equation 3.13.

For a given ϵ, $EDRS_\epsilon(A, B)$ is therefore the soft edit cost of a trace t^* for which the soft edit cost is minimum:

$$EDRS_\epsilon(A, B) = sec_{t^*}(\epsilon, A, B) \tag{3.15}$$

An example of the effects of the new soft cost can be seen in the following example of three one-dimensional sequences: $A = (1, 2, 3, 4, 8)$, $B = (8, 4, 3, 2, 1)$ and $C = (10, 1, 2, 3, 4)$. The matching threshold for the following computations is $\epsilon = \min(\Psi(A), \Psi(B)) = \min(\Psi(A), \Psi(C)) = 2.7$, where $\Psi(A)$, $\Psi(B)$ and $\Psi(C)$ are the standard deviations of A, B and C respectively. Clearly, C is more simmilar to A than B: A and C are essentially the same (except for noise), while B is structurally different to A (in fact, it is its exact reversal). The EDR distance between A and B, however, is the same as the EDR distance between A and C. Specifically, $EDR_\epsilon(A, B) = 2$,

resulting from the replacements $1-8$, $8-1$ (both at cost 1) and the matchings $2-4$, $3-3$ and $4-2$ (all of them at cost 0), and $EDR_\epsilon(A,C) = 2$, resulting from the insertion of 10 and the deletion of 8 (both at cost 1) and the matchings $1-1$, $2-2$, $3-3$ and $4-4$ (all of them at cost 0). On the other hand, the EDRS distance is smaller for C, as desired. More precisely, $EDRS_\epsilon(A,C) = 2 < EDRS_\epsilon(A,B) = 3.5$. The replacements and matchings yielding the value of $EDRS_\epsilon(A,B)$ are the same as those considered for $EDR_\epsilon(A,B)$, but in the soft case the penalties assigned to two of the matchings are different from zero (matchings $2-4$ and $4-2$ are both penalized with 0.75). The matching cost assigned by EDR is too coarse, and can not distinguish subtle differences in the matched elements.

Instance-to-Class Edit Distance on Real sequence

This section presents a further extension to the distance presented in the previous section, that aims at improving the results of certain sequence classification methods based on EDR in cases of large intra-class variability and small training sets.

Classification methods can be roughly divided into: (a) Learning-based classifiers, that require an intensive parameter learning phase, and (b) Non-parametric classifiers, for which learning is based mostly in memorization of the training data. The latter have several attractive features. Remarkably, no calibration phase is required, which avoids large retraining periods in presence of new data and potential overfitting of parameters. Among the variants in the non-parametric group, the most common methods are those based in the *Nearest-Neighbor* (NN) principle [DHS01], which assigns a query instance the class of its nearest neighbor in the training dataset.

As pointed out by [BSI08], the use of *Instance-to-Instance* (I2I) distance can lead to poor results for NN-based methods in certain situations. Intra-class variability increases the distance between instances of the same class, potentially hurting performance. When the number of available training instances is low, the recognition rate can be severely degraded.

Inspired by [BSI08], we incorporate the idea of computing *Instance-to-Class* (I2C) distances (as opposed to I2I) to EDRS. The resulting sequence

classification method calculates the distance between a query sequence and those of a given class by matching points from the query with points of any of the sequences of that class. As a result, the generalization capabilities of NN methods using EDR-based distances are improved. The presented method exploits the information from different training sequences, reducing the effect of intra-class variations. Furthermore, as the I2C concept is adapted to EDR, the temporal order of the aligned points is specifically taken into account.

Given a sequence $A = (a_1, a_2, \dots a_N)$ and a set of K sequences $C = \{C_1, C_2, \dots, C_K\}$ all of them with the same lengths M, and having $C_k = (c_{1k}, c_{2k}, \dots, c_{Mk})$ for $1 \leq k \leq K$, and a vector ϵ of K matching thresholds, we define the *Instance to Class Edit Distance on Real sequence* (I2CEDR) between A and C as:

$$I2CEDR_\epsilon(A,C) = \begin{cases} |A| & \text{if } M = 0 \\ |C_1| & \text{if } N = 0 \\ \min \begin{cases} I2CEDR_\epsilon(Rest(A), Rests(C)) \\ \quad + cost_{I2C}(\epsilon, a_1, (c_{11}, \dots, c_{1k}))), \\ I2CEDR_\epsilon(Rest(A), C) + 1, \\ I2CEDR_\epsilon(A, Rests(C) + 1) \end{cases} & Otherwise \end{cases} \tag{3.16}$$

where $Rest(S)$ again denotes the subsequence of S obtained by removing its first point, $Rests(W)$ denotes the set obtained by applying $Rest$ to each sequence in W (i.e. $Rests(W) = \{Rest(W_k) | 1 \leq k \leq |W|\}$) and $cost_{I2C}$ is defined as:

$$cost_{I2C}(\epsilon, a, b) = \min_{1 \leq k \leq |b|} cost_{edrs}(\epsilon_k, a, b_k) \tag{3.17}$$

Given a point a, a sequence of points b and a vector ϵ of $|b|$ matching thresholds, $cost_{I2C}(\epsilon, a, b)$ returns the minimum matching cost between a and every possible point in b. For a given $1 \leq k \leq |b|$, the cost of matching a with b_k is computed using $cost_{edrs}$ as defined in 3.13, using the threshold ϵ_k. Thus, for a given position, the point of A at that position is compared for

matching against every point in a specific position in a sequence of C. In all our experiments, we set the value of ϵ_k to $\min(\Psi(A), \Psi(C_k))$ where $\Psi(A)$ and $\Psi(C_k)$ are the sum of the coordinate-wise standard deviations of A and C_k respectively.

Note that $I2CEDR_\epsilon(A, C)$ effectively considers the alignment of A with different sequences obtained by combining points from the sequences in C. More specifically, it tries every sequence in $comb(C)$, where $comb(C) = \{B|(\ \forall\ 1 \leq i \leq |B|)\ ((\exists k)(\ 1 \leq k \leq |C|) \wedge (c_{ik} = b_i))\}$. By considering every possible sequence in $comb(C)$, it is possible to obtain a low value for the distance between A and C, even if distances between A and the individual sequences in C are large. A point a_i in A can be matched to points of $|C|$ different sequences. If A belongs to the same class as the sequences in C, the chances of finding a point similar to a_i at the same position in any of the $|C|$ sequences is large.

To further clarify the notion of I2CEDR distance, we extend the notion of trace to describe the alignment of between a sequence and a set of sequences. Formally, given a sequence $A = (a_1, a_2, \ldots a_N)$ and a set of sequences $C = \{C_1, C_2, \ldots, C_K\}$ all of them with the same length M, where $C_k = (c_{1k}, c_{2k}, \ldots, c_{Mk})$ for $1 \leq k \leq K$, an (N, M, K)-*extended trace* (or simply an extended trace when N, M and K are clear) from A to C is a set t of ordered triples (i, j, k) of integers satisfying:

(1) $1 \leq i \leq N, 1 \leq j \leq M$ and $1 \leq k \leq K$;

(2) for any two distinct triples (i_1, j_1, k_1) and (i_2, j_2, k_2) in t:

   (a) $i_1 \neq i_2$ and $j_1 \neq j_2$;
   (b) $i_1 < i_2 \iff j_1 < j_2$.

A triple (i, j, k) can be seen as a line joining point i of sequence A with point j of sequence C_k. We say that the line (i, j, k) *touches* positions i and j, and that points a_i and c_{jk} are *connected*. Condition (1) states that i and j are actually withing the limits of the sequences, and that k refers to a sequence in C. Condition (2a) ensures each position (either in A or in C) is touched by at most one line. Note this implies that, for a given position, at most one

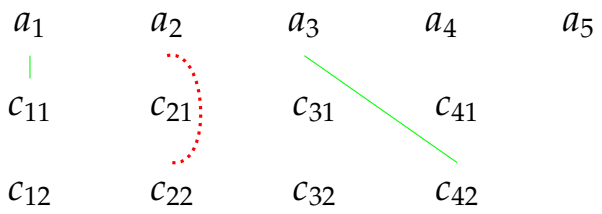

Figure 3.3: A schematic example of an extended trace.

sequence in C is touched by a line at that position. Condition (2b) states that lines cannot cross.

A line (i, j, k) indicates either a match or a replacement operation. If $d(a_i, c_{jk}) < \epsilon_k$, a_i matches c_{jk} and a_i is left unchanged. Otherwise, a_i is replaced by c_{jk}. Positions of A not touched by any line represent points of A deleted by the series of operations. Similarly, untouched positions of C represent points inserted in A.

Figure 3.3 shows a schematic example of an extended trace. Replacements are shown in dotted red lines, while matchings are shown in green. In the example, the first and the third points in A are matched with the first point in C_1 and the fourth point in C_2 respectively, the second point in A is replaced by the second point in C_2, the fourth and fifth elements in A are deleted, and either c_{31} or c_{32} is inserted into A.

We call *Instance-to-Class soft edit cost* the measure optimized by I2CEDR over all possible extended traces. Let t be an extended trace between sequence $A = (a_1, a_2, \ldots a_N)$ and a set of sequences $C = \{C_1, C_2, \ldots, C_K\}$ all of them with the same length M, where $C_k = (c_{1k}, c_{2k}, \ldots, c_{Mk})$ for $1 \leq k \leq K$, and a vector ϵ of K matching thresholds. If I and D are the number of positions in A and C respectively left untouched by lines in the extended trace, the Instance-to-Class soft edit cost $i2csec_t(\epsilon, A, C)$ is defined as:

$$i2csec_t(\epsilon, A, C) = I + D + \sum_{(i,j,k)\in t} cost_{edrs}(\epsilon_k, a_i, c_{jk}) \tag{3.18}$$

wher $cost_{edrs}(\cdot)$ is definied as in Equation 3.13.

For a given $\epsilon \in \mathbb{R}^K$, $I2CEDR_\epsilon(A, B)$ is therefore the Instance-to-Class soft edit cost of an extended trace t^* for which the Instance-to-Class soft edit cost is minimum:

$$I2CEDR_\epsilon(A,B) = i2csec_{t^*}(\epsilon, A, B) \tag{3.19}$$

Note that several extended traces may have the same associated Instance-to-Class soft edit cost. For example, let t be an extended trace including the tuple (i,j,k) and ϵ the used vector of thresholds. If $cost_{edrs}(\epsilon_k, a_i, c_{jk}) >= 1$ (that is, the line corresponds to a replacement operation), (i,j,k) can be replaced by any other tuple (i,j,k') for wich $cost_{edrs}(\epsilon_k, a_i, c_{jk'}) >= 1$, with no change in the Instance-to-Class soft edit cost of the extended trace.

To illustrate the benefits of the I2C approach, consider now the following toy example of a nearest-neighbor based sequence classification problem. Sequence $A = (1,1,1,5,5,5)$ has to be classified into one of two classes. Training data includes two sets of sequences C^1 and C^2. The first set has the training data for class 1, namely sequences $C_1^1 = (1.3,1,0.9,2.8,3.1,3)$ and $C_2^1 = (3,3.1,2.9,5,4.9,5)$. The second set has the training data for class 2, namely sequences $C_1^2 = (1,1,1,1,1.1,1.2)$ and $C_2^2 = (1,1,1,1.1,1.2,1)$. Note that class 1 corresponds roughly to sequences consisting of three low numbers (with an approximate value of 2), followed by three larger numbers (with an approximate value of 4). Class 2, on the other hand, is better described by a constant sequence with a value of 1 at each position. It is clear that A should be closer to class 1 than to class 2. However, due to intra-class variations, A is neither really similar (in terms of EDRS distance) to C_1^1 nor to C_2^1. The problem is that the first three numbers of A are noticeably lower that 2, while its last three numbers are noticeably larger than 4. The training sequences in class 1 contain examples where either one or the other of these two things happen, but no both. Just like A, C_1^1 has its first tree values lower than 2 but, unlike A, its last three values are lower than 4. The inverse happens with C_2^1. Its last three values are larger than 4 but its first three values are larger than 2.

As a result, neither C_1^1 nor C_2^1 yield a low EDRS value when compared to A. For example, when using a matching threshold $\epsilon = \min(S_A, S_{C_1^1}) = 1.05$ (S_A and $S_{C_1^1}$ are the sum of the coordinate-wise standard deviations of A and C_1^1 respectively), three operations of cost 1 are required to transform A into C_1^1. Figure 3.4 illustrates this situation.

A	1	1	1	5	5	5
	0.28	0	0.09			
$\mathbf{C_1^1}$	1.3	1	0.9	2.8	3.1	3

$$\mathbf{EDRS(A, C_1^1) = 3.38}$$

(a)

A	1	1	1	5	5	5
				0	0.05	0
$\mathbf{C_2^1}$	3	3.1	2.9	5	4.9	5

$$\mathbf{EDRS(A, C_2^1) = 3.05}$$

(b)

Figure 3.4: Traces and EDRS distances between a query sequence A and two training sequences C_1^1 (3.4a) and C_2^1 (3.4b). The computed distances are larger than expected. See text for description.

Unfortunately, even though the last three points of A are not matched with any point in C_1^2, the first three points of the sequences match exactly, yielding a distance of EDRS distance of 3, which is lower than the values obtained for C_1^1 and C_2^1. The same thing happens with C_2^2. This is illustrated in Figure 3.5. As a consequence, A is classified as part of class 2.

On the other hand, the desired result is obtained if I2CEDR is used instead of EDRS. When computing the I2CEDR distance between A and C^1, the first three elements of A are matched with the first three elements of C_1^1, and the last three elements of A are matched with the last three elements of C_2^1. Even though the number of matches obtained when comparing A with C_1^1 or C_2^1 alone is small, the I2C approach manages to reveal the high similarity between A and C^1. The key is its ability to match points of the query sequence with points from different training sequences. The I2CEDR distance between A and C^2 is the same as the EDRS distance between A and C_1^2 or C_2^2, because none of the sequences in C^2 has large values in the last three positions. Therefore, A is classified as part of class 1. Figure 3.6a

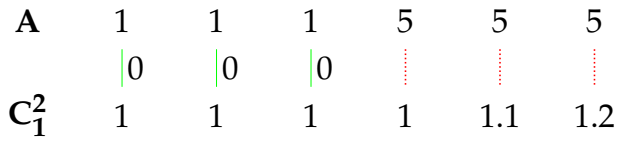

$\mathbf{EDRS}(\mathbf{A}, \mathbf{C_1^2}) = \mathbf{3}$

(a)

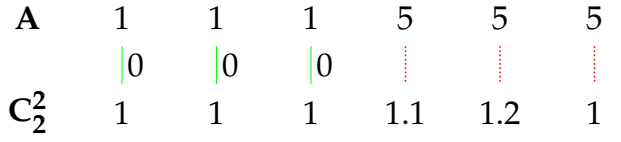

$\mathbf{EDRS}(\mathbf{A}, \mathbf{C_2^2}) = \mathbf{3}$

(b)

Figure 3.5: Traces and EDRS distances between a query sequence A and two training sequences C_1^2 (3.5a) and C_2^2 (3.5b). See text for description.

illustrates the situation.

Similar to EDR, the I2CEDR definition in Equation 3.16 suggests a dynamic programming approach to compute the distance. Given a sequence $A = (a_1, a_2, \ldots, a_N)$ of length N, and a set of sequences $C = \{C_1, C_2, \ldots, C_K\}$, all of them with the same length M, and a vector ϵ of K matching thresholds, we now describe an algorithm implementing such an approach to compute $I2CEDR_\epsilon(A, C)$. Through the description, we use $First(A, m)$ to denote the subsequence obtained by taking the first m elements of A, i.e., given $0 \leq m \leq N$, we define $First(A, m) = (a_1, a_2, \ldots, a_m)$. Moreover, we overload $First$ and use it to denote the the set of sequences resulting from taking the first m elements of each sequence in the set C. That is, given a set of sequences C of the same length M, and $0 \leq m \leq M$ we define $First(C, m) = \{First(C_i, m) | 1 \leq i \leq K\}$.

As with EDR, the algorithm uses a matrix $D \in \mathbb{R}^{(N+1)\times(M+1)\times K}$ indexed from zero to store the cumulative distance. The distance between $First(A, i)$ and $First(C, j)$ is stored at $\arg\min_{1\leq k\leq K} D_{i,j,k}$. Like EDR, the value in $D_{i,j,k}$ can be computed from the values of a set of predecessors. Namely, the follow-

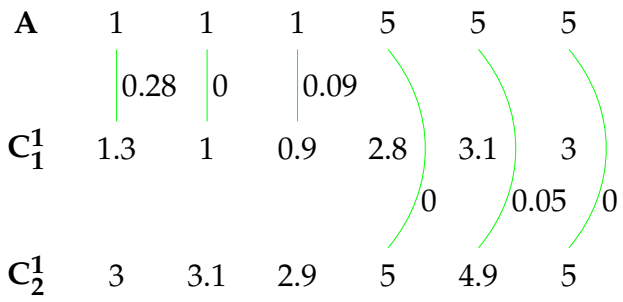

$\mathbf{I2CEDR}(\mathbf{A}, \mathbf{C^1}) = \mathbf{0.43}$

(a)

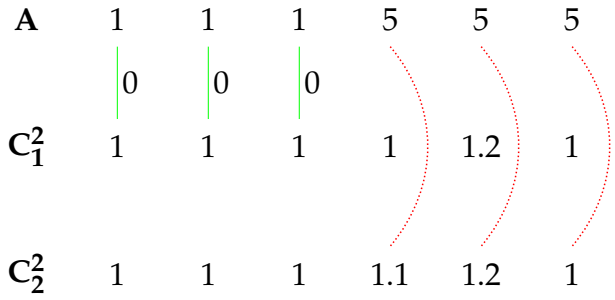

$\mathbf{I2CEDR}(\mathbf{A}, \mathbf{C^2}) = \mathbf{3}$

(b)

Figure 3.6: Extended traces and I2CEDR distances between a query sequence A and two sets of training sequences C^1 and C^2. See text for description.

ing $3K$ values need to be taken into account $D_{\{(i-1,j-1),(i-1,j),(i,j-1)\}\times\{1,\ldots,K\}}$. As with EDR, reusing previous results can be achieved by computing the values of D in a particular order. The value of $I2CEDR_\epsilon(A,C)$ is stored at $\arg\min_{1\leq k\leq K} D_{i,j,k}$. An initialization step sets $D_{0,j,k} = j \;\; \forall\, 0 \leq j \leq M, \;\; 1 \leq k \leq K$ and $D_{i,0,k} = i \;\; \forall\, 1 \leq i \leq N, \;\; 1 \leq k \leq K$. Pseudo-code of the described approach is shown in Algorithm 2.

Algorithm 2 Compute I2CEDR distance

Require: Time series $A = (a_1, a_2, \ldots a_N)$, set $C = \{C_1, C_2, \ldots, C_K\}$ of time series such that $C_i = (c_{1i}, c_{2i}, \ldots, c_{Mi})$, vector $\epsilon \in \mathbb{R}^K$ of matching thresholds.

1: **function** I2CEDR(A, C, ϵ)
2: $D \leftarrow$ *new matrix* $\in \mathbb{R}^{(N+1)\times(M+1)\times K}$
3: $D_{0,j,k} = j \;\; \forall\, 0 \leq j \leq M, \;\; 1 \leq k \leq K$
4: $D_{i,0,k} = i \;\; \forall\, 0 \leq i \leq N, \;\; 1 \leq k \leq K$
5: **for** $i \leftarrow 1, N$ **do**
6: **for** $j \leftarrow 1, M$ **do**
7: $ins \leftarrow \min D_{\{(i,j-1)\}\times\{1,\ldots,K\}}$
8: $del \leftarrow \min D_{\{(i-1,j)\}\times\{1,\ldots,K\}}$
9: $mr \leftarrow \min D_{\{(i-1,j-1)\}\times\{1,\ldots,K\}}$
10: **for** $k \leftarrow 1, K$ **do**
11: $mr \leftarrow mr + cost_{edrs}(\epsilon_k, a_i, c_{jk})$
12: $D_{i,j,k} \leftarrow \min(ins, del, mr)$
13: **end for**
14: **end for**
15: **end for**
16: **return** $\min D_{\{(N,M)\}\times\{1,\ldots,K\}}$
17: **end function**

The algorithm has three nested loops. The two outer loops traverse the N positions of A and the M positions of the sequences in C. The inner loop traverse the K sequences in C. Besides the inner loop, three minimum searches among K elements are performed for each position (i, j). All of the remaining steps have a temporal complexity of $\mathcal{O}(1)$. The time complexity

of the algorithm is thus $\mathcal{O}(MN(4K)) = \mathcal{O}(MNK)$, which can be reduced to $\mathcal{O}(MN)$ when $K \ll \min(M, N)$, as often happens in many real world action recognition tasks.

3.2.3 Action recognition with I2CEDR

In this section we describe our proposed action recognition method based on I2CEDR. The method classifies a query video based on its similarity with several sets of labeled videos (the training data).

As explained in Section 1.1.1, the posture of the actor at a specific instant is given by a skeleton, consisting of the 3D coordinates of a set of body joints. If we let J be the number of joints, then a skeleton contains the location information of each joint j, i.e. $l_j = (x_j, y_j, z_j)$ where $1 \leq j \leq J$. A sequence of skeletons serves in turn as the raw representation of an action execution, encoding the temporal evolution of the actor's pose.

Several transformations are applied to this basic raw representation to make it more suitable for action classification. This section makes explicit those transformations and details the classification procedure for a new skeleton sequence.

Skeleton normalization

In order to achieve scale, translation and orientation invariance, three normalizations proposed in [VAC14] are applied to the raw skeleton data.

Translation invariance is achieved by subtracting from each joint location the location of the hip center. This effectively express the posture information in hip-centered coordinate system, abstracting from the relative locations of the actor and the camera.

The second normalization concerns body sizes. The lengths of the segments connecting adjacent joints (limbs) in a skeleton depends on the considered subject. This fact increases intra-class variability, making action recognition more difficult. As this information is not relevant for determining the performed action, we impose the same limbs lengths for all the skeletons. To this end, we take one skeleton from the training data as ref-

erence, and modify the joint locations in the rest of the skeletons in such a way that their limbs have the same lengths as the reference skeleton, but without changing the angles between the limbs. Recall from Section 1.1.1 that a skeleton can be seen as a tree. Starting from a root joint in the tree, the employed procedure moves down the branches modifying each joint location, such that the length of the affected limb becomes the same as in the reference skeleton, while preserving its direction.

To further gain orientation invariance, we rotate the skeletons such that the x-component of the vector joining the left hip with the right hip has the same direction as the x-axis.

Skeleton descriptor

Skeleton data can be used directly for classification. However, using a skeleton descriptor instead tends to improve the performance. An action execution is therefore better represented by a sequence of skeleton descriptors.

As commented in Section 2.1.1, many interesting skeleton descriptors have been proposed in the past. In this work, we compute the pairwise relative position of the joints (RJP), a popular option that has been used many times before [VAC14, YT12, WLWY12a, CZN+11]. The following paragraphs explain the descriptor.

Recall that given a joint $1 \leq j \leq J$, its (normalized) 3D location is $l_j = (x_j, y_j, z_j)$. The descriptor d_j for joint j is computed by taking the difference between l_j and l_i, for any $1 \leq i \leq J \ \wedge \ i \neq j$:

$$d_j = (d_{j1}, d_{j2}, \ldots, d_{j(j-1)}, d_{j(j+1)}, \ldots, d_{jJ}) \tag{3.20}$$

where $d_{ji} = l_j - l_i$.

Note that d_j is a $3(J-1)$ length vector. The RJP descriptor is a $3(J-1)J$ length vector, obtained by concatenating the descriptors of the J joints:

$$d = (d_1, d_2, \ldots, d_J) \tag{3.21}$$

Relative positions describe human posture more naturally than raw joint locations. For example, the statement "hand next to the head" is an intuitive

way of describing the action *talking on the phone*. In practice, this descriptor has stand out as a discriminative feature, and offered satisfactory performance in many previous works.

Sequence length standardization

Recall from Equation 3.16 that I2CEDR distance is defined for a sequence A and a set of sequences C, *all of the same length*. Thus, the length of the skeleton descriptor sequences need to be standardized in the training data to allow for the use of I2CEDR. Specifically, for every action in the considered dataset, sequences labeled with that action have to be brought to the same number of skeleton descriptors. We now describe how this is done in this work.

Let $C^i = \{C^i_1, C^i_2, \ldots, C^i_{K^i}\}$ be the set of skeleton descriptor sequences labeled with action i. The *standarized length* M^i for class i is chosen to be the average length of all the sequences in C^i:

$$M^i = \frac{\sum_{k=1}^{K^i} |C^i_k|}{K^i} \tag{3.22}$$

where $|\cdot|$ denotes length.

For a given i and k, with $1 \leq k \leq K^i$ sequence $C^i_k = (C^i_{1k}, C^i_{2k}, \ldots, C^i_{|C^i_k|k})$, consisting of $|C^i_k|$ descriptors is transformed into a new sequence $C^{i\prime}_k = (C^{i\prime}_{1k}, C^{i\prime}_{2k}, \ldots, C^{i\prime}_{M^ik})$ of length M^i. This is achieved by applying a simple coordinate-wise cubic spline interpolation [DB78], which is explained next.

As described in Equation 3.21, each skeleton descriptor is a $3(J-1)J$ length vector, where J is the number of joints. For any given $1 \leq c \leq 3(J-1)J$, consider the real sequence $C^i_k(c) = (C^i_{1k}(c), C^i_{2k}(c), \ldots, C^i_{|C^i_k|k}(c))$ obtained by retaining only coordinate c from each skeleton descriptor in C^i_k. A cubic spline S is fit to the values in $C^i_k(c)$. The cubic spline S is a peacewise function:

$$S[x] = \begin{cases} S_1[x] \;\; for \;\; 1 \leq x \leq 2 \\ S_2[x] \;\; for \;\; 2 \leq x \leq 3 \\ \dots \\ S_{|C_k^i|-1}[x] \;\; for \;\; |C_k^i| - 1 \leq x \leq |C_k^i| \end{cases} \tag{3.23}$$

where each S_t, for $1 \leq t \leq |C_k^i| - 1$, is a cubic polynomial.

Fitting the spline means finding the coefficients of S_t for $1 \leq t \leq |C_k^i| - 1$ that let S fulfill certain conditions. The first set of conditions requires that S equals $C_k^i(j)$ at $1 \leq t \leq |C_k^i|$:

$$S_t[t] = C_k^i(j)[t] \;\; \wedge \;\; S_t[t+1] = C_k^i(j)[t+1] \qquad \forall \;\; 1 \leq t \leq |C_k^i| - 1 \tag{3.24}$$

The second set of conditions intends to make S smooth, by equating the first and second derivatives of adjacent polynomials at the internal points:

$$S_t'[t+1] = S_{t+1}'[t+1] \;\; \wedge \;\; S_t''[t+1] = S_{t+1}''[t+1] \qquad \forall \;\; 1 \leq t \leq |C_k^i| - 2 \tag{3.25}$$

Finally, the second derivatives are required to equal zero at the endpoints. These conditions lead to a linear system that can be easily solved to find the polynomials coefficients.

The resulting spline is used to find the values in $C_k^i(c)'$, the transformed 1-dimensional sequence of standardized length M^i. For example, the f^{th} value in $C_k^i(c)'$, with $1 \leq f \leq M^i$ is found by evaluating S at $f\frac{|C_k^i|}{M^i}$.

Choice of the matching threshold

Recall from Equation 3.16 that the I2CEDR distance between a sequence A and set of sequences $C = \{C_1, C_2, \dots, C_K\}$ depends on a vector $\epsilon \in \mathbb{R}^K$ of matching thresholds. The values in ϵ play a crucial role in determining the cost of the considered edit operations, as seen in equations 3.13 and 3.17.

In all our experiments we use the following formula to obtain the value of ϵ_k for a given $1 \leq k \leq K$:

$$\epsilon_k = \min(\Psi(A), \Psi(C_k)) \tag{3.26}$$

where given a sequence A of d dimensional points, $\Psi(A)$ is the sum of the coordinate-wise standard deviations of A:

$$\Psi(A) = \sum_{c=1}^{d} \sigma_{A(c)} \tag{3.27}$$

In Equation 3.27 $\sigma_A(c)$ denotes the standard deviation of the sequence obtained by retaining only coordinate c from the points in A. For clarity, in the following we omit the ϵ when mentioning EDR, EDRS and I2CEDR.

Video classification procedure

The ultimate goal of the presented method is to predict the action label of a query video, based on the available training data. Training data consists in turn of several videos, each of them with an assigned action label.

As refreshed at the beginning of Section 3.2.3, actions are represented as sequences of skeletons. Thus, our method attempts to classify a query skeleton sequence based on several training skeleton sequences. Raw training data is preprocessed using the techniques explained before in this section: normalization, descriptor computation and length standardization. When labeling a query skeleton sequence A, the first two techniques are also applied to A before classification. Therefore, action prediction for a query sequence A consists of three steps:

1. Obtain a sequence of normalized skeletons by normalizing each skeleton in A,
2. Obtain a sequence of skeleton descriptors by computing a descriptor for each skeleton normalized in the previous step,
3. Classify the sequence of skeleton descriptors obtained in the previous step.

Training sequences are organized in sets, according to their label. If L is the number of possible action labels, the training data consists of L sets C^i

for $1 \leq i \leq L$. Step 3 above classifies a sequence A of skeleton descriptors by comparing it with each of the L sets. The comparison between A and a given set C^i is done by computing the $I2CEDR$ distance between them. A possible classification approach is therefore obtained by choosing the predicted action label l^* as:

$$l^* = \arg\min_{1 \leq i \leq L} I2CEDR(A, C^i). \tag{3.28}$$

Multi-part approach

Following a trend used in several works [WLWY12a,SVB+13,WWY13], this basic classification approach is improved by grouping skeleton joints into *body parts*, and solving the problem stated in Equation 3.28 for each part.

Specifically, joints are grouped into five body parts. As an example, part 4 consists of the joints 13 (right hip), 14 (right knee), 15(right ankle) and 16 (right hip), thus corresponding to the right leg. Recall from equations 3.20 and 3.21 that a skeleton descriptor is a $3(J-1)J$ length vector $d = (d_1, d_2, \ldots, d_J)$, where J is the number of joints in the skeleton and d_i is the $3(J-1)$ length vector corresponding to joint i. For a given set p, we define a function f_p that, given a skeleton descriptor, it preserves the coordinates associated with joints in p, and discards the rest. Formally, if $p = \{p_1, p_2, \ldots, p_z\}$ is a set of z integers such that $1 \leq p_i \leq J \ \ \forall\ 1 \leq i \leq z$, f_p is a function $f_p : \mathbb{R}^{3(J-1)J} \rightarrow \mathbb{R}^{3(J-1)z}$ such that:

$$f_p((d_1, d_2, \ldots, d_J)) = (d_{p_1}, d_{p_2}, \ldots, d_{p_z}) \tag{3.29}$$

We overload f_p to describe a function that takes a sequence of skeleton descriptors $A = (a_1, a_2, \ldots, a_N)$ and applies f_p to each of them:

$$f_p(A) = (f_p(a_1), f_p(a_2), \ldots, f_p(a_N)) \tag{3.30}$$

Further, given a set of skeleton descriptors sequences $C = \{C_1, C_2, \ldots, C_K\}$, we overload f_p as:

$$f_p(C) = \{f_p(C_1), f_p(C_2), \ldots, f_p(C_K)\} \tag{3.31}$$

The multi-part approach determines the predicted action label l^* as:

$$l^* = \arg\min_{1 \leq i \leq L} \sum_{p \in P} \frac{I2CEDR(f_p(A), f_p(C^i))}{G_p(A)} \tag{3.32}$$

where $G_p(A)$ is a normalization factor, defined as:

$$G_p(A) = \sum_{i=1}^{L} I2CEDR(f_p(A), f_p(C^i)) \tag{3.33}$$

3.3 Results

In this section we detail and discuss experimental results for the proposed action recognition method. In our evaluation, we use 4 different datasets: MSRDailyActivity3D, MSRAction3D, UTKinect and Florence3D. See section 2.2 for a thorough description of the datasets.

3.3.1 Evaluation of the proposed EDR extensions

In Section 3.2.2, we present two extensions to original ERD distance. The first one introduces a soft matching mechanism between points. Allegedly, this results in a more accurate distance measure (EDRS), since it can now capture smaller differences between sequences. The second one incorporates the idea of computing I2C distances to EDRS. We argue that the resulting distance measure (I2CEDR) brings improved performance to nearest neighbor sequence classification in cases of large intra-class variability and small training sets.

In order to support these claims, we experimentally compare the three distance measures (EDR, EDRS and I2CEDR) for the problem of action classification. Both EDR and EDRS are tested on a classical nearest neighbor classification scheme: query videos are assigned the action label of the closest (according to EDR or EDRS) video. On the other hand, I2CEDR is tested using the instance-to-class scheme explained in Section 3.2.3. We further include a fourth variant in the comparison, corresponding to the multi-part method described in Section 3.2.3, to evaluate the benefits of using I2CEDR for that approach.

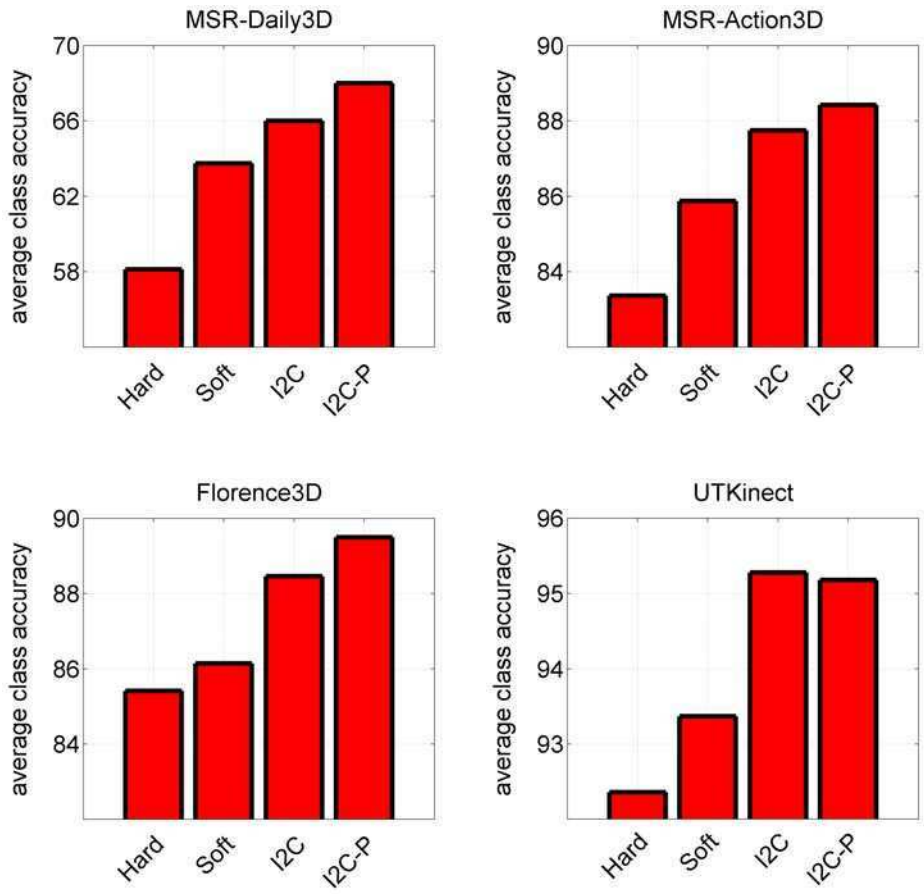

Figure 3.7: Evaluation of the proposed EDR extensions. The original EDR distance is referred to as *Hard*, while *Soft* and *I2C* denote EDRS and I2CEDR respectively. The term *I2C-P* denotes the use of I2CEDR combined with the multi-part approach. See text for details.

Figure 3.7 shows the average class accuracy of the compared variants, for the four considered datasets. The original EDR distance is referred to as *Hard*, reflecting the fact that a hard mechanism is used for point matching. The soft matching extension EDRS is noted by *Soft*. *I2C* indicates in turn the instance-to-class extension I2CEDR. Lastly, *I2C-P* denotes the use of I2CEDR combined with the multi-part approach.

The figure show that EDRS consistently outperforms EDR on every considered dataset, in some cases by a remarkable amount. Likewise, I2CEDR outperforms EDRS in every case. The multi-part approach gives some improvement in every database, except in UTKinect. Results support our be-

lief that the extensions introduced in Section 3.2.2 enhance the original EDR distance. Moreover, they suggest that performance can be further benefited by using them in conjunction with the multi-part approach of Section 3.2.3.

3.3.2 Comparison of the proposed EDR extensions with other elastic matching similarity measures

In order to compare EDRS and I2CEDR with other elastic similarity measures between sequences, we implemented four other distance functions, and use them for action classification. Among the considered functions, two of them (the classical Frechet and DTW) are more related to EDRS than to I2CEDR, in the sense that they compute distances between two sequences. As such, they are used in a classic Instance-to-Instance nearest neighbor classification scheme. The other two are Instance-to-Class versions of the formers, and thus more related to I2CEDR. They are *Instance-to-Class Frechet* (I2CFrechet) and *Instance-to-Class Dynamic Time Warping* (I2CDTW). I2CDTW was originally proposed in [WLL+14] for the problem of face recognition.

Figure 3.8 shows the average class accuracy obtained with each distance function for the four considered datasets.

Frechet obtains the worst performance on every dataset. This is expected (see Section 3.2.1) since its dependence on a maximum measure makes it very sensitive to noise and outliers, which tend to be frequent in sequences of skeleton descriptors. The I2C extension of Frechet shows better results, although the improvement over the I2I version varies depending on the dataset. Moreover, it is consistently outperformed by the classical I2I DTW, suggesting that the replacement of the maximum measure by a sum measure is more beneficial for performance than the switch from an I2I to an I2C approach. Regarding our proposed distance functions, the I2CEDR based method consistently yields the best performance. Further, EDRS is only surpassed by I2CEDR (on every dataset) and I2CDTW (on two of the datasets). EDRS outperforms DTW on every dataset, supporting the effectiveness of distance quantization combined with soft thresholding.

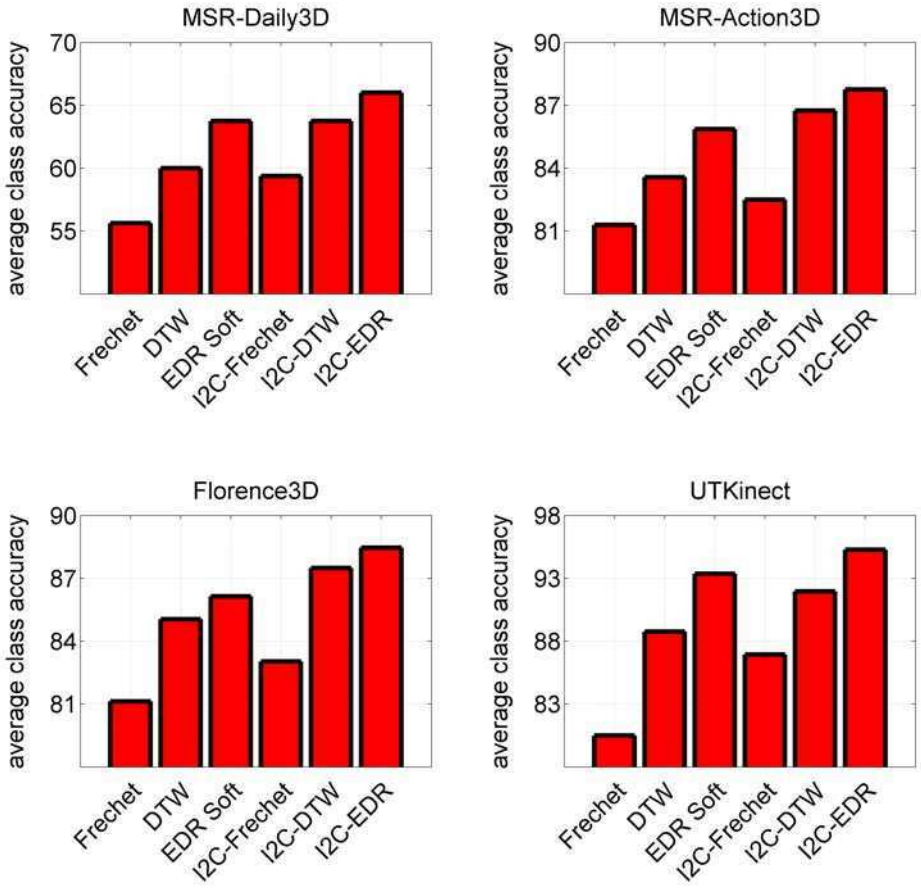

Figure 3.8: Comparison of I2CEDR with other elastic matching similarity measures. The presented functions EDRS (referred as *EDR Soft*) and I2CEDR (referred as *I2C-EDR*) are compared with four other measures: Frechet, Dynamic Time Warping (*DTW*), Instance-to-Class Frechet (*I2C-Frechet*) and Instance-to-Class Dynamic Time Warping (*I2C-DTW*). See text for details.

It is worth noting that all the results correspond to the basic single-part classification approach. For simplicity, the multi-part approach described in Section 3.2.3 was no used for these experiments.

The results support the claim about the superiority of our method for action classification with respect to methods using on other sequence distance functions.

3.3.3 Robustness analysis

In this section we detail a number of experiments aimed at testing the robustness of the proposed action recognition method. First, we analyze the effect of adding independent identically distributed white noise to the skeletons. Then, we study the impact of local temporal shifts in the sequences.

Our approach is compared with several other methods, based on different modelings of the temporal information. Besides the methods based on distance functions over raw sequence representations considered in Section 3.3.2 (Frechet, DTW, I2CFrechet and I2CDTW), two other approaches are included in the comparison: Fourier Temporal Pyramids (FTP) from [WLWY12b], and Hidden Markov Model (HMM) from [LN06]. See Section 2.1.1 for a description of the methods. In every case, the optimal parameters for FTP and HMM were found by leave-one-actor-out cross-validation (see Section 2.2 for a description of the technique) on the training actors.

Experiments were carried out for two datasets: MSRDailyActivity3D and UTKinect. In both cases, we show the relative accuracy obtained by each of the tested methods, which is defined as the ratio between the average class accuracy under the perturbed scenario and the average class accuracy under the non-perturbed scenario.

Robustness to noise

We evaluated the robustness of the proposed approach to noise, along with that of several other methods. For this purpose, we corrupted the skeletons by adding noise from a Gaussian distribution with mean zero and variance one. We compute the relative accuracy of each method for different amounts

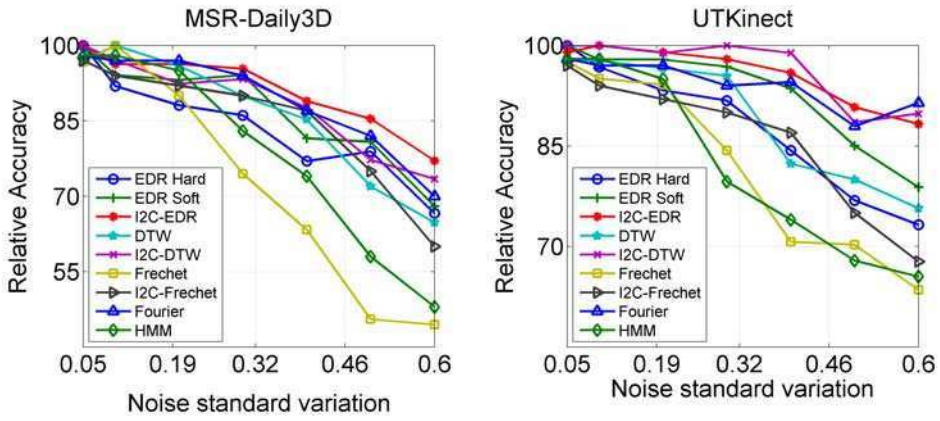

(a) (b)

Figure 3.9: Relationship between the relative accuracy and the noise standard variation for several methods on two datasets: MSRDailyActivity3D (3.9a) and UTKinect (3.9b).

of noise, and studied the resulting behaviors.

Figure 3.9 shows the results for the two considered datasets. While, as expected, relative accuracy decays with noise in every case, the degree in which this happens varies depending on the method. Moreover, results on MSRDailyActivity3D are generally worse than results on UTKinect, which is reasonable considering that the former is a more challenging dataset.

Frechet exhibits the worst behavior in terms of robustness. The negative effects of the maximum measure employed by this distance are evidenced once again. Its I2C version (I2CFrechet) achieves some improvement on the MSRDailyActivity3D dataset, although it shows less robustness than most of the other methods. Hidden Markov Model results almost as sensitive to noise as Frechet, presumably because of the instability of the procedure used by HMM to compute the hidden states. DTW and EDR (indicated as *EDR Hard* in the figure) offer similar robustness, suggesting that the quantization of point distances is not, by itself, enough to make of EDR a more robust measure than DTW. On the other hand, the incorporation of the soft matching mechanism seems to give EDR the edge over DTW in terms of robustness, as EDRS shows larger relative accuracy than DTW for most of the scenarios. Fourier Temporal Pyramid, I2CDTW and I2CEDR stand out as

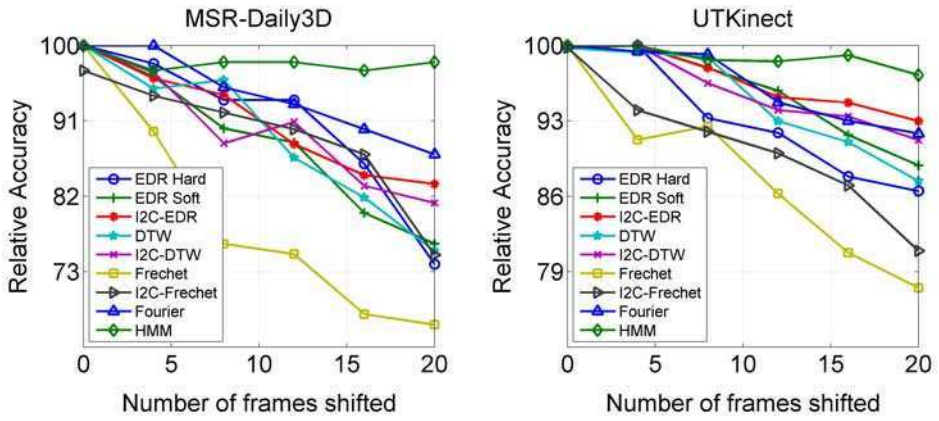

(a) (b)

Figure 3.10: Relationship between the relative accuracy and the temporal misalignment for several methods on two datasets: MSRDailyActivity3D (3.10a) and UTKinect (3.10b).

the most robust methods according to the tests. Dropping the Fourier coefficients associated to high frequency components makes Fourier Temporal Pyramid highly resilient to noise. The increased robustness of I2CDTW and I2CEDR with respect to its I2I versions comes presumably from their ability to match points from different sequences within a sequence set, thus mitigating the effects of noisy points.

Robustness to temporal misalignment

To test the robustness of our method to temporal misalignment, we circularly shifted every skeleton descriptor sequence in the training data. The (uncorrupted) testing data was classified by a given method several times, each corresponding to a different number of shifted frames. Again, we compare the relative accuracy of our approach with that of the other methods.

Figure 3.10 shows the results for the two datasets. Accuracy deteriorates for most of the methods as the number of shifted frames increases. The exception is HMM, which achieves almost the same accuracy for every scenario. This was expected as it is well known that HMM performance does not depend on the sequences being aligned. A variety of behaviors is observed for the rest of the methods.

Frechet once again gives the worst results on both datasets. This can also be attributed to the instability caused by the maximum computation. DTW, EDR, and EDRS show roughly the same robustness. This makes sense, as the main difference between the three methods does not lie in the ability to deal with time shifting. A similar reasoning can be used to explain the behavior of I2CEDR and I2CDTW. While achieving slightly better results than their I2I versions for 15 and 20 shifted frames, they show nearly the same robustness than those methods in most of the scenarios. FTP shows considerable robustness in every case, thanks to its usage of the frequency domain. Overall, we see that the proposed I2CEDR shows considerable tolerance to temporal misalignment and stands out as one of the more robust methods among the compared approaches.

3.3.4 Comparison with the state-of-the-art

In this section, we compare the results obtained by our proposed action recognition approach with those of several state-of-the-art methods. In order to make a fair comparison, we only consider those works focusing on skeleton-based action classification. That is, we do not include results corresponding to methods employing depth or RGB information.

Table 3.1 shows the average class accuracy of each method for the four considered datasets. In comparison to the state-of-the-art our method is able to be on par with previously reported results, achieving competitive performance on the four datasets. On the Florence3D dataset, it even outperforms the best accuracy known to us (85.20%) by 4.30%. On the rest of the datasets, it is among the top performing approaches.

It is worth mentioning that many of the methods referenced in Table 3.1 ([CPLFR13, YT12, XCA12, ATSS15, SVB+13]) use skeleton descriptors different to the RJP (described in Section 3.2.3) employed in our approach, as well as different preprocessing techniques. For example, [CPLFR13] considers a descriptor that extends RJP with joint offset and velocity information, [YT12] further improves that descriptor by applying Principal Component Analysis (PCA), [XCA12] uses histograms of joints positions, and [SVB+13]

MSRDailyActivity3D dataset	
Fourier Temporal Pyramid [WLWY12b]	68.00
Weakly-aligned Bag of Poses [SVB+13]	70.00
Proposed method	68.00

MSRAction3D dataset	
Hidden Markov Model [XCA12]	78.97
Naive-Bayes-Nearest-Neighbor [YT12]	82.30
Joint Angle Similarities [OBT13]	83.53
Elastic Functional Coding [ATSS15]	85.16
Fourier Temporal Pyramid [WLWY12b]	88.20
DTW Nominal Curve + FTP [VAC14]	88.23
Bag of Temporal and Spatial Part-Sets [WWY13]	90.22
Random Forest [ZCG13]	90.90
Recurrent Neural Networks [DWW15]	94.49
Proposed method	88.42

UTKinect dataset	
Random Forest [ZCG13]	87.90
Hidden Markov Model [XCA12]	90.92
Elastic Functional Coding [ATSS15]	94.87
DTW Nominal Curve + FTP [VAC14]	95.58
Proposed method	95.28

Florence3D dataset	
Weakly-aligned Bag of Poses [SVB+13]	82.00
DTW Nominal Curve + FTP [VAC14]	85.20
Proposed method	89.50

Table 3.1: Comparison of the proposed approach with the state-of-the-art.

models the human torso as a rigid part, expressing the position of the joints in a coordinate system derived from the torso orientation. Therefore, Table 3.1 should be approached with caution in terms of temporal modeling comparison, as the differences in accuracies may be caused by several other factors. Nevertheless, the table shows that the proposed method can yield very satisfactory results, and encourages the use of the I2CEDR distance for action recognition based on skeleton sequences.

3.4 Resumen

En este capítulo se presenta el primero de los dos métodos propuestos en la tesis para el reconocimiento de acciones en videos de profundidad. El mismo está basado en una nueva técnica para comparar secuencias, obtenida como resultado de dos modificaciones a una conocida medida de similaridad entre secuencias.

La sección 3.1 presenta un repaso general a los enfoques elegidos por trabajos anteriores para modelar la evolución temporal de secuencias de esqueletos. Dicho repaso analiza los principales defectos de los métodos descriptos y sirve como motivación para presentar el enfoque propuesto en la tesis.

La sección 3.2 presenta la nueva técnica para comparar secuencias y el método de reconocimiento de acciones basado en ella. Primero (sección 3.2.1), se repasan varias técnicas clásicas para comparación de secuencias, poniendo especial énfasis en un grupo de técnicas que calcula la distancia entre secuencias buscando el mejor (de acuerdo a una determinada función de costo) alineamiento posible entre los puntos de las secuencias comparadas. Entre ellas se encuentra la medida conocida como *Edit Distance on Real sequence* (EDR), que tiende a ser más precisa y más robusta al ruido que otras técnicas del grupo. La sección 3.2.2 introduce la técnica propuesta en la tesis, obtenida mediante dos modificaciones clave a EDR. La primera consiste en la introducción de una función de costo *suave* para el alineamiento de puntos, que apunta a hacer de EDR una medida más precisa, permitiendo caracterizar diferencias más sutiles entre los puntos alineados. La segunda

modificación incorpora la noción de distancia *Instancia-a-Clase* (I2C, por el término en inglés *Instance-to-Class*) a EDR, y permite alinear puntos de la secuencia a clasificar con puntos pertenecientes a distintas secuencias, mejorando la capacidad de generalización de clasificadores no-paramétricos en casos de alta variabilidad intra-clase y pocos datos de entrenamiento. Al ser derivada a partir de EDR, la técnica propuesta tiene especialmente el ordenamiento temporal a la hora de alinear puntos. Como un beneficio adicional, no requiere aprendizaje de parámetros. La sección 3.2.3 describe el método propuesto para reconocimiento de acciones basado en secuencias de esqueleto. El método clasifica una secuencia dada basándose en la similaridad de la misma con varios conjuntos de secuencias de entrenamiento. Dicha similaridad es medida utilizando la técnica propuesta en la sección 3.2.2. La sección detalla el modo exacto en que la técnica es usada, así como varios preprocesamientos aplicados a las secuencias originales de esqueletos antes de la clasificación.

La sección 3.3 presenta los resultados de los experimentos realizados con el método propuesto en cuatro bases de datos. En particular, se evalúan las mejoras obtenidas respecto de métodos basados en EDR y en otras medidas de alineamiento de secuencias. Además, se evalúa la robustez del método respecto al ruido y al desfasaje temporal. Por último, se compara el rendimiento del mismo con el estado del arte.

Chapter 4

Action recognition using Citation-kNN on bags of time-stamped poses

This chapter describes the second novel method for action recognition presented in the thesis. Its main feature is a new Multiple Instance Learning (MIL) approach to the problem. Section 4.1 explains the reasoning behind the MIL approach. Section 4.2 reviews MIL concepts needed to understand our proposal and presents the action recognition method. Finally, Section 4.3 experimentally evaluates our method and compares it with the state-of-the-art.

4.1 Introduction

As discussed in Section 1.1.1, modeling the temporal evolution of skeleton descriptors is a challenging task, due mainly to the noisy joints, and the inherently large intra-class variability/inter-class similarity (in skeleton spatial configurations as well as in execution speed and temporal misalignment). This challenges have been addressed in a variety of ways in previous works. Sections 1.1.1 and 3.1 detail many of the existent approaches to the problem.

Most of those approaches attempt to capture the main features of the

temporal evolution in a single representation, either by training a model or classifier specifically suited for time series, by using distance functions appropriate for temporal patterns, or by computing a high level description of the temporal sequence based on the individual skeletons. In doing so, they face the challenges commented above. The proposed representation has to be general enough as to abstract away the inherent intra-class variability and the noisy skeletons, and, at the same time, it has to be able to discriminate between very similar sequences corresponding to different actions. The proposed solutions are typically sophisticated, highly hand-crafted and require a lot of tuning.

In contrast, we explicitly acknowledge that the number of discriminative skeletons in a sequence might be low. The rest of the skeletons might be noisy, correspond to subject-specific poses, occur at uncommon frames, or have a configuration common to several actions (for example, a *sit still* configuration). In other words, we know that certain actor poses, when occurring at specific times, provide discriminative information about the performed action. But we do not know exactly which poses (in terms of configuration and time location) those are. At the same time, many other poses may provide no information, or may even be misleading or ambiguous.

Thus, the problem can be naturally treated as a Multiple Instance Learning (MIL) problem. In MIL, training instances are organized into bags. A bag from a given class contains some instances that are characteristic of that class, but might (and most probably will) contain instances that are not. Following this idea, we represent videos as bags of time-stamped skeleton descriptors, and we propose a new framework based on Citation-kNN [WZ00] for action recognition.

Approaching the task using a MIL framework allows our method to condense all the descriptors in a loose representation to decide the sequence class. As long as a few representative descriptors occur at the right time, the query video has a good chance of being correctly classified. We found that our approach is effective in dealing with the large intra-class variability/inter-class similarity nature of the problem. The proposed framework is simple and provides a clear way or regulating tolerance to noise and temporal mis-

alignment.

To the best of our knowledge we are the first to use Citation-kNN for this problem. MIL has been considered before [YHC+12] for skeleton-based action recognition. However, their main reason for using a MIL approach is the presence of irrelevant actions in the videos as a consequence of inaccurate manual segmentation. Furthermore, their goal is the classification of actions involving two people. On the other hand, we aim at exploring the MIL ability to deal with the large intra-class variability/inter-class similarity of the single-person action recognition problem.

Experimental results support the validity of the proposed approach. Extensive tests on four datasets verify the robustness of our method and show that it compares favorably to other state-of-the-art action recognition methods.

4.2 Recognizing actions with Citation-kNN on bags of time-stamped poses

This section describes the Multiple Instance Learning (MIL) approach proposed for skeleton-based action recognition. Sections 4.2.1 and 4.2.2 review MIL and Citation-kNN, the specific MIL method used by our approach. Section 4.2.3 presents a modified version of Citation-kNN. Finally, Section 4.2.4 presents our method for action recognition based on Citation-kNN.

4.2.1 Multiple Instance Learning

Multiple Instance Learning (MIL) is a variant of supervised machine learning in which the training examples come in the form of *bags*. A bag is a set of feature vectors, called *instances*. Each training bag has, as in traditional supervised learning, an assigned class label. The goal is to learn a model capable of predicting class labels for unseen query bags. Note how this setting considerably differs from classical single instance supervised learning, in which training data is organized as individual feature vectors, and a class label is available for each vector. Following the usual procedure in

the literature, we present MIL as a binary classification task. Multiple-class classification can be obtained following typical one-vs-one or one-vs-rest strategies [Bis06], although other approaches are possible (see for example our proposed method in Section 4.2.4).

More formally, a bag is defined as a set of instances $X = \{x_1, \ldots, x_M\}$ where each of the instances x_i is a vector in a d-dimensional space, i.e. $x_i \in \mathbb{R}^d \quad \forall \quad 1 \leq i \leq M$. The goal in MIL is to learn a classification function $\mathcal{C}(X) \in [0, 1]$ that predicts 1 if and only if X is estimated to be positive. The training set $\mathcal{T} = \{(X_1, y_1), \ldots, (X_N, y_N)\}$ consists of N bags and its labels. For each bag X_i, its label $y_i \in \{0, 1\}$ indicates whether X_i is positive ($y_i = 1$) or negative ($y_i = 0$).

A variety of approaches to the MIL task have been proposed over the years [DLLP97, MLP98, WFP03, ZG01, ATH02, ZX07, CBW06, Don06]. Every method relies on a specific assumption about the relationship between a bag label and the instances within that bag. Early works [DLLP97, MLP98] assume that every instance has an assigned hidden label, and that every bag with a positive label contains at least one positive instance. Further, negative bags do not contain any positive instances. This assumption is known as the *standard MI assumption*. A considerable part of the most recent works [WFP03, SZB05, CBW06, Don06], however, relaxes this assumption. In particular, the approach used in this work (see Section 4.2.2) is based on the very loose assumption that bags that are similar according to a given distance measure are likely to have the same class label. The key aspect of the approach is, of course, the distance measure considered for comparing bags.

4.2.2 Citation-kNN

Citation-kNN is presented in [WZ00] as a way of adapting the *k-Nearest Neighbors* (kNN) approach to the multiple instance task. In the single instance variant of kNN, traditional distance functions such as L_p norms can be used to compare examples. In MIL though, proper distance functions between bags have to be used instead. Moreover, the usual kNN method for

selecting the label of a query example based on the majority class of the closest neighbors may not lead to good classification results. Therefore, other ways of combining the labels of the nearest bags have to be considered.

The chosen distance function in Citation-kNN is a modified version of the Hausdorff distance. Given two set of points $A = \{a_1, \ldots, a_M\}$ and $B = \{b_1, \ldots, b_N\}$, the Hausdorff distance is defined as:

$$H(A, B) = \max(h(A, B), h(B, A)) \tag{4.1}$$

where

$$h(A, B) = \max_{a \in A} \min_{b \in B} \|a - b\| \tag{4.2}$$

and $\|\cdot\|$ is a norm on the points of A and B.

The function $h(A, B)$ is known as the *directed Hausdorff distance* from A to B. If we denote by a the point in A that is farthest from any point in B, then $h(A, B)$ is the distance from a to its nearest neighbor in B. Note that if $h(A, B) = d$, then each point of A is within distance d of at least one point in B and, further, there is some point in A that is exactly at distance d from its nearest neighbor in B. For future reference, we call A the *source set* and B the *target set*.

The Hausdorff distance measures the degree in which the compared sets A and B differ from one another. It does it by measuring the distance of the point in A that is farthest from any point in B and vice versa. A Hausdorff distance of d indicates that every point in A is within distance d from some point in B, and that every point in B is within distance d from some point in A. Therefore, two sets are similar if each point in one set is close to some point in the other set, and vice versa.

A small Hausdorff distance is obtained if and only if every point of one set is near some point of the other set. Thus, a single outlier can severely distort the distance. In order to increase its robustness with respect to outliers, a modified version of the distance is used in [WZ00]. The modified measure considers a different function for the directed Hausdorff distance from A to B, $h(A, B)$. Specifically, each point in A is *ranked* by the distance to its nearest point in B, and the R-th ranked such point determines the modi-

fied distance. Formally, if M is the number of points in A and $1 \leq S \leq M$, $h_S(A, B)$ is defined as:

$$h_S(A, B) = \underset{a \in A}{S^{th}} \min_{b \in B} \|a - b\|, \tag{4.3}$$

where $\underset{a \in A}{S^{th}}$ is the S-th ranked distance in the set of distances (one for each element in A).

The value of S is usually defined indirectly by specifying a fraction $0 \leq K \leq 1$ of the points in A. Therefore, after ranking each of the M points in A by the distance to its nearest point in B, the value corresponding to position $S = \max(\lfloor KM \rfloor, 1)$ of the ranking is the modified directed distance. Note that when $K = 1$, the largest distance in the ranking is used, and thus $h_S(A, B)$ is the same as $h(A, B)$. On the other hand, when $K \leq \frac{1}{M}$, the minimal of the M point distances decides the modified directed distance.

The modified Hausdorff distance is given by:

$$H_{SL}(A, B) = \max(h_S(A, B), h_L(B, A)) \tag{4.4}$$

where S and L indicate the considered number of points from A and B respectively.

Again, S and L are usually determined using a single K value. Specifically, if M is the number of points in A and N is the number of points in B, then $S = \max(\lfloor KM \rfloor, 1)$ and $L = \max(\lfloor KN \rfloor, 1)$. Setting $K = 1$ results in $S = M$ and $L = N$ (i.e. the standard Citation-kNN), while setting K to a value such that $K \leq \frac{1}{M}$ and $K \leq \frac{1}{N}$ results in $S = L = 1$. This last variant is typically called *minimal Hausdorff distance*.

In [WZ00], the conventional kNN procedure for selecting the label of a query example was found not to be optimal for the MIL scenario. In their experiments with binary classification, the authors observed that negative examples might frequently contain more positive bags than negative bags among their nearest neighbors. Thus, predicting an example label based on the majority class of the closest neighbors will generally yield low accuracy. This phenomena might be due to the presence of false positive instances in the positive bags, that may attract negative bags. This situation is explained

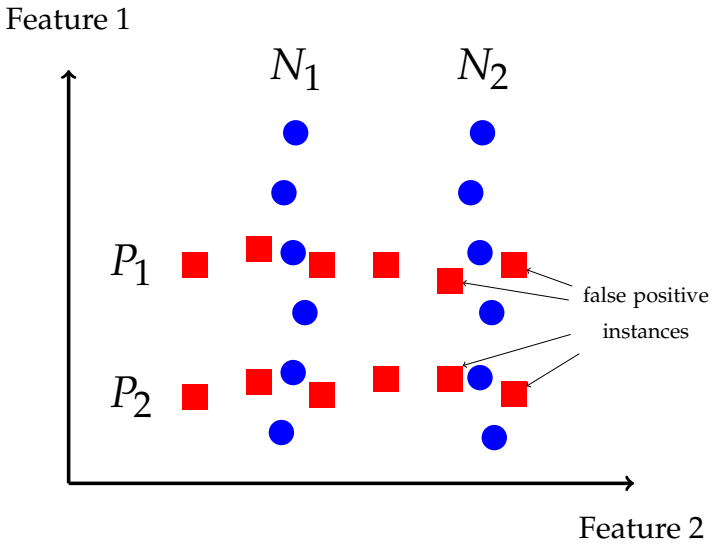

Figure 4.1: The traditional kNN method for combining neighbors labels to obtain the label of a query is not directly applicable to the MIL setting. The figure illustrates how false positive instances contained in positive bags attract negative bags. For example, given $\{P_1, P_2, N_1\}$ as training bags, N_2 will be classified as positive when the minimal Hausdorff distance is used.

in Figure 4.1.

If bags P_1, P_2 and N_1 are used for training, then the query bag N_2 will be classified as positive (for simplicity, we assume the minimal Hausdorff distance is used, although the problem can persist for different values of S and L in 4.4). The false positive instances in P_1 and P_2 are close to instances in N_2, and thus N_2 is closer (in terms of minimal Hausdorff distance) to the positive bags than it is to N_1.

To overcome this problem, [WZ00] incorporates the notion of *citation* into the voting mechanism used to decide the label of a query bag. Instead of only taking into account the neighbors of the query bag (called *references*), the proposed mechanism considers also the bags that count the query as a neighbor (called *citers*). According to the authors, this is inspired by a well-known method from the field of library and information science [GM79] used to find related papers.

The proposed approach defines the *R-nearest references* of an example A as the R nearest neighbors of A. Moreover, it defines the *C-nearest citers* of

A to be the set that includes any given bag X if and only if A is one of the C nearest neighbors of X. Note that, in general, the number of *C-nearest citers* is not C.

The class of a query bag is derived by combining the votes of its R-nearest references with those of its C-nearest citers. For binary classification, the number of positive votes p is determined by summing the number of positive references R_p and positive citers C_p, i.e. $p = R_p + C_p$. Likewise, if the number of positive and negative references are R_n and C_n respectively, the number of negative votes is $n = R_n + C_n$. The query is predicted positive if $p > n$, and negative otherwise.

4.2.3 Modified Citation-kNN

This section presents a modified version of Citation-kNN, which introduces two changes to the original method. First, it extends it to allow for multiple-class classification. Second, it adjusts the voting mechanism by incorporating weighted votes. Both changes are a natural application of ideas commonly used in the kNN method.

The voting procedure described in Section 4.2.2 was thought for binary classification. Like other binary methods, this procedure can be combined with (for example) a one-vs-one or one-vs-rest strategy to allow for multiple-class classification. However, a more natural extension to the multiple class scenario can be devised for Citation-kNN. We now present such extension.

Let L be the set of possible labels. For a given query bag X, assume $\{r_1, \ldots, r_{n_r}\}$ and $\{c_1, \ldots, c_{n_c}\}$ are the class labels of its n_r nearest references and its n_c nearest citers respectively. In our extension, the predicted label l^* for X is obtained by summing the votes of citers and references as:

$$l^* = \arg\max_{l \in L} \left(\sum_{i=1}^{n_c} \delta(l, c_i) + \sum_{j=1}^{n_r} \delta(l, r_j) \right) \tag{4.5}$$

where $\delta(a, b) = 1$ if $a = b$ and $\delta(a, b) = 0$ otherwise.

The criteria presented in Equation 4.5 assigns the same importance to the vote of any citer or reference. However, it seems reasonable to pay more attention to those neighbors that are closer to the query bag. In other words,

examples that are closer to the query should count for more. This can be achieved by using weighted voting. Formally, let X be the query example, L be the set of possible labels, and assume $\{R_1, \ldots, R_{n_r}\}$ and $\{C_1, \ldots, C_{n_c}\}$ are the sets of nearest references and citers of X respectively. Further, let $\{r_1, \ldots, r_{n_r}\}$ and $\{c_1, \ldots, c_{n_c}\}$ be the class labels of its nearest references and its nearest citers respectively. Then, the weighted voting approach for predicting label l^* for X is:

$$l^* = \arg\max_{l \in L} \left(\sum_{i=1}^{n_c} \alpha_i \delta(l, c_i) + \sum_{i=1}^{n_r} \beta_i \delta(l, r_i) \right) \tag{4.6}$$

where α_i is the weight for citer C_i and β_i is the weight for reference R_i.

Clearly, the weight for a particular example should be a decreasing function of its distance to X. In this work we use the following popular choice for kNN:

$$\alpha_i = \frac{1}{H(X, C_i)} \qquad \beta_i = \frac{1}{H(X, R_i)} \tag{4.7}$$

where $H(\cdot)$ is the modified Hausdorff distance described in Equation 4.4 (we omit the S and L subscripts here for clarity).

Note that the weight functions in Equation 4.7 are not defined when the distance between the compared examples is zero. Therefore, when a neighbour matches the query exactly, we directly assign l^* to be the label of such neighbour.

4.2.4 Citation-kNN on bags of time-stamped poses

This section describes the proposed method for action recognition based on Citation-kNN. As explained in Chapter 1.2, the raw representation of an action execution is given by a sequence of skeletons, that encodes the temporal evolution of the actor's pose (see Section 3.2.3 for details).

In this method, skeletons are normalized using the same procedure as in Section 3.2.3. Furthermore, the relative position of the joints (RJP), detailed in Section 3.2.3 is used as skeleton descriptor.

In the following, we introduce the specific representation for descriptor sequences used by the presented method, and we study the application of Hausdorff distance on such representation. Then, we describe the classification procedure for new skeleton sequences.

Representing skeleton descriptor sequences as bags of time-stamped skeleton descriptors

Any given skeleton descriptor sequence contains descriptors that are representative of the action being performed. However, at the same time, many other descriptors in the sequence provide no information (or worse, they are misleading) about the action label. As explained in sections 1.1.1 and 4.1, this is due not only to the nature of action sequences (which have large inherent inter-class similarity and intra-class variability), but also to the high degree of noise and outliers present in sequences captured with typical depth devices.

Formally, given a sequence $X = (x_1, x_2, \ldots, x_N)$ with N skeleton descriptors, its time-stamped bag representation is the set $B_X = \{b_1, b_2, \ldots, b_N\}$, where $b_i = (x_i, \alpha\frac{i}{N})$ is the ordered pair obtained by appending a single value to descriptor x_i. The appended value $\alpha\frac{i}{N}$ adds temporal information to the original descriptor. It is computed by multiplying the relative temporal position of the descriptor (i.e. the video frame at which the descriptors is located divided by the total number of frames in the video) by a constant α, that regulates the weight of the temporal information. We refer to α as the *frame weight* and to b_i as a *time-stamped descriptor*. Bags of time-stamped descriptors are compared using the modified Hausdorff distance given in Equation 4.4. We now present a series of examples that aim at gaining further insight into the proposed bag representation and the chosen distance function.

Comparing bags of skeletons descriptors using the Hausdorff distance

Figure 4.2 illustrates how the Hausdorff distance between two bags of descriptors is obtained. The compared bags correspond to the actions *cheer*

up and *drink*. For clarity purposes, the original sequences (belonging to the dataset MSRDailyActivity3D described in Section 2.2) were brought to a length of only 6 frames.

Figure 4.2a shows the distance between each descriptor in the *cheer up* bag and its nearest neighbor in the *drink* bag. I.e., it shows the values involved in the computation of the directed Hausdorff distance (Equation 4.2) from the *cheer up* bag to the *drink bag*. Figure 4.2b illustrates in turn the directed Hausdorff distance from the *drink* bag to the *cheer up* bag. In both figures, descriptors are linked to their nearest neighbor by an arrow. Note how multiple descriptors from one set can be map to the same descriptor in the other set. Arrows are colored according to the color scale shown on the right. Arrow color serves as an additional indication of the distance between the linked descriptors. Observe that each descriptor is represented by its corresponding skeleton (that is, the skeleton from which it was obtained). Moreover, skeletons are shown in the order they appear in the original sequence. In this example, frame information was not considered. That is, a frame weight $\alpha = 0$ was used.

For both figures 4.2a and 4.2b, it can be seen that descriptors corresponding to neutral poses (located roughly at the beginning and at the end of the sequences) are relatively close to their nearest neighbors. This is expected behavior, since the neutral pose is common to both actions. On the other hand, the more representative poses of each action (both hands above the head in the case of *cheer up* and one hand next to the head in the case of *dink*) lead to larger distances. The largest distances are produced by the most characteristic poses of the *cheer up* sequence. In particular, one of those distances (91.13) determines the final Hausdorff distance when $K = 1$ is used.

This example illustrates an important assumption of our approach: Even though two differently labeled action sequences may (and most probably will) contain many similar poses, at least one of the sequences will contain poses that differentiate it from the other sequence. Therefore, when comparing the bag representations of those sequences, descriptors originated in such differentiating poses will be at large distance from their nearest neighbors in the other bag. As a consequence, the Hausdorff distance will be

large. On the contrary, two sequences with the same label will *share* most of their poses, causing the Hausdorff distance between their corresponding bags to be small.

Taking temporal information into account

In the example of Figure 4.2 time was not taken into account. While this may not be a problem for some actions, ignoring temporal information can severely hurt classification performance in other cases. This is illustrated in figures 4.3a and 4.3b. The figures show the comparison of a query *sit down* bag with two other bags: another *sit down* bag and *stand up* bag. A frame weight $\alpha = 0$ was used. For future reference, we call the bags Q, A and B respectively. Specifically, Figure 4.3a illustrates the directed Hausdorff distance from the A to Q, $h(A, Q)$, while Figure 4.3a illustrates the directed Hausdorff distance from the B to Q, $h(B, Q)$. For clarity, only one direction of the Hausdorff distance is shown for each comparison. Take into account, however, that considering both directions is important for achieving good results.

Clearly, it is desirable that $h(B, Q) < h(A, Q)$, because Q and B are labeled with the same action, and Q and A are not. However, as both actions *sit down* and *stand up* involve similar poses, $h(A, Q)$ is smaller than desired. In general, *sit down* bags contain skeleton descriptors that are similar to the ones found in *stand up* bags, namely those corresponding to siting and standing poses. As a consequence, every descriptor in one bag has a close nearest neighbor in the other bag, yielding a small distance between bags. In this example, even though the distances involved in the computation of $h(B, Q)$ are also small, a few of them are slightly larger than the ones involved in the computation of $h(A, Q)$, causing $h(B, Q) > h(A, Q)$. The unexpected behavior came from discarding temporal information. The compared actions can be easily confused if the temporal order is not taken into account.

The effect of choosing an adequate value for the frame weight is illustrated in Figure 4.4. The figure shows the same comparisons described in Figure 4.3. In this case, however, time information is taken into account.

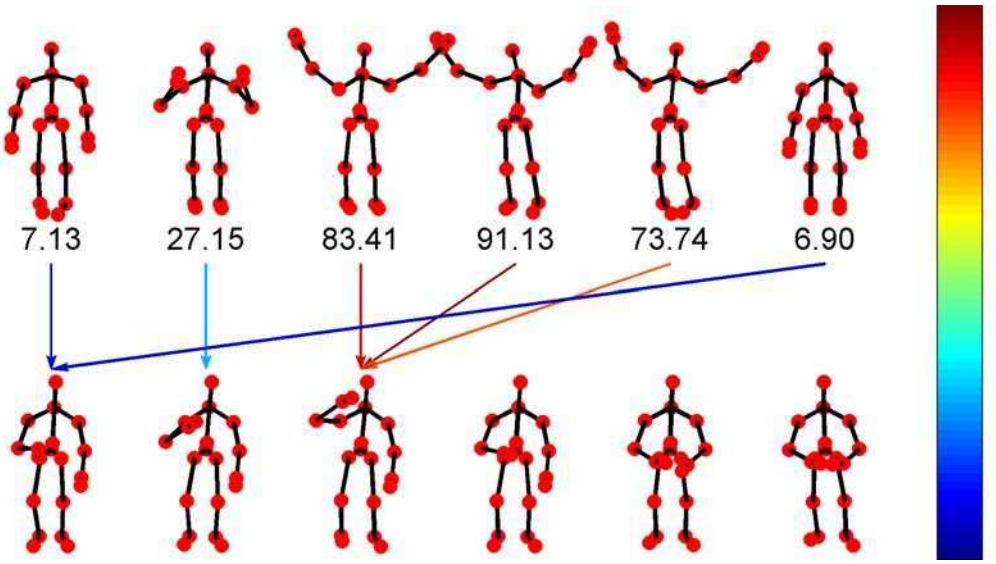

(a)

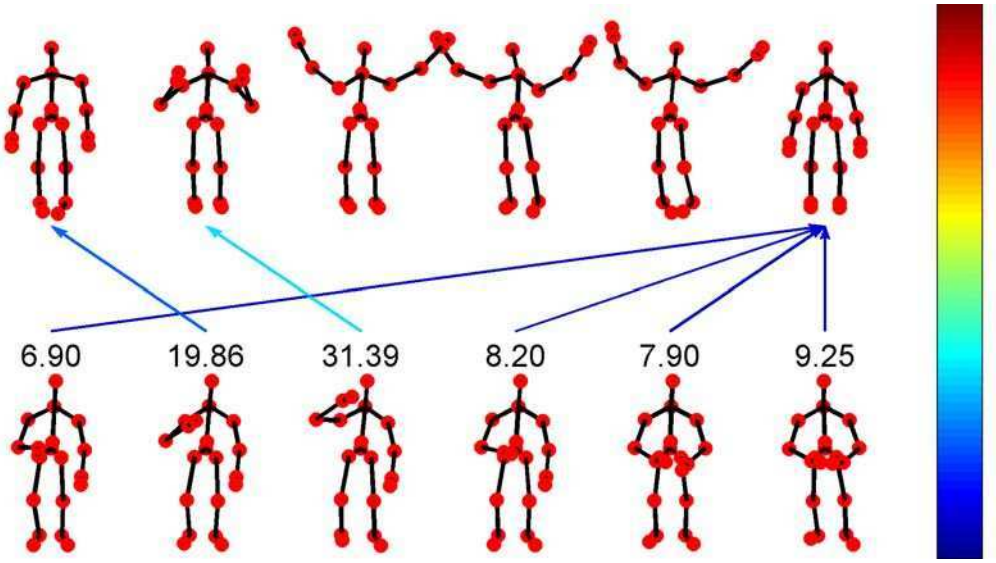

(b)

Figure 4.2: Illustration of the Hausdorff distance between two bags of skeleton descriptors, corresponding to the actions *cheer up* and *drink*. Figure 4.2a describes the directed Hausdorff distance from the *cheer up* bag to the *drink* bag. Figure 4.2b describes the distances for the directed Hausdorff distance from the *drink* bag to the *cheer up* bag. Each descriptor in the source bag is linked by an arrow to its nearest neighbor in the target bag. The distance to such nearest neighbor is indicated both by the color of the arrow (following the color scale shown on the right side) and by the number next to the arrow. See text for details.

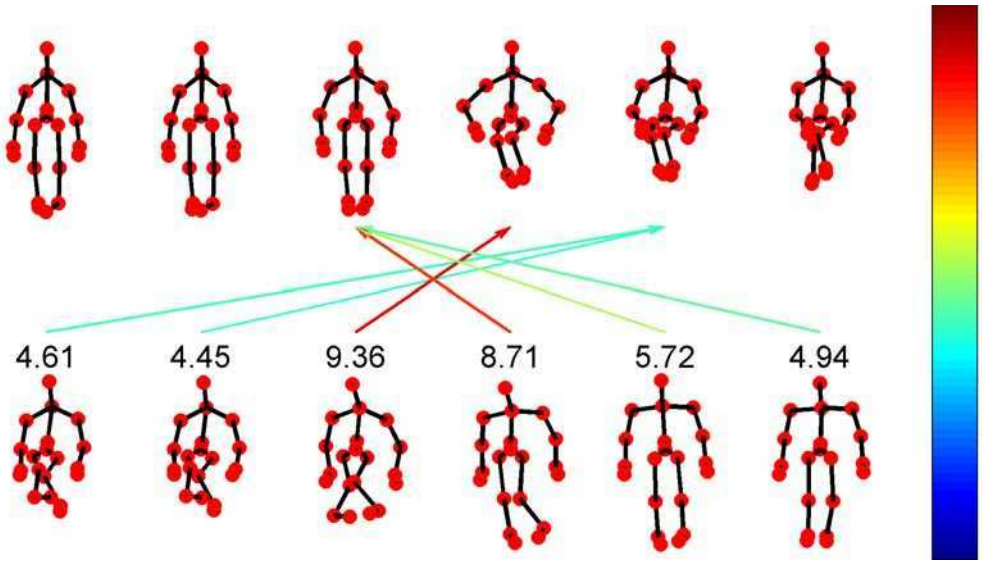

(a)

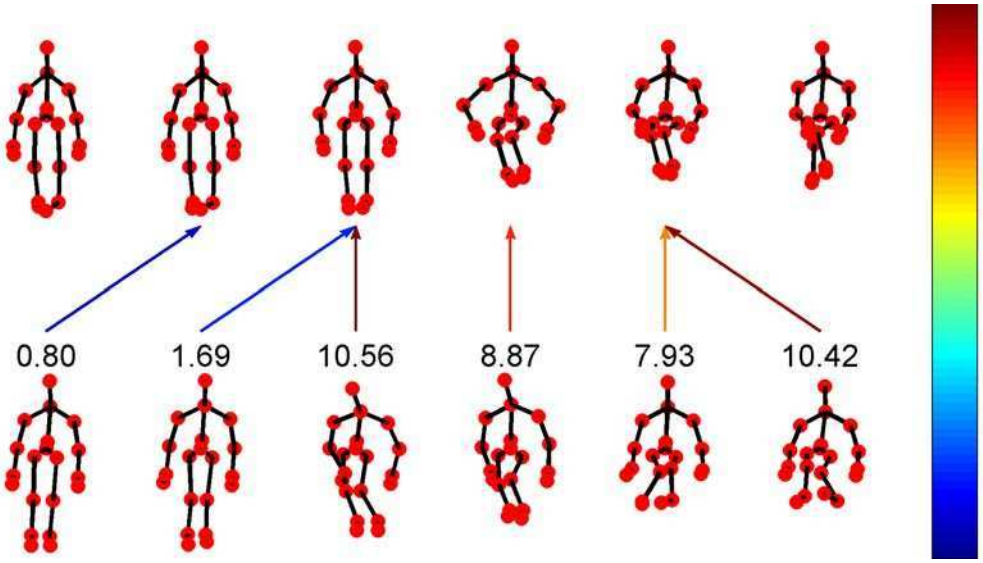

(b)

Figure 4.3: Illustration of the Hausdorff distance between a query bag and two training bags of skeleton descriptors. The query bag corresponds to the action *sit down*. Training bags are labeled with the actions *sit down* and *stand up*. Figure 4.3a describes the directed Hausdorff distance from the *stand up* bag to the query bag. Figure 4.3b describes the directed Hausdorff distance from the *sit down* training bag to the query bag. Temporal order is not considered. Descriptors in the source bag are linked by an arrow to their nearest neighbors in the target bag. The distance to such nearest neighbor is indicated both by the color of the arrow (following the color scale shown on the right side) and by the number next to the arrow. See text for details.

Note how the temporal information forces each descriptor to be linked to a descriptor located at a similar temporal position. This has particularly beneficial effects on the comparison between the *sit down* and the *stand up* bags, shown in Figure 4.4a. For example, the rightmost descriptor in the bottom row (corresponding to the standing pose) cannot longer be (costless) linked to a descriptor located in left-half of the top row (as it happens in Figure 4.3a). In other words, it is forced to find its nearest neighbor among descriptors with which is not similar in terms of pose. Compared to example in Figure 4.3a, the computation of the Hausdorff distance between *sit down* bag and the *stand up* bag involves larger values, causing bags to be further apart. On the other hand, the Hausdorff distance between the two *sit down* bags does not change significantly, because similar poses are located at similar temporal locations in the original sequences. The ultimate consequence is that the query bag is closer to the *sit down* bag than the *stand up* bag, as desired.

The effect of the K parameter

Recall from Section 4.2.2 that the modified Hausdorff distance can be tuned by specifying the parameter $0 \leq K \leq 1$. This parameter indicates the fraction of the points that are to be considered to compute the similarity between the two bags. In other words, $1 - K\%$ of the points is ignored when computing the modified Hausdorff distance.

To illustrate the effect of the K parameter, Figure 4.5 compares a query *cheer up* bag with two other bags. Specifically, Figure 4.5a compares the query with another *cheer up* bag, and Figure 4.5b compares it with a *drink* bag. As in the example of the previous section, we use the names Q, A and B for the considered bags, where Q is the query, A is the other *cheer up* bag and B is the *drink* bag. In each figure, the values involved in the computation of the modified Hausdorff distance (Equation 4.4) are shown. Note that, for clarity purposes, only one direction of the modified Hausdorff distanceis shown for each comparison. More precisely, Figure 4.5a illustrates $h_S(A, Q)$, while Figure 4.5b illustrates $h_S(Q, A)$. We intentionally choose the directions that produce the larger final distance in each case. Recall from

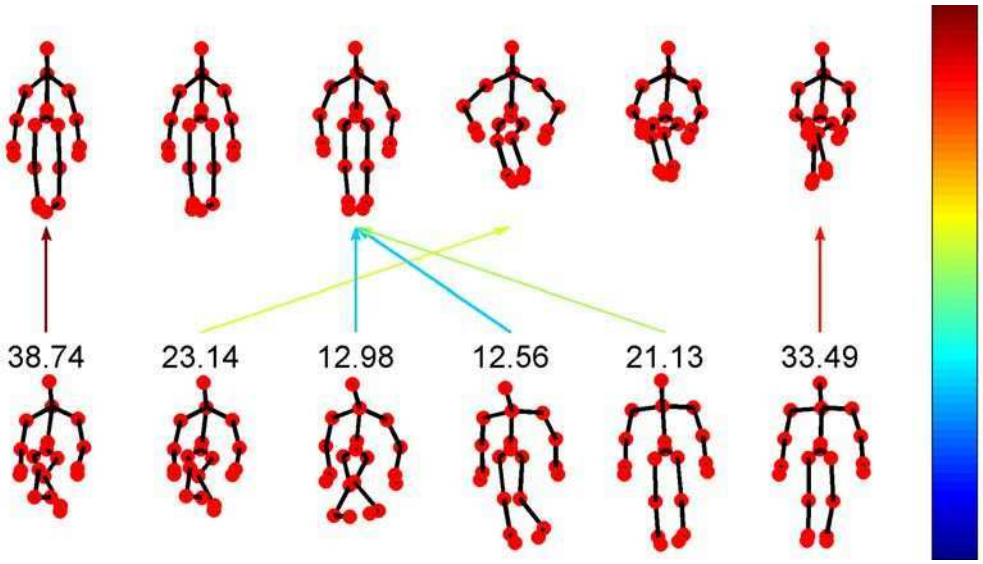

(a)

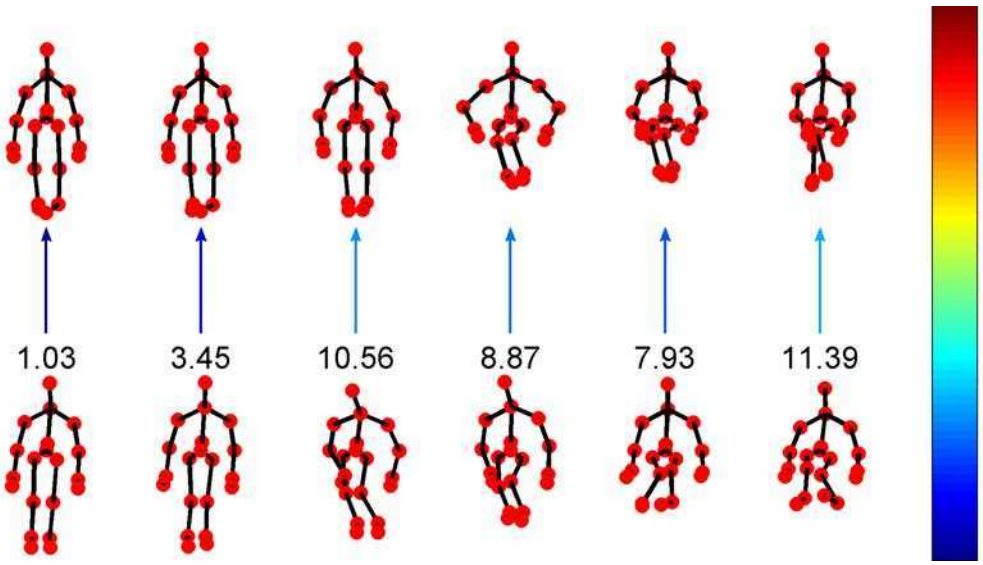

(b)

Figure 4.4: Illustration of the Hausdorff distance between a query bag and two training bags of skeleton descriptors. The compared bags are the same as in Figure 4.3. Different from the scenario illustrated in that Figure, the example shown here takes into account temporal information. See text for details.

Section 4.2.2 that the value of S is determined by K as $S = \max(\lfloor K6 \rfloor, 1)$.

It is desired that $h_L(A, Q) < h_L(Q, B)$, since Q and A have the same label, while Q and B do not. However, a different result is obtained using $K = 1$ (and thus $L = 6$). This is due to a very noisy skeleton in A. Specifically, the fourth skeleton from the right is severely perturbed by noise. As a consequence, its associated descriptor lies far away from every descriptor in Q, causing $h_6(A, Q)$ to be large. On the other hand, while $h_6(Q, B)$ involves some large distances (as expected, because Q and B have different labels), none of them is as large as the one associated with the noisy skeleton in A. In the end, $h_6(A, Q) = 121.59 > h_6(Q, B) = 55.67$, which differs from the expected result.

The desired behavior can be obtained, however, by letting $K = \frac{5}{6}$ (and thus $L = 5$). After ranking each of the 6 points in A by the distance to its nearest point in Q, the value corresponding to position 5 of the ranking is the modified directed distance from A to Q, $h_5(A, Q) = 33.91$. Similarly, the modified directed distance from Q to B is $h_5(Q, B) = 40.89$. Note that, as desired, $h_5(A, Q) < h_5(Q, B)$.

It might seem that reducing K is always beneficial. However, note that setting $K = \frac{3}{6}$ (and thus $L = 3$) again gives the undesired result $h_3(A, Q) = 18.78 > h_3(Q, B) = 13.68$. The problem comes from the fact the three more discriminative poses in Q (namely, those in which both hands are above the head) are ignored in the computation of $h_3(Q, B)$.

The following important conclusion can be drawn about the role of the K parameter based on the previous example. It is possible to make the distance robust against noisy and outlying descriptors by adjusting the value of K. More precisely, if $n\%$ of the descriptors in a bag are known to be noise or outliers, then using a value of K such that $K < 1 - n$, leaves those descriptors out of the computations, avoiding their undesired effects on the final distance. However, if the value of K is too low, then the descriptors that differentiate one bag from the other might also be ignored. Specifically, if the fraction of noisy and discriminative descriptors are known to be of $n\%$ and $d\%$ respectively (assume, for simplicity, that the fractions are the same for both bags), then setting K to a value less than $1 - n - d$ discards not only

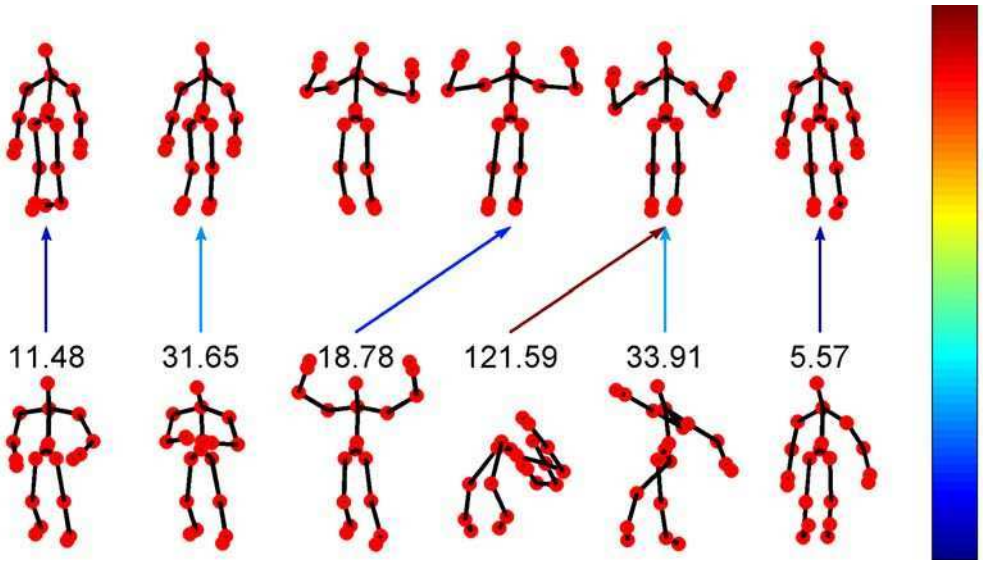

(a)

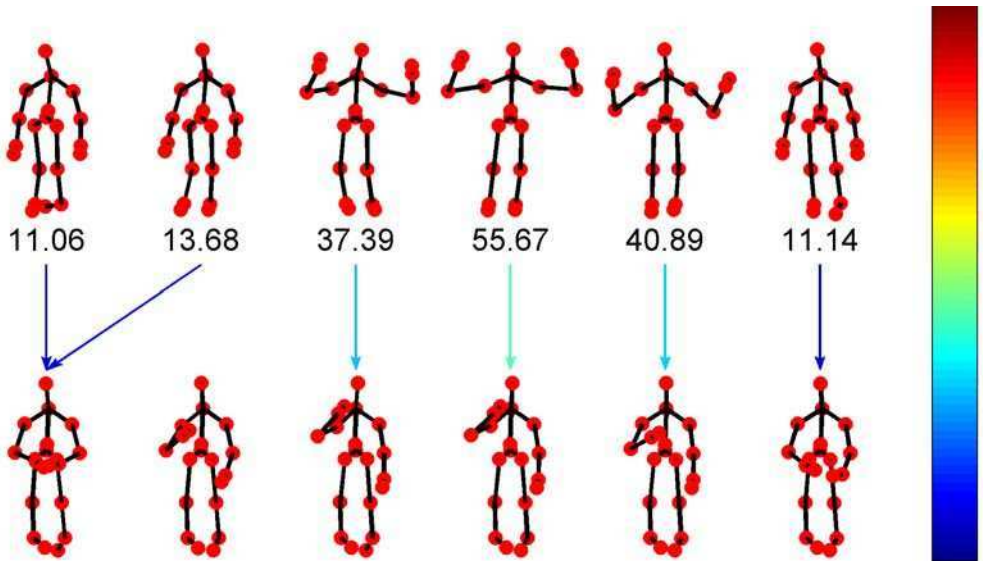

(b)

Figure 4.5: Illustration of the Hausdorff distance between a query bag and two training bags of skeleton descriptors. The query bag corresponds to the action *cheer up*. Training bags are labeled with the actions *cheer up* and *drink*. Figure 4.5a describes the directed Hausdorff distance from the *cheer up* bag to the query bag. Figure 4.5b describes the directed Hausdorff distance from the query bag to the *cheer up* training bag. One of the descriptors in the *cheer up* training bag is very noisy. Descriptors in the source bag are linked by an arrow to their nearest neighbors in the target bag. The distance to such nearest neighbor is indicated both by the color of the arrow (following the color scale shown on the right side) and by the number next to the arrow. See text for details.

the noisy descriptors but also the informative ones. Thus, the optimal K must lie at some point between $1-n$ and $1-n-d$. Of course, n and d vary depending on the bags, and are generally not known in advance. Therefore, the value of K has to be decided empirically.

Video classification procedure

This section presents an overview of the main steps involved in the classification of a query video. Recall from the beginning of this section and from Chapter 1 that the raw representation of action sequence is given by a sequence of skeletons. Therefore, our presented method attempts to predict the action label of a query skeleton sequence, based on labeled training sequences.

After skeleton normalization and descriptor computation (see the beginning of Section 4.2.4), the original sequences in the training data are transformed into bags of time-stamped descriptors, as explained in Section4.2.4. The same procedure is applied for a query sequence before classification. Therefore, action prediction for a query sequence A consists of three steps:

1. Obtain a sequence of normalized skeletons by normalizing each skeleton in A,
2. Obtain a sequence of skeleton descriptors by computing a descriptor for each skeleton normalized in the previous step,
3. Obtain a bag of time-stamped skeleton descriptors by appending temporal information to each descriptor computed in the previous step,
4. Classify the bag of the time-stamped skeleton descriptors obtained in the previous step.

Step 4 above predicts the label of the sequence A using the multi-class distance-weighted classification approach presented in Section 4.2.3.

Multi-part approach

Similar to the method described in Section 3.2.3, we improve the basic classification step using a multi-part approach. Recall from equations 3.20 and

3.21 that a skeleton descriptor is a $3(J-1)J$ length vector $d = (d_1, d_2, \ldots, d_J)$, where J is the number of joints in the skeleton and d_i is the $3(J-1)$ length vector corresponding to joint i. In addition, recall that when considering time-stamped descriptors the value corresponding to the temporal information is appended to the original descriptor. That is, if d is the ith descriptor in a sequence with N elements, its associated time-stamped descriptor b is a $3(J-1)J+1$ length descriptor such that $b = (d_1, d_2, \ldots, d_J, \alpha\frac{i}{N})$.

For a given set p, we define a function f_p that, given a skeleton descriptor, it preserves the coordinates associated with joints in p and the temporal information, and discards the rest. Formally, if $p = \{p_1, p_2, \ldots, p_z\}$ is a set of z integers such that $1 \leq p_i \leq J \quad \forall\ 1 \leq i \leq z$, f_p is a function $f_p : \mathbb{R}^{3(J-1)J+1} \rightarrow \mathbb{R}^{3(J-1)z+1}$ such that:

$$f_p((d_1, d_2, \ldots, d_J, \alpha\frac{i}{N})) = (d_{p_1}, d_{p_2}, \ldots, d_{p_z}, \alpha\frac{i}{N}) \tag{4.8}$$

We overload f_p to describe a function that takes a bag of time-stamped descriptors $A = \{a_1, a_2, \ldots, a_N\}$ and applies f_p to each of them:

$$f_p(A) = \{f_p(a_1), f_p(a_2), \ldots, f_p(a_N)\} \tag{4.9}$$

Further, for a given set of time-stamped skeleton descriptors bags $C = \{C_1, C_2, \ldots, C_K\}$, we overload f_p as:

$$f_p(C) = \{f_p(C_1), f_p(C_2), \ldots, f_p(C_K)\} \tag{4.10}$$

As in Section 3.2.3, we group joints into five body parts. For each part, the problem stated in Equation 4.6 is solved. Formally, let A be the query bag, L be the set of possible labels and T the set of all training bags. Assume $\{R_1^p, \ldots, R_{n_r^p}^p\}$ and $\{C_1^p, \ldots, C_{n_c^p}^p\}$ are the sets of nearest references and citers of $f_p(A)$ in $f_p(T)$, respectively. Further, let $\{r_1^p, \ldots, r_{n_r^p}^p\}$ and $\{c_1^p, \ldots, c_{n_c^p}^p\}$ be the class labels of those references and citers respectively. We define $sim_l^p(A)$, the similarity measure between $f_p(A)$ and class l, as:

$$sim_l^p(A) = \sum_{i=1}^{n_c^p} \alpha_i^p \delta(l, c_i^p) + \sum_{i=1}^{n_r^p} \beta_i^p \delta(l, r_i^p) \tag{4.11}$$

where $\delta(a,b) = 1$ if $a = b$ and $\delta(a,b) = 0$ otherwise, and α_i^p and β_i^p are the weights for citer C_i^p and reference R_i^p respectively, determined using the Hausdorff distance $H(\cdot)$ as:

$$\alpha_i^p = \frac{1}{H(f_p(A), C_i^p)} \qquad \beta_i^p = \frac{1}{H(f_p(A), R_i^p)} \tag{4.12}$$

Then, the multi-part approach for predicting label l^* for A is:

$$l^* = \arg\max_{l \in L} \sum_{p \in P} \frac{sim_l^p(A)}{G_p(A)} \tag{4.13}$$

where $G_p(A)$ is a normalization factor, defined as:

$$G_p(A) = \sum_{l \in L} sim_l^p(A) \tag{4.14}$$

4.3 Results

This section presents and discuss experimental results for our proposed action recognition method. As in Section 3.3, we use 4 different datasets: MSRDailyActivity3D, MSRAction3D, UTKinect and Florence3D. See section 2.2 for a thorough description of the datasets.

4.3.1 Parameter selection

Along Section 4.2, we describe several parameters that control the behavior of the presented method. In order to select appropriate values for those parameters, we optimize the performance of our approach by cross-validation on the training data. As the optimal parameters vary depending on the dataset, we carry out such optimization procedure for each dataset.

The considered parameters are the frame weight α (see Section 4.2.4), the K parameter for the modified Hausdorff distance (see Section 4.2.4), and the values R and C that determine the number of references and citers of the Citation-kNN method respectively.

A *gradient ascent* procedure is employed to obtain find optimal values for the parameters. Specifically, such values are searched among the points of

a grid that (roughly) divides the parameter space. Starting from a reasonable point, the current point is updated at each iteration of the grid search. More precisely, for each immediate neighbor of the current point, the average class accuracy for that point is computed using the leave-one-actor-out cross-validation (LOAOCV) technique (see Section 2.2) on the training data. After considering all the neighbors, the algorithm moves to the point that produced the largest average class accuracy. Note that, as we have four parameters to optimize, the grid is four-dimensional and the number of neighbors for a grid point can be as large as 81. However, caching results of previous points helps in reducing computation times. The grid search finishes when no improvement is observed in the optimized measure. The main reason for using this approach for parameter selection is its convenient time complexity. In general, performing the gradient ascent is much faster than evaluating every point in the grid. The price paid for the low temporal complexity is that potentially optimal grid points might be not taken into account.

4.3.2 Parameter influence

To evaluate the influence of the different parameters, we study the change in performance obtained when varying one of them while leaving the rest fixed. Specifically, the average class accuracy is computed using LOAOCV on the training data for several values of the studied parameter. Such values belong to a short range centered at the optimal value found by the grid search described in Section 4.3.1. The remaining parameters are fixed at their optimal values (also found by the grid search).

Figures 4.6a, 4.6b, 4.7a and 4.7b show the results for the MSRDailyActivity3D dataset, the MSRAction3D dataset, the UTKinect dataset and the Florence3D dataset respectively. In addition to the average class accuracy computed by LOAOCV on the training data, the figures show the average class accuracy computed on the test data (using the standard train-test regime for each dataset, as described in Section 2.2). The former is denoted as *train* in the figures, while the latter is denoted as *test*.

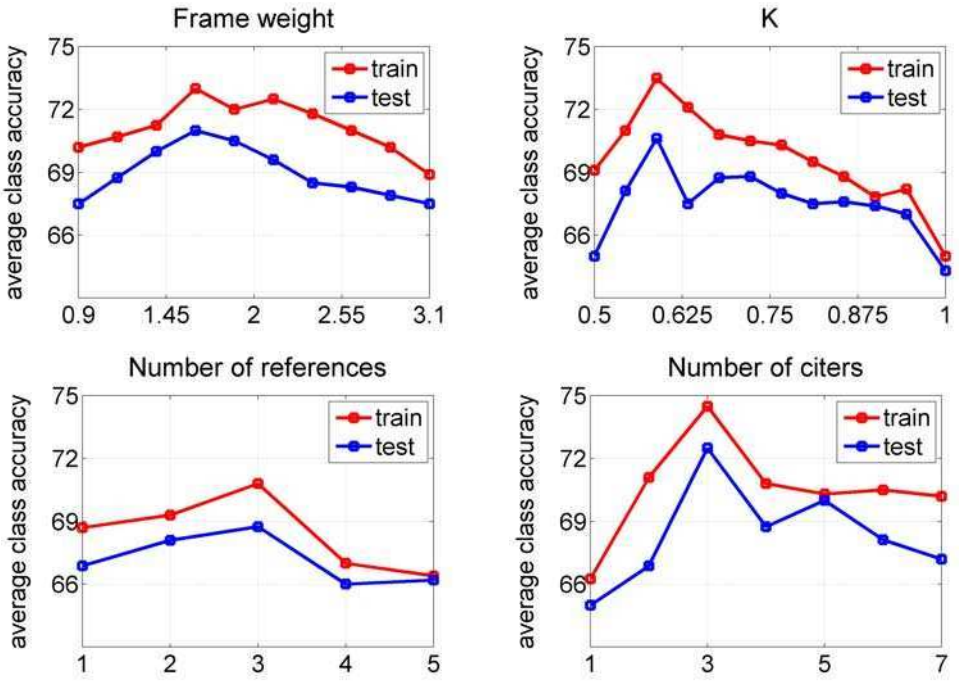

(a) Parameter influence for the MSRDailyActivity3D dataset.

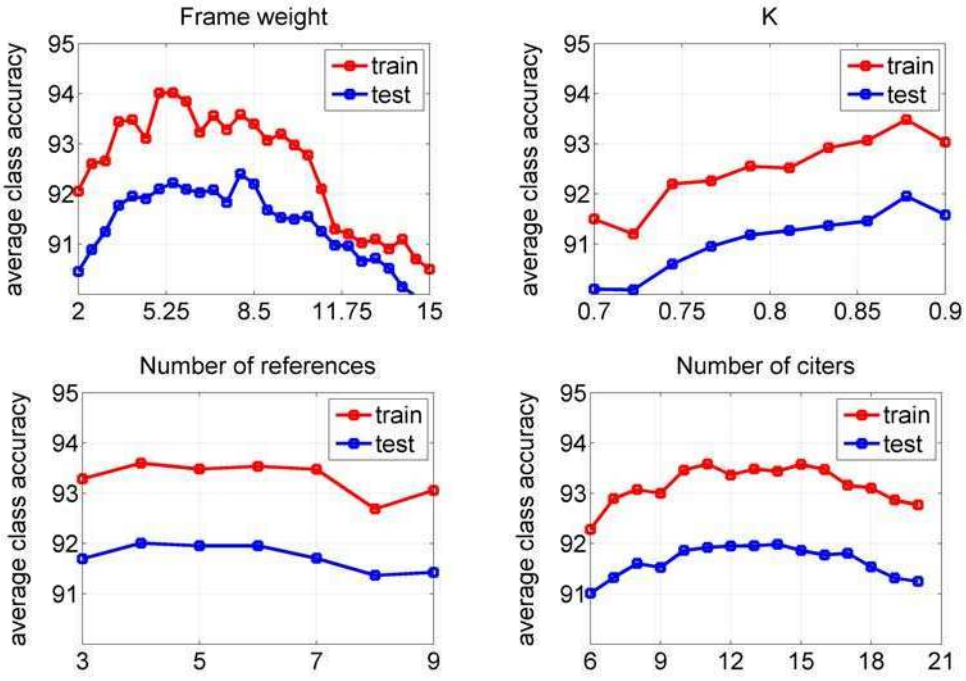

(b) Parameter influence for the MSRAction3D dataset.

Figure 4.6: Parameter influence for two of the four considered datasets.

Note that the influence of the parameters varies depending on the dataset.

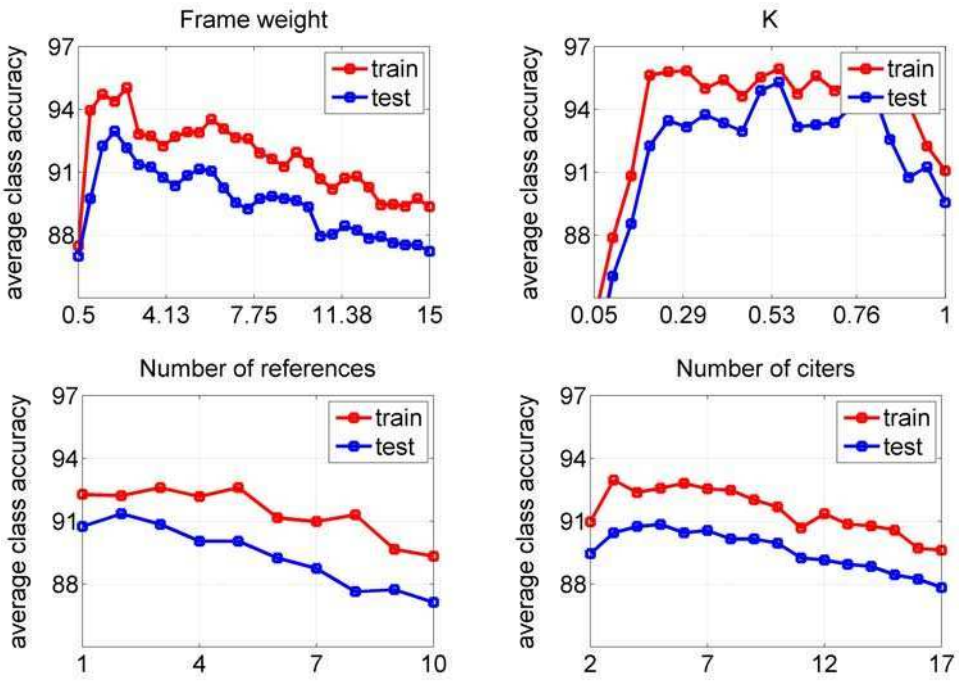

(a) Parameter influence for the UTKinect dataset.

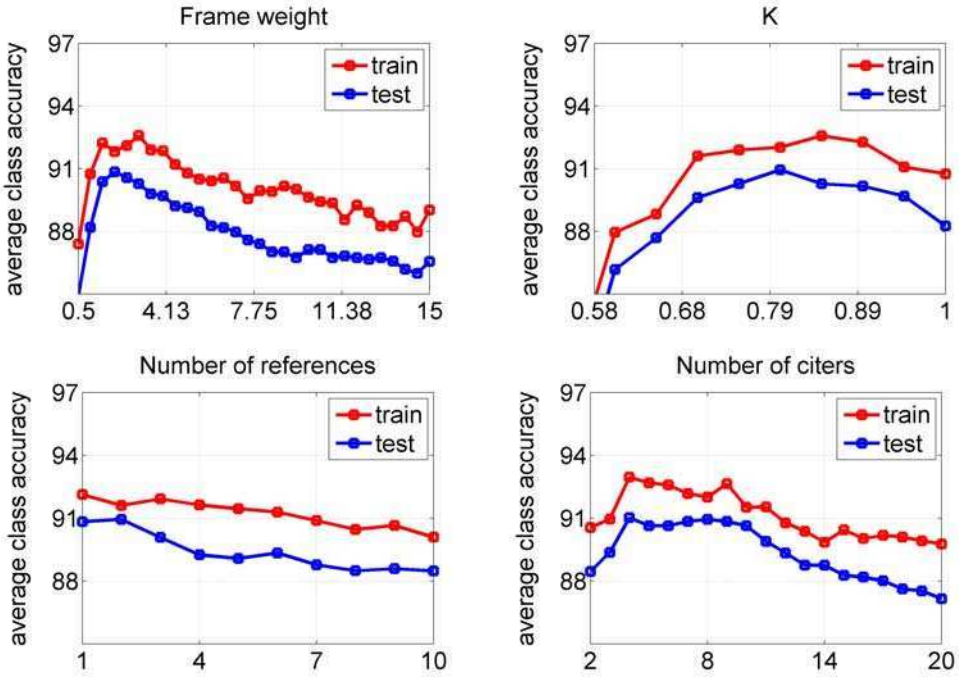

(b) Parameter influence for the Florence3D dataset.

Figure 4.7: Parameter influence for two of the four considered datasets.

For example, the optimal K is around 0.55 for MSRDailyActivity3D, while

it is around 0.88 for MSRAction3D. However, many behaviors common to all datasets exist, as we discuss next.

In every considered dataset, performance drops somewhat drastically when the frame weight is set below a specific threshold. Presumably, such threshold corresponds to the point below which crucial temporal information is discarded. Values above that threshold also lead to worse performance. However, decrement is slower in this case, which suggests that giving excessive (but reasonable) importance to temporal order is less harmful than ignoring it. It is worth commenting that, even if not shown in the plots, an extremely large frame weight indeed shatters performance, as it allows no temporal flexibility at all.

Figures also show a common pattern regarding the K parameter. Specifically, high performance is achieved within a certain range, while low performance is obtained outside the range. This is consistent with the observations in Section 4.2.4. Namely, that the optimal K must be low enough as to leave noisy and outlying descriptors out of the computations, but not as low as to ignore informative descriptors. Despite this common pattern, note how the range varies for the different datasets. For example, it is (roughly) $[0.2, 0.76]$ for the UTKinect dataset and $[0.66, 0.88]$ for the Florence3D dataset, which can be interpreted as the latter containing videos with a smaller percentage of informative descriptors (indicated by the fact that $0.88 - 0.66 < 0,76 - 0.2$) and a smaller percentage of noisy descriptors (because $0.88 > 0.76$).

In general, performance is not very sensitive to the number of references and citers. While large deviations from the optimal values do cause a change in accuracy, results show that such change tends to be smooth. This is presumably due to the weighted voting mechanism explained in Section 4.2.3, that reduces the influence in the voting of those references and citers located far away from the query bag.

4.3.3 Evaluation of the main components of the action recognition procedure

In this section, we experimentally study on two datasets (MSRDailyActivity3D and UTKinect) the impact on performance caused by the main components of our method for action recognition. Specifically, we evaluate the benefits of time-stamped descriptors (Section 4.2.4), weighted-voting (Section 4.2.3) and the multi-part approach (Section 4.2.4).

We report results considering each component separately, but also for all possible combinations of two and three components. Moreover, we include results for basic variant of our method that does not use any of the components. The basic version is indicated by *Citation-kNN*. Variants considering only time-stamped descriptors, weighted voting or the multi-part approach are indicated as *Citation-kNN + time*, *Citation-kNN + weighted* or *Citation-kNN + parts* respectively. Names for the solutions accounting for more than one component together are indicated by combining the names of the single-component variants. For example, *Citation-kNN + time + weighted* indicates the combined use of time-stamped descriptors and weighted voting.

For each variant, the involved parameters were optimized using the gradient ascent technique described in Section 4.3.1, and refined using the procedure explained in Section 4.3.2. Note that, depending on the variant, different parameters need to be considered. For example, in the case of *Citation-kNN + parts + weighted*, the frame weight parameter does not exist, because temporal information is not taken into account. The reported measure is the average class accuracy computed on the test data (using the standard train-test regime for each dataset, as described in Section 2.2).

Table 4.1 shows the results. In both datasets, performance of the basic Citation-kNN is considerably improved by the proposed method (i.e. the variant than combines the three evaluated components). The table also shows that every single-component variant yields better results than the basic approach. Further, it shows that the performance of any given variant can be improved by extending it with any of its missing components.

Even though the exact relative benefit brought by each variant to the ba-

sic approach depends on the dataset, improvements are consistent across datasets for most of the variants. For example, the variant *Citation-kNN + parts + time* yields an average class accuracy about 15% larger than the basic approach on both datasets. However, two variants show particularly different behaviors in both datasets, in terms of the improvements to the basic variant. The first one is *Citation-kNN + weighted*, that allows for an improvement of 8% for the MSRDailyActivity3D dataset, but of only 1.7% for the UTKinect. A possible explanation for this result could lie in the higher noise levels of the MSRDailyActivity3D dataset (see Section 2.2). In that scenario, it seems reasonable to find a relatively large number of misleading (i.e. labeled with a different action) neighbors among the citers and references of the query bag. On the contrary, it is expect for such number to be low in a less noisy scenario. Therefore, the benefit of weighting neighbors votes by distance can be more noticeable in the noisy dataset.

The second variant that shows an interesting behavior is *Citation-kNN + time*. For the UTKinect dataset, it allows for an improvement of aorund 12% compared to the basic variant. However, such an improvement is of only 5% for the MSRDailyActivity3D dataset. This suggests that using time-stamped descriptors is more beneficial for the former dataset than it is for the latter. Presumably, this is due to the fact that the relative number of actions for which temporal order is decisive is lager in the UTKinect dataset. This explanation is consistent with the *frame weight* plots in Figures 4.6a and 4.7a. Those figures show that a quite large frame weight does not deteriorate performance on the UTKinect dataset significantly, while small increments in such weight cause a large decrease in performance on the MSRDailyActivity3D.

To further study the effects of time-stamped descriptors on performance, we analyze the misclassified actions on both datasets when time information is not taken into account. Figures 4.8a and 4.8b show confusion matrices for the UTKinect dataset. The former corresponds to the the variant *Citation-kNN + parts + weighted*, that uses the multi-part approach and weighted voting, but ignores temporal order. The latter corresponds to the full method *Citation-kNN + parts + weighted + time*, that also take time into

	UTKinect	MSRDaily
Citation-kNN	80.90 %	61.88 %
Citation-kNN + weighted	82.31 %	66.87 %
Citation-kNN + time	91.26 %	65.00 %
Citation-kNN + parts	85.02 %	66.87 %
Citation-kNN + weighted + time	92.36 %	69.37 %
Citation-kNN + parts + time	93.77 %	70.63 %
Citation-kNN + parts + weighted	86.94 %	68.13 %
Citation-kNN + parts + weighted + time	95.38 %	72.50 %

Table 4.1: Average class accuracy on datasets MSRDailyActivity3D and UTKinect for different variants of the proposed method.

acount. Note how a considerable amount of error in Figure 4.8a comes from confusing action *sit down* with action *stand up*, and action *push* with action *pull*. The confused actions involve similar poses, meaning that any pose in one of the actions can be found in the other action, and vice versa. The differentiating aspect between those actions lies in the temporal location of the poses. This is supported by Figure 4.8b, that shows a drastic reduction in the confusion between them when using time-stamped descriptors.

Figures 4.9a and 4.9b show the confusion matrices corresponding to the same variants for the MSRDailyActivity3D dataset. Note how the variant that ignores temporal information confuses actions *sit down* and *stand up*. Specifically, 60% of the videos labeled with one of the two actions is erroneously classified as corresponding to the other. When time is considered, the confusion between them drops to 0%.

4.3.4 Robustness analysis

This section analyzes the tolerance of the proposed method to noise and temporal misalignment. Similarly to Section 3.3.3, we study both the performance in presence of independent identically distributed white noise in the skeletons, and the impact of local temporal shifts on the descriptor sequences.

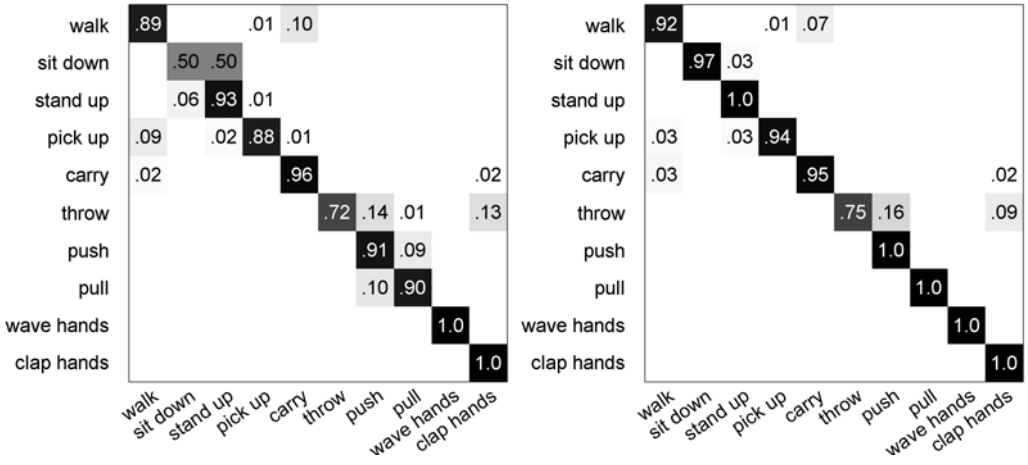

(a) (b)

Figure 4.8: Confusion matrices for the UTKinect dataset. Figure 4.8a shows the results obtained when time information is ignored. Figure 4.8b shows the results obtained when taking temporal information into account.

Our approach is compared with two popular methods: Fourier Temporal Pyramids (FTP) from [WLWY12b], and Hidden Markov Model (HMM) from [LN06]. See section 2.1.1 for a description of the methods. In every case, the optimal parameters for FTP and HMM were found by leave-one-actor-out cross-validation (see 2.2 for a description of the technique) on the training actors. On the other, parameters for our method were optimized using the gradient ascent technique described in Section 4.3.1, and refined using the procedure explained in Section 4.3.2.

Experiments were carried out for two datasets: MSRDailyActivity3D and UTKinect. In both cases, we show the relative accuracy obtained by each of the tested methods, which is defined as the ratio between the average class accuracy under the perturbed scenario and the average class accuracy under the non-perturbed scenario.

Robustness to noise

We evaluated the noise robustness of the proposed approach, along with that of several other methods. For this purpose, we corrupted the skeletons by adding noise from a Gaussian distribution with mean zero and variance

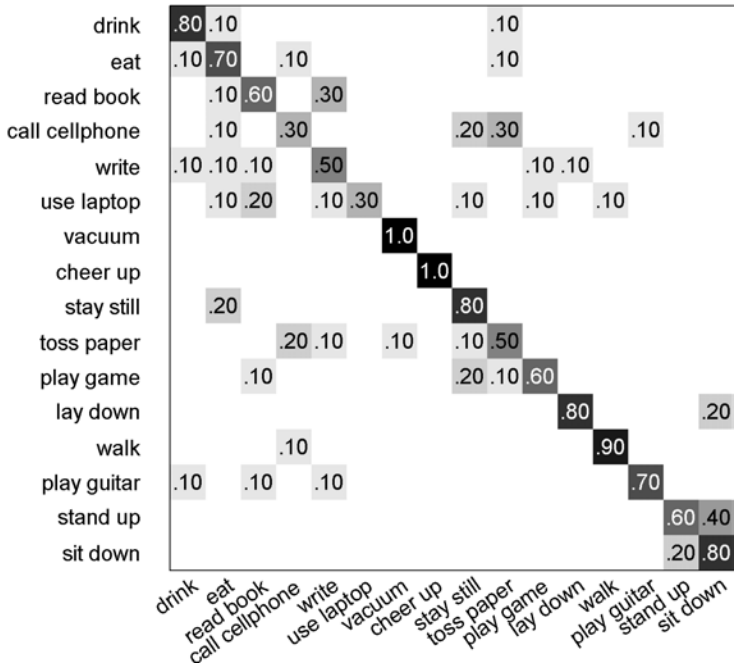

(a)

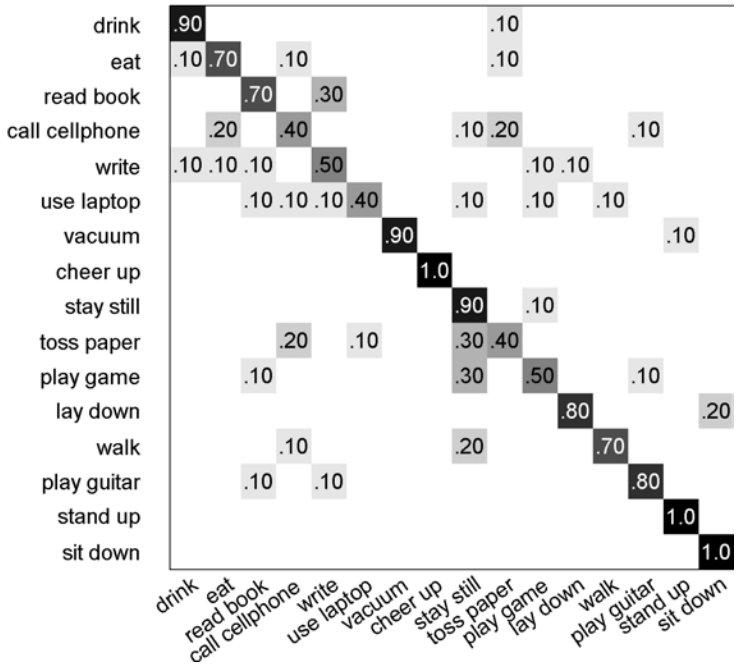

(b)

Figure 4.9: Confusion matrices for the MSRDailyActivity3D dataset. In Figure 4.9a time information is ignored, while in Figure 4.9b it is not.

one. We compute the relative accuracy of each method for different amounts of noise, and studied the resulting behaviors.

Figure 4.10 shows the results for the two considered datasets. While, as expected, relative accuracy decays with noise in every case, the degree in which this happens varies depending on the method. Moreover, results on MSRDailyActivity3D are generally worse than results on UTKinect, which is reasonable considering that the former is a more challenging dataset.

HMM shows the least robustness on both datasets. This is somewhat expected, since it is well known that the procedure used by this method to compute the hidden states is quite sensitive to noise. Our method and FTP show a similar behavior. While the proposed approach seems to slightly outperform FTP in terms of robustness on the MSRDailyActivity3D, both methods obtain almost the same relative accuracy for most of the scenarios on the UTKinect. As commented in 2.1.1, dropping the Fourier coefficients associated to high frequency components makes FTP highly resilient to noise. Encouragingly, our method achieves similar robustness. We argue that a possible explanation lies mainly in two aspects of the proposed multiple instance learning approach. First, the skeletons more affected by noise can be ignored by the modified Hausdorff distance, as described in Section 4.2.4. Second, the citation approach (improved by the weighted voting mechanism presented in Section 4.2.3) mitigates the effect of misleading neighbors (potentially increased by noise).

Robustness to temporal misalignment

We compared the tolerance to temporal misalignment of the same methods considered in Section 4.3.4. To that aim, we circularly shifted every skeleton sequence in the training data, and kept the testing data uncorrupted. The relative accuracy of our approach and that of FTP and HMM was computed for several scenarios, each corresponding to a different number of shifted frames.

Results for the two considered datasets are shown in Figure 4.11. It is well known that the performance of HMM is not affected by sequence alignment. This is reflected in its relative accuracy, that remains close to

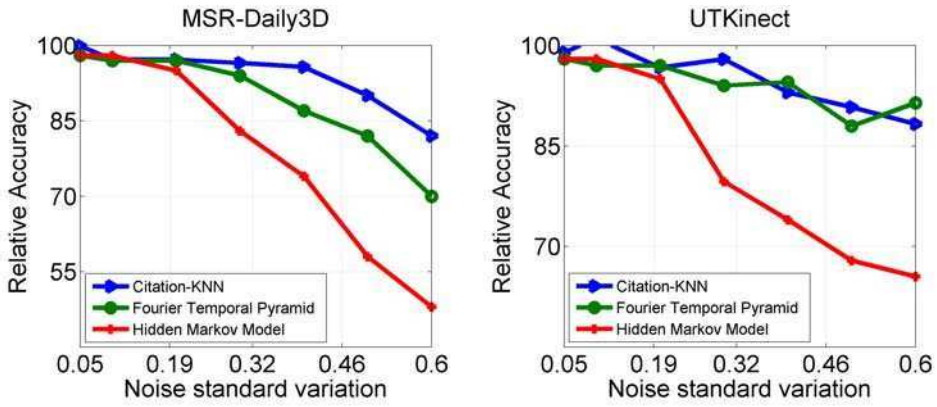

(a) (b)

Figure 4.10: Relationship between the relative accuracy and the noise standard variation for several methods on two datasets: MSRDailyActivity3D (4.10a) and UTKinect (4.10b).

100% for every scenario on both datasets. Our method shows a robustness comparable to that of FTP. Indeed, despite a somewhat erratic behavior, it clearly outperforms such method on the MSRDailyActivity3D dataset. On the other hand, both methods show very similar performance on UTKinect dataset.

This test suggests that our method is more sensitive to temporal shifts than HMM. Nevertheless, it shows competitive robustness, retaining a large percentage of the average class accuracy obtained in the non-perturbed scenario. This is presumably due to the same aspects commented in Section 4.3.4 for the noise experiments. Namely, the benefits brought by both the Hausdorff distance and the citation approach with weighted voting. The former reduces the effect of those skeletons shifted to unusual temporal positions. Such skeletons lead to misleading time-stamped descriptors, than can be seen as noisy instances in the bag representation. The latter offers resilience against a potentially larger number of misleading neighbors, caused by the larger presence of misleading time-stamped descriptors in the bags.

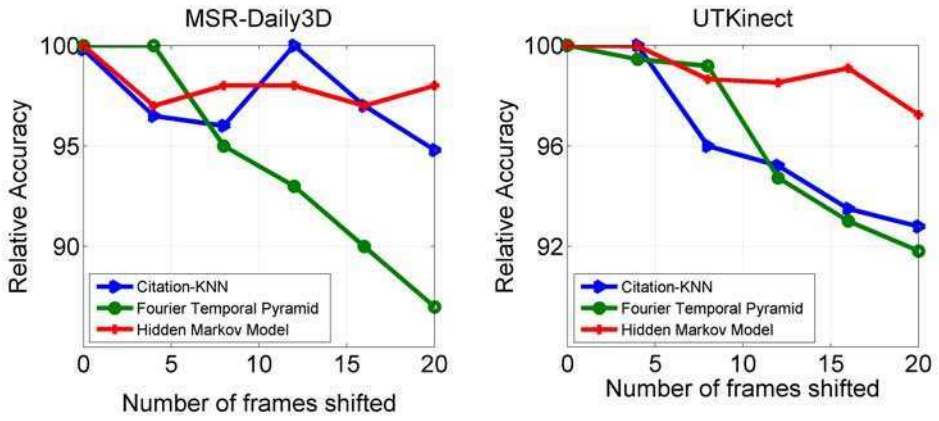

(a) (b)

Figure 4.11: Relationship between the relative accuracy and the temporal misalignment for several methods on two datasets: MSRDailyActivity3D (4.11a) and UTKinect (4.11b).

4.3.5 Comparation with the state-of-the-art

In this section, we compare the results obtained by our proposed action recognition approach with those of several state-of-the-art methods. In order to make a fair comparison, we only consider those works focusing on skeleton-based action classification. That is, we do not include results corresponding to methods employing depth or RGB information.

Table 4.2 shows the average class accuracy of each method for the four considered datasets. Results of our method are competitive on the four datasets. On two of them, it outperforms the rest of the methods. Specifically, it surpass the best result among the considered methods by 2.5% on the MSRDailyActivity3D dataset and by 5.83% on the Florence3D dataset. On the UTKinect dataset, performance is slightly worse than that of [VAC14]. On the MSRAction3D dataset, it is the second best method.

It is worth mentioning that many of the methods referenced in Table 3.1 ([CPLFR13, YT12, XCA12, ATSS15, SVB+13]) use skeleton descriptors different to the RJP (described in Section 3.2.3) employed in our approach, as well as different preprocessing techniques. For example, [CPLFR13] considers a descriptor that extends RJP with joint offset and velocity information, [YT12] further improves that descriptor by applying Principal Component

MSRDailyActivity3D dataset	
Fourier Temporal Pyramid [WLWY12b]	68.00
Weakly-aligned Bag of Poses [SVB+13]	70.00
Proposed method	72.50

MSRAction3D dataset	
Hidden Markov Model [XCA12]	78.97
Naive-Bayes-Nearest-Neighbor [YT12]	82.30
Joint Angle Similarities [OBT13]	83.53
Elastic Functional Coding [ATSS15]	85.16
Fourier Temporal Pyramid [WLWY12b]	88.20
DTW Nominal Curve + FTP [VAC14]	88.23
Bag of Temporal and Spatial Part-Sets [WWY13]	90.22
Random Forest [ZCG13]	90.90
Recurrent Neural Networks [DWW15]	94.49
Proposed method	92.22

UTKinect dataset	
Random Forest [ZCG13]	87.90
Hidden Markov Model [XCA12]	90.92
Elastic Functional Coding [ATSS15]	94.87
DTW Nominal Curve + FTP [VAC14]	95.58
Proposed method	95.38

Florence3D dataset	
Weakly-aligned Bag of Poses [SVB+13]	82.00
DTW Nominal Curve + FTP [VAC14]	85.20
Proposed method	91.03

Table 4.2: Comparison of the proposed approach with the state-of-the-art.

Analysis (PCA), [XCA12] uses histograms of joints positions, and [SVB+13] models the human torso as a rigid part, expressing the position of the joints in a coordinate system derived from the torso orientation. Therefore, Table 4.2 should be approached with caution in terms of temporal modeling comparison, as the differences in accuracies may be caused by several other factors. Nevertheless, the table shows that our method can yield very satisfactory results, and encourages the use of the proposed MIL approach for action recognition based on skeleton sequences.

4.4 Resumen

En este capítulo se presenta el segundo método de reconocimiento de acciones en videos de profundidad propuesto en la tesis. Su rasgo distintivo es el enfoque de *Aprendizaje Multi Instancia* (MIL por el término en inglés *Multiple Instance Learning*) que utiliza. En MIL, las instancias de entrenamiento vienen organizadas en conjuntos, generalmente denominados *bags*. Cada bag de entrenamiento tiene asignada una etiqueta que indica la clase a la que pertenece. Un bag etiquetado con una determinada clase contiene instancias que son características de la clase, pero puede (y generalmente así ocurre) también contener instancias que no lo son. Notar que, a diferencia de lo que ocurre en el aprendizaje supervisado tradicional, las etiquetas de los datos de entrenamiento están disponibles a nivel de bag, y no de instancia.

La sección 4.1 justifica la pertinencia del enfoque MIL para el problema de reconocimiento de acciones a partir de secuencias de esqueleto. La observación clave es que, en una secuencia dada, ciertas poses del actor pueden proveer información característica de la acción ejecutada cuando ocurren en determinados instantes, pero dichas poses "conviven" con otras que pueden ser no informativas y hasta causantes de ambigüedad (debido a ruido, a desfasaje temporal, a la existencia de poses comunes a varias acciones, etc.).

La sección 4.2 detalla el método propuesto. Primero se repasan algunos conceptos de MIL, poniendo especial énfasis en la técnica de MIL considerada en la tesis, conocida como Citation-kNN. Dicha técnica adapta el

clásico esquema de *k vecinos más cercanos* (kNN por el término en inglés *k-nearest-neighbors*). Luego, se proponen tres modificaciones al planteo original de Citation-kNN. La primera modificación es un extensión natural de la técnica al problema de clasificación multi-clase. La segunda incorpora pesos ajustados por distancia en la votación de los vecinos más cercanos. La tercera adapta el método para trabajar sobre múltiples secuencias obtenidas a partir de la secuencia original a clasificar, lo cual permite emplear un enfoque multi-parte al trabajar con secuencias de esqueletos. La sección 4.2.4 introduce una nueva representación para las secuencias de esqueletos, que permite su clasificación mediante Citation-kNN. Específicamente, se representa una secuencia dada como un bag de descriptores de esqueleto con marcas de tiempo. La sección analiza también varios aspectos de la representación propuesta. Además, dicha sección detalla el método completo para clasificar nuevas secuencias a partir de los datos de entrenamiento.

La sección 4.3 evalúa experimentalmente el método propuesto y lo compara con el estado del arte. En particular, el rol jugado por cada uno de los parámetros es analizado, y la robustez del método frente al ruido y al desfasaje temporal es evaluada, con muy buenos resultados. Además, los beneficios proporcionados por las modificaciones a Citation-kNN son verificados. A pesar de la simplicidad del enfoque propuesto, los experimentos muestran que, cuando se lo utiliza en conjunto con un descriptor de esqueleto robusto, es posible obtener resultados altamente competitivos. Creemos que esto es un indicio de que utilizar un enfoque MIL para el problema es apropiado, y prepara el terreno para posteriores investigaciones en esta dirección.

Chapter 5

Conclusions and perspective

In this thesis we have presented and evaluated two novel methods for the problem of skeleton-based action recognition. Both methods make use of machine learning techniques to predict the action encoded in a sequence of skeletons based on a set of labeled training sequences.

Section 3.2 described the first method. At its core lies a new technique for comparing sequences, that computes the distance between a query sequence and a given class by searching for the best possible alignment between the query and the training sequences in the class, according to a specific criteria. Such technique, called *Instance-to-Class Edit Distance on Real sequence* (I2CEDR) is the result of two modifications to a popular distance function known as *Edit Distance on Real sequence* (EDR): (1) A soft matching cost is used to align sequence points, allowing small differences between aligned points to be taken into account. (2) An Instance-to-Class approach is incorporated into the sequence comparison, that matches points from the query with points from any sequence within a set of sequences, improving generalization capabilities of non-parametric classification methods in cases of large intra-class variability and small training sets. Being derived from EDR, the proposed technique specifically takes into account temporal ordering when comparing sequences. As a further benefit, it requires no learning of parameters. An efficient dynamic programming algorithm is presented for computing I2CEDR.

Our proposed approach obtained highly competitive results (Section 3.3)

on four popular datasets. Moreover, it stood out as a very robust method, both in terms of noise and temporal misalignment. We believe this shows that alignment-based distances can be successfully used to compare skeleton sequences and that, when coupled with a robust skeleton descriptor, they can lead to state-of-the art methods. We see the encouraging results as an invitation to explore further variations of alignment-based distances that might be beneficial for the action recognition problem. A concrete topic for future work would be to train a cost function which assigns different penalties to edit operations depending on the involved skeleton. Consider for example the computation of I2CEDR between a query sequence and a set associated with action label l. Insertions of skeletons corresponding to poses frequently found in videos of action l should receive a large penalty, because the absence of such skeletons indicates the action in the query is probably not l. An analogous reasoning can be done for deletions. Another interesting concrete topic would be to devise a new criteria for choosing the threshold ϵ (See section 3.2.2), maybe by learning appropriate values from training data.

Section 4 presented a novel Multiple Instance Learning (MIL) approach to the problem of skeleton-based action recognition. The method involves a new way of handling skeleton sequences, that represents them as bags of time-stamped skeleton descriptors. Bags are classified using an modified version of Citation-kNN, a classical and simple MIL method. Both the benefits of the MIL approach to the problem, and the improvements brought by the proposed modifications to Citation-kNN are supported by the extensive experiments described in Section 4.3. Such experiments also showed that the proposed method is very tolerant to noise and temporal misalignment, and exposed the role played by the different parameters.

Regarding future work, it would be interesting to devise an efficient and effective method to learn different values for the K parameter (see Section 4.2.4) depending on the considered action. Likewise, using different values for the frame weight α might improve performance, as the importance of temporal information could vary depending on the action. Another attractive topic is the incorporation of data mining techniques to select useful

training skeletons before applyin Citation-kNN. By filtering out uninformative skeletons, typical MIL problems such as the one described in Figure 4.1 can be mitigated. More generally, we think the work in this thesis opens the door to the application of new MIL methods to the action recognition problem. The MIL literature is vast, and many other of its methods can be found to be useful apart from the one explored in this work.

A number of research directions apply to both methods presented in this thesis. One such direction involves the development of new skeleton descriptors and distance functions to compare them. As commented in Section 2.1.1, many previous works have done contributions regarding these aspects. We believe, however, there is still room for improvement. As a concrete example, it would be interesting to *plug* our proposed methods into a framework that learns weights for each joint depending on its discriminative power, similar to the one presented in [DWW15]. Another direction is the incorporation of raw depth information into our methods, a common trend in the literature that we intentionally avoid to focus on skeletal data. Taking raw depth information into account can be crucial for distinguishing actions involving nearly identical movements but different objects, such as *having a cup of coffee* and *having a glass of water*. The exact way in which this information can be incorporated into the presented methods is not trivial, but previous works suggest this might be a promising research avenue.

Capítulo 5

Conclusiones y perspectiva

En esta tesis hemos presentado y evaluado dos métodos novedosos para el reconocimiento de acciones basado en esqueletos. Ambos métodos usan técnicas de aprendizaje automático para predecir la acción codificada en una secuencia de esqueletos a partir de un conjunto se secuencias de entrenamiento etiquetadas.

La sección 3.2 describió el primer método. Una parte fundamental del mismo es una nueva técnica para comparar secuencias, que computa la distancia entre una secuencia dada y una determinada clase buscando el mejor alineamiento posible entre dicha secuencia y las secuencias de entrenamiento de esa clase, de acuerdo a un criterio específico. Esta técnica, llamada *Instance-to-Class Edit Distance on Real sequence* (I2CEDR) es el resultado de dos modificaciones a una conocida función de distancia entre secuencias conocida como *Edit Distance on Real sequence* (EDR): (1) Una función de costo *suave* es usada para el alineamiento de puntos. (2) Un enfoque *Instancia-a-Clase* (I2C, por el término en inglés *Instance-to-Class*) es incorporado a la comparación de secuencias, permitiendo el alineamiento de puntos de una secuencia dada con puntos de varias secuencias incluidas en un conjunto, mejorando la capacidad de generalización de métodos de clasificación no-paramétricos en casos de alta variabilidad intra-clase y pocos datos de entrenamiento. Al ser derivada a partir de EDR, la nueva técnica tiene específicamente en cuenta el ordenamiento temporal al comparar las secuencias. Como beneficio adicional, no requiere aprender parámetros. Un algoritmo

eficiente de programación dinámica es presentado para computar I2CEDR.

El método propuesto para reconocimiento de acciones obtuvo resultados altamente competitivos (Sección 3.3) en cuatro bases de datos utilizadas con frecuencia en la literatura. Asimismo, resultó muy robusto , tanto en términos de ruido como de desfasaje temporal. Creemos que esto muestra que las distancias basadas en alineamiento de puntos pueden ser usadas con éxito para comparar secuencias de esqueletos y que, combinadas con un descriptor de esqueleto robusto, permiten la obtención de métodos al nivel del estado del arte. Vemos estos resultados alentadores como una invitación a continuar explorando variantes de distancias basadas en alineamiento de puntos que puedan resultar benéficas para el problema de reconocimiento de acciones. Un posible tema concreto para trabajos futuros consiste en entrenar una función de costo que asigne diferentes penalidades a las operaciones de edición de acuerdo al esqueleto involucrado. Consideremos por ejemplo el cálculo de I2CEDR entre una secuencia dada s y un conjunto de secuencias asociado a la acción l. La inserción de esqueletos correspondientes a poses frecuentemente encontradas en videos de la acción l debería recibir una penalidad alta, ya que la ausencia de dichos esqueletos indica que la acción en la secuencia s sea probablemente distinta a l. Un razonamiento análogo puede hacerse con el la operación de borrado. Otro tema concreto que podría resultar interesante es el diseño de nuevos criterios para determinar el umbral ϵ (Ver sección 3.2.2), quizás mediante el aprendizaje de valores apropiados a partir de los datos de entrenamiento.

La sección 4 presentó un novedoso enfoque de *Aprendizaje Multi Instancia* (MIL por el término en inglés *Multiple Instance Learning*) para el problema de reconocimiento de acciones basado en esqueletos. El método involucra una nueva manera de manejar secuencias de esqueletos, que las representa como conjuntos (o *bags*) de descriptores de esqueleto con marcas de tiempo. Los bags son clasificados usando una versión modificada de Citation-kNN, un método de MIL clásico y simple. Tanto los beneficios del enfoque basado en MIL como las mejoras logradas a través de las modificaciones propuestas para Citation-kNN son avaladas por detallados experimentos descriptos en la sección 4.3. Dichos experimentos mostraron también que el método

propuesto es muy tolerante al ruido y al desfasaje temporal, y pusieron de manifiesto el rol jugado por los diferentes parámetros.

Con respecto al trabajo futuro, sería interesante diseñar un método eficiente y efectivo para aprender diferentes valores para el parámetro K (ver sección 4.2.4) dependiendo de la acción considerada. De la misma manera, utilizar distintos valores para el peso α asignado a la información temporal de los descriptores podría mejorar la performance del método, dado que la importancia de dicha información puede variar de acuerdo a la acción. Otro tema atractivo es la utilización de técnicas de minería de datos para seleccionar esqueletos útilos para el entrenamiento antes de aplicar Citation-kNN. Mediante la eliminación de esqueletos no informativos es posible mitigar problemas típicos de los métodos basados en MIL, como el descripto en la figura 4.1. En líneas más generales, creemos que el trabajo en esta tesis abre la puerta para la aplicación de nuevo métodos basados en MIL para el problema de reconocimiento de acciones. La literatura de MIL es vasta, y muchos otros métodos propuestos en ella podrían resultar útiles además del explorado en este trabajo.

Ciertas direcciones de investigación aplican a ambos métodos presentados en esta tesis. Una de ellas involucra el desarrollo de nuevos descriptores de esqueleto y nuevas funciones de distancia para compararlos. Como se comenta en la sección 2.1.1, muchos trabajos anteriores han hecho contribuciones en este aspecto. Creemos, sin embargo, que todavía queda mucho por mejorar. A manera de ejemplo, sería interesante integrar nuestros métodos en un framework que aprenda pesos por cada articulación del esqueleto en base a su poder discriminativo, de manera similar a la propuesta de [DWW15]. Otra dirección posible es el desarrollo de métodos que incorporen la información de profundidad en bruto a las técnicas presentadas en la tesis, una tendencia común en la literatura que evitamos intencionalmente en este trabajo para concentrarnos en los datos de esqueleto. Tener en cuenta la información de profundidad en bruto puede ser crucial para distinguir acciones que involucren movimientos casi idénticos y objetos diferentes, como *tomar una taza de café* y *tomar un vaso de agua*. Si bien la incorporación de este tipo de datos a los métodos presentados no es trivial,

varios trabajos previos sugieren que la misma puede constituir una dirección de trabajo prometedora.

Bibliography

[ATH02] Stuart Andrews, Ioannis Tsochantaridis, and Thomas Hofmann, *Support vector machines for multiple-instance learning*, Advances in neural information processing systems, 2002, pp. 561–568.

[ATSS15] Rushil Anirudh, Pavan Turaga, Jingyong Su, and Anuj Srivastava, *Elastic functional coding of human actions: From vector-fields to latent variables*, Proceedings of the IEEE Conference on Computer Vision and Pattern Recognition, 2015, pp. 3147–3155.

[Bis06] Christopher M Bishop, *Pattern recognition*, Machine Learning (2006).

[BSI08] O. Boiman, E. Shechtman, and M. Irani, *In defense of nearest-neighbor based image classification*, CVPR08, 2008, pp. 1–8.

[BW95] Armin Bruderlin and Lance Williams, *Motion signal processing*, Proceedings of the 22nd annual conference on Computer graphics and interactive techniques, ACM, 1995, pp. 97–104.

[CBW06] Yixin Chen, Jinbo Bi, and James Z Wang, *Miles: Multiple-instance learning via embedded instance selection*, Pattern Analysis and Machine Intelligence, IEEE Transactions on **28** (2006), no. 12, 1931–1947.

[Cha02] Shih-Fu Chang, *The holy grail of content-based media analysis*, MultiMedia, IEEE **9** (2002), no. 2, 6–10.

[CN04] Lei Chen and Raymond Ng, *On the marriage of lp-norms and edit distance*, Proceedings of the Thirtieth international conference on Very large data bases-Volume 30, VLDB Endowment, 2004, pp. 792–803.

[CÖO05] Lei Chen, M Tamer Özsu, and Vincent Oria, *Robust and fast similarity search for moving object trajectories*, Proceedings of the 2005 ACM SIGMOD international conference on Management of data, ACM, 2005, pp. 491–502.

[CPLFR13] A.A. Chaaraoui, J.R. Padilla Lopez, and F. Florez Revuelta, *Fusion of skeletal and silhouette-based features for human action recognition with rgb-d devices*, 2013, pp. 91–97.

[CZN+11] Cheng Chen, Yueting Zhuang, Feiping Nie, Yi Yang, Fei Wu, and Jun Xiao, *Learning a 3d human pose distance metric from geometric pose descriptor*, Visualization and Computer Graphics, IEEE Transactions on **17** (2011), no. 11, 1676–1689.

[DB78] Carl De Boor, *A practical guide to splines. number 27 in applied mathematical sciences*, 1978.

[DHS01] R.O. Duda, P.E. Hart, and D.G. Stork, *Pattern classification*, Wiley, 2001.

[DLLP97] Thomas G Dietterich, Richard H Lathrop, and Tomás Lozano-Pérez, *Solving the multiple instance problem with axis-parallel rectangles*, Artificial intelligence **89** (1997), no. 1, 31–71.

[Don06] Lin Dong, *A comparison of multi-instance learning algorithms*, Ph.D. thesis, Citeseer, 2006.

[DWW15] Yong Du, Wei Wang, and Liang Wang, *Hierarchical recurrent neural network for skeleton based action recognition*, Proceedings of the IEEE Conference on Computer Vision and Pattern Recognition, 2015, pp. 1110–1118.

[EM94] Thomas Eiter and Heikki Mannila, *Computing discrete fréchet distance*, Tech. report, Citeseer, 1994.

[FF10] James Foulds and Eibe Frank, *A review of multi-instance learning assumptions*, The Knowledge Engineering Review **25** (2010), no. 01, 1–25.

[FS97] Yoav Freund and Robert E Schapire, *A decision-theoretic generalization of on-line learning and an application to boosting*, Journal of computer and system sciences **55** (1997), no. 1, 119–139.

[G+12] Alex Graves et al., *Supervised sequence labelling with recurrent neural networks*, vol. 385, Springer, 2012.

[GD+95] DM Gavrila, LS Davis, et al., *Towards 3-d model-based tracking and recognition of human movement: a multi-view approach*, International workshop on automatic face-and gesture-recognition, Citeseer, 1995, pp. 272–277.

[GM79] Eugene Garfield and Robert King Merton, *Citation indexing: Its theory and application in science, technology, and humanities*, vol. 8, Wiley New York, 1979.

[GTHES13] Mohammad Abdelaziz Gowayyed, Marwan Torki, Mohammed Elsayed Hussein, and Motaz El-Saban, *Histogram of oriented displacements (hod): Describing trajectories of human joints for action recognition.*, IJCAI, 2013.

[HKT99] Yka Huhtala, Juha Karkkainen, and Hannu T Toivonen, *Mining for similarities in aligned time series using wavelets*, AeroSense'99, International Society for Optics and Photonics, 1999, pp. 150–160.

[HS97] Sepp Hochreiter and Jürgen Schmidhuber, *Long short-term memory*, Neural computation **9** (1997), no. 8, 1735–1780.

[HXL+11] Weiming Hu, Nianhua Xie, Li Li, Xianglin Zeng, and Stephen Maybank, *A survey on visual content-based video indexing and re-*

trieval, Systems, Man, and Cybernetics, Part C: Applications and Reviews, IEEE Transactions on **41** (2011), no. 6, 797–819.

[LN06] Fengjun Lv and Ramakant Nevatia, *Recognition and segmentation of 3-d human action using hmm and multi-class adaboost*, Computer Vision–ECCV 2006, Springer, 2006, pp. 359–372.

[LS13] Li Liu and Ling Shao, *Learning discriminative representations from rgb-d video data*, Proceedings of the Twenty-Third International Joint Conference on Artificial Intelligence, IJCAI '13, AAAI Press, 2013, pp. 1493–1500.

[LSP06] Svetlana Lazebnik, Cordelia Schmid, and Jean Ponce, *Beyond bags of features: Spatial pyramid matching for recognizing natural scene categories*, Computer Vision and Pattern Recognition, 2006 IEEE Computer Society Conference on, vol. 2, IEEE, 2006, pp. 2169–2178.

[LZL10] W.Q. Li, Z.Y. Zhang, and Z.C. Liu, *Action recognition based on a bag of 3d points*, CVPR4HB10, 2010, pp. 9–14.

[MHK06] Thomas B Moeslund, Adrian Hilton, and Volker Krüger, *A survey of advances in vision-based human motion capture and analysis*, Computer vision and image understanding **104** (2006), no. 2, 90–126.

[MLP98] Oded Maron and Tomás Lozano-Pérez, *A framework for multiple-instance learning*, Advances in neural information processing systems (1998), 570–576.

[MLSS94] Richard M Murray, Zexiang Li, S Shankar Sastry, and S Shankara Sastry, *A mathematical introduction to robotic manipulation*, CRC press, 1994.

[MR06] Meinard Müller and Tido Röder, *Motion templates for automatic classification and retrieval of motion capture data*, Proceedings of the 2006 ACM SIGGRAPH/Eurographics sym-

posium on Computer animation, Eurographics Association, 2006, pp. 137–146.

[MWLF05] Vasileios Megalooikonomou, Qiang Wang, Guo Li, and Christos Faloutsos, *A multiresolution symbolic representation of time series*, Data Engineering, 2005. ICDE 2005. Proceedings. 21st International Conference on, IEEE, 2005, pp. 668–679.

[OBT13] E. Ohn-Bar and M.M. Trivedi, *Joint angles similarities and hog2 for action recognition*, Computer Vision and Pattern Recognition Workshops (CVPRW), 2013 IEEE Conference on, June 2013, pp. 465–470.

[OL13] Omar Oreifej and Zicheng Liu, *Hon4d: Histogram of oriented 4d normals for activity recognition from depth sequences*, In CVPR, 2013.

[Pav73] Theodosios Pavlidis, *Waveform segmentation through functional approximation*, Computers, IEEE Transactions on **100** (1973), no. 7, 689–697.

[PM02] Ivan Popivanov and Renee J Miller, *Similarity search over time-series data using wavelets*, Data Engineering, 2002. Proceedings. 18th International Conference on, IEEE, 2002, pp. 212–221.

[Pop10] Ronald Poppe, *A survey on vision-based human action recognition*, Image and vision computing **28** (2010), no. 6, 976–990.

[RDE11] Miguel Reyes, Gabriel Domínguez, and Sergio Escalera, *Featureweighting in dynamic timewarping for gesture recognition in depth data*, Computer Vision Workshops (ICCV Workshops), 2011 IEEE International Conference on, IEEE, 2011, pp. 1182–1188.

[RKH11] Michalis Raptis, Darko Kirovski, and Hugues Hoppe, *Real-time classification of dance gestures from skeleton animation*, Proceedings of the 2011 ACM SIGGRAPH/Eurographics symposium on computer animation, ACM, 2011, pp. 147–156.

[SMA11] Samsu Sempena, Nur Ulfa Maulidevi, and Peb Ruswono Aryan, *Human action recognition using dynamic time warping*, Electrical Engineering and Informatics (ICEEI), 2011 International Conference on, IEEE, 2011, pp. 1–5.

[SPL+05] Sudeep Sarkar, P Jonathon Phillips, Zongyi Liu, Isidro Robledo Vega, Patrick Grother, and Kevin W Bowyer, *The humanid gait challenge problem: Data sets, performance, and analysis*, Pattern Analysis and Machine Intelligence, IEEE Transactions on **27** (2005), no. 2, 162–177.

[SPSS11] Jaeyong Sung, Colin Ponce, Bart Selman, and Ashutosh Saxena, *Human activity detection from rgbd images.*, plan, activity, and intent recognition **64** (2011).

[SS15] Erik E Stone and Marjorie Skubic, *Fall detection in homes of older adults using the microsoft kinect*, Biomedical and Health Informatics, IEEE Journal of **19** (2015), no. 1, 290–301.

[SSK+13] J.J.D. Shotton, T. Sharp, A. Kipman, A. Fitzgibbon, M. Finocchio, A. Blake, M. Cook, and R. Moore, *Real-time human pose recognition in parts from single depth images*, CACM **56** (2013), no. 1, 116–124.

[SVB+13] Lorenzo Seidenari, Vincenzo Varano, Stefano Berretti, Alberto Del Bimbo, and Pietro Pala, *Recognizing actions from depth cameras as weakly aligned multi-part bag-of-poses*, Computer Vision and Pattern Recognition Workshops (CVPRW), 2013 IEEE Conference on, IEEE, 2013, pp. 479–485.

[SZ96] Hagit Shatkay and Stanley B Zdonik, *Approximate queries and representations for large data sequences*, Data Engineering, 1996. Proceedings of the Twelfth International Conference on, IEEE, 1996, pp. 536–545.

[SZB05] Stephen Scott, Jun Zhang, and Joshua Brown, *On generalized*

multiple-instance learning, International Journal of Computational Intelligence and Applications **5** (2005), no. 01, 21–35.

[VAC14] Raviteja Vemulapalli, Felipe Arrate, and Rama Chellappa, *Human action recognition by representing 3d skeletons as points in a lie group*, Computer Vision and Pattern Recognition (CVPR), 2014 IEEE Conference on, IEEE, 2014, pp. 588–595.

[VKG02] Michail Vlachos, George Kollios, and Dimitrios Gunopulos, *Discovering similar multidimensional trajectories*, Data Engineering, 2002. Proceedings. 18th International Conference on, IEEE, 2002, pp. 673–684.

[VSRCC09] Ashok Veeraraghavan, Anuj Srivastava, Amit K Roy-Chowdhury, and Rama Chellappa, *Rate-invariant recognition of humans and their activities*, Image Processing, IEEE Transactions on **18** (2009), no. 6, 1326–1339.

[VZQ15] Vivek Veeriah, Naifan Zhuang, and Guo-Jun Qi, *Differential recurrent neural networks for action recognition*, arXiv preprint arXiv:1504.06678 (2015).

[wan12] *Robust 3d action recognition with random occupancy patterns*, Springer, October 2012.

[WF74] Robert A Wagner and Michael J Fischer, *The string-to-string correction problem*, Journal of the ACM (JACM) **21** (1974), no. 1, 168–173.

[WFP03] Nils Weidmann, Eibe Frank, and Bernhard Pfahringer, *A two-level learning method for generalized multi-instance problems*, Machine Learning: ECML 2003, Springer, 2003, pp. 468–479.

[WLL+14] Xingjie Wei, Chang-Tsun Li, Zhen Lei, Dong Yi, and Stan Z Li, *Dynamic image-to-class warping for occluded face recognition*, Information Forensics and Security, IEEE Transactions on **9** (2014), no. 12, 2035–2050.

[WLWY12a] J. Wang, Z.C. Liu, Y. Wu, and J.S. Yuan, *Mining actionlet ensemble for action recognition with depth cameras*, CVPR12, 2012, pp. 1290–1297.

[WLWY12b] Jiang Wang, Zicheng Liu, Ying Wu, and Junsong Yuan, *Mining actionlet ensemble for action recognition with depth cameras*, CVPR 2012, 2012.

[WRB11] Daniel Weinland, Remi Ronfard, and Edmond Boyer, *A survey of vision-based methods for action representation, segmentation and recognition*, Computer Vision and Image Understanding **115** (2011), no. 2, 224–241.

[WWY13] Chunyu Wang, Yizhou Wang, and Alan L Yuille, *An approach to pose-based action recognition*, Computer Vision and Pattern Recognition (CVPR), 2013 IEEE Conference on, IEEE, 2013, pp. 915–922.

[WZ00] Jun Wang and Jean-Daniel Zucker, *Solving multiple-instance problem: A lazy learning approach*.

[XCA12] Lu Xia, Chia-Chih Chen, and JK Aggarwal, *View invariant human action recognition using histograms of 3d joints*, Computer Vision and Pattern Recognition Workshops (CVPRW), 2012 IEEE Computer Society Conference on, IEEE, 2012, pp. 20–27.

[XY04] Yimin Xiong and Dit-Yan Yeung, *Time series clustering with arma mixtures*, Pattern Recognition **37** (2004), no. 8, 1675–1689.

[YHC+12] Kiwon Yun, J. Honorio, D. Chattopadhyay, T.L. Berg, and D. Samaras, *Two-person interaction detection using body-pose features and multiple instance learning*, Computer Vision and Pattern Recognition Workshops (CVPRW), 2012 IEEE Computer Society Conference on, June 2012, pp. 28–35.

[YT12] Xiaodong Yang and YingLi Tian, *Eigenjoints-based action recognition using naive-bayes-nearest-neighbor*, Computer Vision and

Pattern Recognition Workshops (CVPRW), 2012 IEEE Computer Society Conference on, June 2012, pp. 14–19.

[YZT12] Xiaodong Yang, Chenyang Zhang, and YingLi Tian, *Recognizing actions using depth motion maps-based histograms of oriented gradients*, Proceedings of the 20th ACM international conference on Multimedia, ACM, 2012, pp. 1057–1060.

[ZCG13] Yu Zhu, Wenbin Chen, and Guodong Guo, *Fusing spatiotemporal features and joints for 3d action recognition*, Proceedings of the 2013 IEEE Conference on Computer Vision and Pattern Recognition Workshops (Washington, DC, USA), CVPRW '13, IEEE Computer Society, 2013, pp. 486–491.

[ZG01] Qi Zhang and Sally A Goldman, *Em-dd: An improved multiple-instance learning technique*, Advances in neural information processing systems, 2001, pp. 1073–1080.

[ZHJR11] Michael Zöllner, Stephan Huber, Hans-Christian Jetter, and Harald Reiterer, *Navi–a proof-of-concept of a mobile navigational aid for visually impaired based on the microsoft kinect*, Springer, 2011.

[ZX07] Zhi-Hua Zhou and Jun-Ming Xu, *On the relation between multi-instance learning and semi-supervised learning*, Proceedings of the 24th international conference on Machine learning, ACM, 2007, pp. 1167–1174.